AERODYNAMIC OPTIMIZATION OF COMPACT ENGINE INTAKES FOR HIGH SUBSONIC SPEED TURBOFAN APPLICATIONS
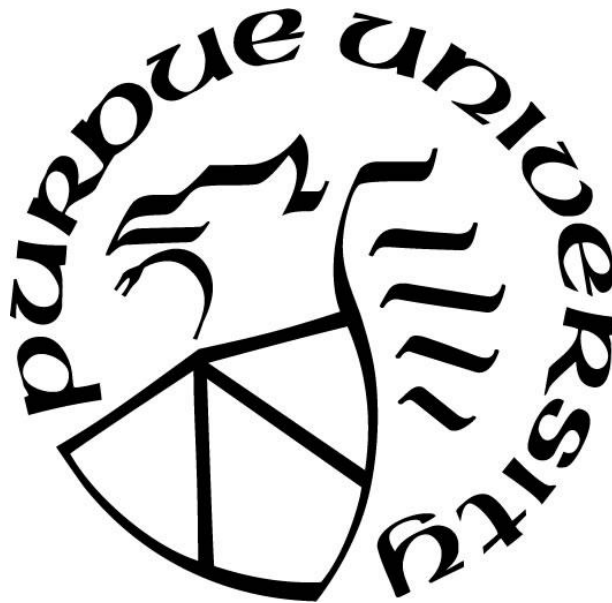
by

Udit Vyas

A Thesis

Submitted to the Faculty of Purdue University

In Partial Fulfillment of the Requirements for the degree of

Master of Science in Mechanical Engineering

Mechanical Engineering

West Lafayette, Indiana

May 2019

THE PURDUE UNIVERSITY GRADUATE SCHOOL
STATEMENT OF COMMITTEE APPROVAL

Dr. Guillermo Paniagua, Chair

Department of Mechanical Engineering

Dr. Tom Shih

Department of Aeronautics and Astronautics

Dr. Steve Son

Department of Mechanical Engineering

Dr. Ganesh Subbarayan

Department of Mechanical Engineering

Approved by:

Dr. Jay Gore

Head of the Graduate Program

To my family: My parents, Hema and Kshitij Vyas, who came to a new country with no money to their name to create opportunity for my brother and me. And to my grandparents, whose success and hard work inspires me every day.

ACKNOWLEDGMENTS

There are many people who have contributed and aided in my success. Naming everyone who has helped me along the way is impossible, so instead I will name a few.

My faculty advisor, Guillermo Paniagua, has been instrumental over the past few years in creating engaging and challenging research opportunities for me. His technical advice and support have helped me grow as an engineer and develop into a better problem solver. His support as I change fields and pursue my passions has been meaningful. He has also cultivated a team environment where technical knowledge and advice is disseminated; resulting in a true team-oriented approach to actively advancing the turbine industry through several inspired turbomachinery concepts.

Over the past year, I have been given the opportunity to work as part of a great team at Purdue (PETAL). Every member of the team has created an atmosphere that allows for fruitful scientific discussion leading to technical knowledge being spread. Being a part of the team has been a true honor, and everyone involved in the team has truly helped me become a better engineer. In particular on the team, I would like to acknowledge and thank Valeria Andreoli, James Braun, Francisco Lozano, and Jorge Saavedra for their technical advice on various topics (this is not a comprehensive list of the team members who are deserving of acknowledgment).

Additionally, I'd like to thank Carleigh Moneybags for encouraging me to channel my inner Michael Scott while completing this work.

Finally, I would like to thank my family and friends, especially my brother, Puna, who helped keep me sane during long and frustrating days. There are countless others who are deserving acknowledgment, but in the interest of brevity, I will just say: know that I am grateful to you for your help.

TABLE OF CONTENTS

LIST OF TABLES

LIST OF FIGURES

LIST OF SYMBOLS

A_{hl}: area at lip inlet of intake

A_t: throat area (inlet area of intake)

L_{ref}: reference length (inlet radius)

$\dot{m}$: massflow (kg/s)

M : Mach number

ρ : density (kg/m^3)

P_0: total pressure (Pa)

P_s: static pressure (Pa)

u : axial component of velocity (m/s)

ABSTRACT

Author: Vyas, Udit. M.S. in Mechanical Engineering
Institution: Purdue University
Degree Received: May 2019
Title: Aerodynamic Investigation and Optimization of Compact Engine Intakes for High
      Subsonic Speed Applications
Committee Chair: Guillermo Paniagua

Within the gas turbine industry, turbofan engines are widely implemented to enhance engine efficiency, specific thrust, and specific fuel consumption. However, these turbofans have yet to be widely implemented into microgas turbine engines. As turbofans become implemented into smaller engines, the need to design engine intakes for high-speed mission becomes more vital. In this work, a design procedure for compact, highly diffusive engine intakes for high subsonic speed applications is set about. The aerodynamic tradeoffs between cruise and takeoff flights are discussed and methods to enhance takeoff performance without negatively impacting high-speed cruise performance is discussed. Intake performance is integrated into overall engine analysis to help guide future mission analyses. Finally, an experimental model for engine intakes is developed for application to linear wind tunnels; allowing future designers to effectively validate numerical results.

A multi-objective optimization routine is performed for compact engine intakes at a Mach number of 0.9. This optimization routine yielded a family of related curves that maximize intake diffusive capability and minimize intake pressure losses. Design recommendations to create such optimal intakes are discussed in this work so that future designers do not need to perform an optimization. Due to high diffusion rate of the intake, the intake performance at takeoff suffers greatly (as measured by massflow ingestion). Methods to enhance takeoff performance, from designing a variable geometry intake, to creating slots, to sliding intake components are evaluated and ranked for future designers to get an order of magnitude understanding of the types of massflow enhancements possible. Then, off-design performance of the intake is considered: with different Mach number flights, non-axial flow conditions, various altitudes, and unsteady engine operation considered. These off-design effects are evaluated to generate an intake map across a wide engine operational envelope. This map is then inputted into an engine model to generate a performance map of an engine; which allows for mission planning

analysis. Finally, various methods to replicate intake flow physics in a linear wind tunnel are considered. It is shown that replicating diffuser curvature in a linear wind tunnel allows for best replication of flow physics. Additionally, a method to non-dimesnsionalize intake performance for application to a wind tunnel is developed.

This work can be utilized by future engine intake designers in a variety of ways. The results shown here can help guide future designers create highly compact diffuser technology, capable of operating across a wide breadth of conditions. Methods to assess intake performance effects on overall engine performance are demonstrated; and an experimental approach to intake analysis is developed.

CHAPTER 1 : INTRODUCTION

As the gas turbine industry advances, turbine concepts become increasingly efficient and powerful. However there exists a need to improve the performance of smaller engines, such as the microgas turbines found in UAV engines. These power plants still have room for notable efficiency improvements, which in UAVs would lead to extended mission duration and range. Concepts exist to improve the power plant performance by converting existing micro-turbojet engines to turbofan engines [1]. For these concepts to be viable, compact engine intakes need to efficiently diffuse high-speed flows down to acceptable speeds for the rest of the engine. In addition to flow diffusion, the intake must meet other aerodynamic requirements for the engine, including maximal total pressure recovery and flow homogeneity; as well as minimal boundary layer development and separation. Mechanical requirements also exist for the intake, including minimal weight (primarily accomplished by minimizing the intake length) as well as physical dimensions such as outlet radius and nose cone outlet radius. A reduced weight intake improves overall engine performance by boosting the specific thrust and specific fuel consumption of the engine. Furthermore, the engine intake must be capable of operating at a wide variety of engine conditions, from takeoff (zero flight speed at sea level conditions) to cruise conditions (high speed flight at high altitudes) minimizing the impact on the fan performance. In compact engine solutions, these varying operating points create design conflicts: the intake's outlet radius is often fixed by downstream engine components, and at cruise conditions a small inlet radius is needed to maintain an inlet to outlet area ratio capable of diffusing the flow; while at takeoff conditions a relatively large inlet radius is needed for the intake to ingest sufficient massflow. The focus of this master's thesis is on the design of high subsonic speed engine intakes considering mechanical constraints while evaluating cruise and takeoff aerodynamic performance; with particular focus on designing engine intakes suitable for use in compact engines such as those found in small compact engines. A methodology for the design of compact, high subsonic speed engine intakes, with mechanical design constraints is developed as part of this thesis.

The methodology developed for this thesis was specifically applied to a high subsonic speed turbofan engine designed to operate at an altitude of 3000m and a Mach number of 0.9 at cruise conditions. This works includes an optimization of the engine intake for cruise conditions. Then the optimized geometry is evaluated at the other aerodynamic extreme: takeoff conditions.

A separate optimization to investigate the parameters controlling takeoff performance is then conducted and the trade-offs between take-off and cruise designs are presented. Methods to enhance takeoff performance while maintaining optimal cruise performance are explored and evaluated for future designers to consider. The analysis of the intake is extended into an overall engine analysis, and a map of engine performance as a function of intake performance at off-design conditions is provided. Furthermore, the effects of unsteadiness from the engine on the engine intake is also considered to quantify the effects that engine components can have on the intake and overall engine performance. Finally, an experimental model for the optimized geometry is developed for future testing in a linear wind tunnel found at Zucrow Labs at Purdue University.

1.1: Problem Motivation

As the design of engine components and turbomachinery continually advances, a new limiting factor in the operation of many engines emerges: the ability of a compact engine intake to diffuse high speed flows while delivering homogenous flow to the engine at every operational point along the mission envelope. Intakes must be capable of delivering diffused flows to desired speeds at high flow rates and minimizing pressure losses while operating at a variety of different altitudes and conditions. These requirements and varying conditions can often make the design of engine intakes difficult to manage, especially in compact engine configurations where the weight of the intake factors heavily into overall engine performance. In particular, the differences between what is required of intakes at high-speed cruise conditions (diffusion of flow, minimal pressure losses and flow distortion) vs. what is required at take-off conditions (maximal mass-flow, minimal pressure losses) creates trade-offs in designing the intake which often leads to a reduction in overall engine capabilities. Another level of complexity is added by the design constraints on weight (length, diameter), size and speed requirements from downstream components. Balancing these requirements and constraints creates a challenging design problem that must be addressed to improve the performance of future compact engines.

The difficulties in engine intake design are amplified in high subsonic speed applications where the diffusion required by the engine intake becomes extreme. The large diffusive requirements combined with low pressure losses and flow distortion leads to a limited designs space. The trade-offs between high speed cruise operation and take-off operation further reduces

the compact engine intake design space since cruise conditions require a large outlet to inlet area ratio, while takeoff operation requires a large inlet area due to large massflow (and thrust) requirements; and meeting both requirements in compact engine design is not always feasible.

Despite the challenges involved in creating engine intakes for compact high subsonic speed engines, the demand for such engine intakes is steadily increasing as the gas turbine industry moves to operating microgas turbines in more efficient configurations, such as in turbofan configurations [1].

1.1.1: Turbofan Engine Configuration in Compact Engines

Traditional turbojet engines pass all the intake air through the downstream engine components; namely the compressor, combustor, and turbine. This means that all intake air is combusted; and therefore, all intake air requires fuel to generate thrust. Turbofan engines offer better thrust to fuel performance by placing a fan downstream of the engine intake and using two flow paths: a core flow path (in which air is sent through the combustor and fuel is used to generate thrust) as well as a bypass flow path (in which thrust is generated with no fuel needed) [2]. The bypass flow is accelerated from the freestream by the fan downstream of the inlet, helping to provide thrust from the bypass flow. Typically, the fan does not significantly increase the fuel required by the core engine, so turbofans offer improvements over traditional turbojet engines by increasing the thrust to fuel consumption ratio [3].
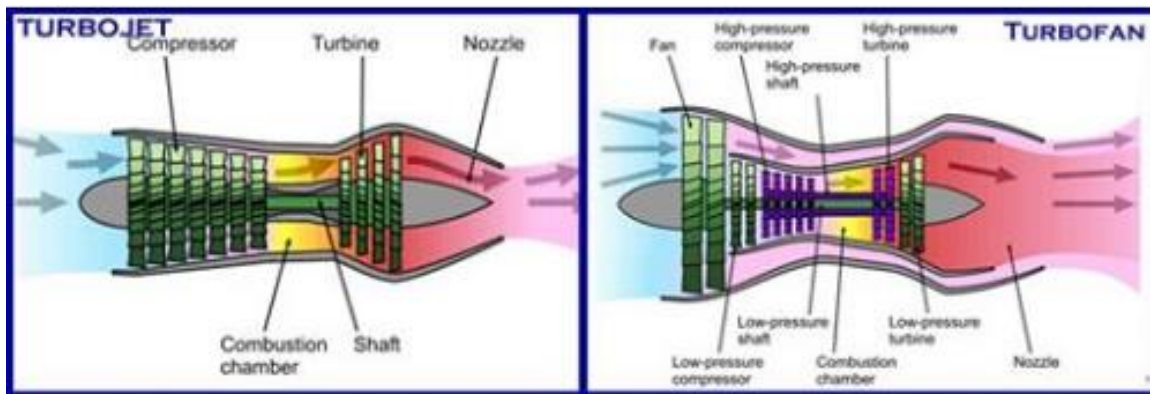
Figure 1-1: Overview of turbojet vs turbofan configurations. The turbofan has a bypass flow path which generates thrust without requiring fuel combustion.

Turbofan engines are widely implemented in large engine configurations, however, in the class of microgas turbines the use of turbofan engines becomes more complicated. Specifically, in the small compact UAV engines turbofan engines have yet to be widely implemented. This is often because turbojet engines are simpler in design, often cheaper to produce and lighter. There have been several investigations on the use of micro turbojet engines in such applications. Chiang and Hsu investigated the use of a small 12 pound thrust turbojet engine for the UAV marketplace. They found that while small turbojet engines were capable of meeting thrust requirements after many cycles, the engines also experienced structural issues during extended use, such as bearing integrity; and found operational issues during quick throttle applications [4]. Such issues severely limit the mission length of what small turbine engines are often applied to: UAV missions. Other challenges of micro turbojet engines include the capital cost for creating small turbine engines as well as the need for an exhaust heat recuperator to increase the cycle efficiency [5].

As mission lengths and duration for UAVs demand further extension, the need for better engine designs emerges. Designs to convert small gas turbojet engines to turbofan engines are being proposed, including the potential conversion of turbojets to turbofan engines via a continuously varying transmission [1,6]. These designs enable the use of turbofans in UAV technology, which will improve the range and fuel consumption of UAV missions and alleviate the issues that turbojet engines have in UAV applications.

1.1.2: Overview of UAV Engine Operation and Applications

In the past few decades the role and prominence of unmanned aerial vehicles (UAVs) has increased as the applications of the technology has become more widespread. UAV technology spans multiple industrial sectors and involve multiple branches of engineering. UAV applications include (but are not limited to) aiding law enforcement in high speed chases and surveillance [7], improving traffic patterns [8-9], collecting geographical data for farming and environmental data [10-11], and military operations. This broad range of UAV applications reveals the versatile nature needed for UAV technology to function properly. UAVs must be capable of performing at a variety of conditions for a variety of purposes.

While UAVs can be deployed in a variety of manners, the primary use of high-speed UAV technology lies in military applications; whether for payload delivery, surveillance,

intelligence, reconnaissance, or target acquisition operations [12]. These missions have varying operational altitudes, range, and duration. During operation, the UAVs have 3 major distinct operational modes: cruise (high-speed flight), loiter, and ascent/descent (takeoff/landing). These conditions create a complex design space due to the variety of operational points hit. Furthermore, UAVs in this environment must be designed in a robust manner capable of covering as many target locations as possible while considering fuel, weather, and mechanical limitations. Optimizations based on current UAV technologies have been performed as the operational limits of UAVs are pushed [8,10]. The next step in UAV development is to increase the speed of the engines and to improve overall engine design.

As UAV technology advances, the design space is moving towards engines capable of high-speed cruise flight. These engines have improved mission range, due to the increased flight velocity. The high-speed cruise flight requirement is often determined by other UAV characteristics, such as engine power, aerodynamic design, endurance requirements, and mission duration [12]. However, challenges still exist in designing these engines efficiently. Due to the small engine size, these UAV engines operate primarily with turbojet engine configurations, leaving room for engine improvement by replacing the turbojet with a turbofan engine [1,6].

Improving the engine operation by replacing the standard turbojet engine with a turbofan configuration increases the mission duration by reducing specific fuel consumption requirements [1]. Designing future UAVs to operate at high speeds will lead to increased mission range. Consequently, it appears that the future of UAV technology is to utilize turbofan engines capable of flying at high speeds. To make such engines possible, a compact engine intake with high pressure recovery and flow diffusion capabilities must be designed. These engine intakes will need to operate at near sonic speeds, as well as possess the ability to perform well at off-design conditions such as takeoff.

1.1.3: Problem Overview

As turbofan engines are implemented into UAV technology, the intake design for engines becomes more complicated. UAVs often need to operate at a variety of speeds and altitudes; and must be capable of performing at off-design (high angle of attack and takeoff) conditions. Innovations in the turbine industry that enable the use of turbofan engines in UAV applications and other compact engine technologies further exacerbates the need to design engine intakes

capable of performing at a wide variety of conditions while satisfying new engine design requirements. The focus of this thesis is on the design of compact engine intakes capable of efficient high subsonic speed cruise flight for applications to microgas turbines; with particular attention paid to the possibility of implementing turbofan engine configurations in future UAV technologies.

1.2: Current Intake Design Methods for Cruise Conditions

Engine intakes serve primarily to diffuse air intake to acceptable speeds for downstream engine components. Typical engine intakes consist of an inlet lip, diffuser, and nose cone. The inlet lip serves to capture air and establish inlet flow, the diffuser serves to diffuse the flow, and the nose cone develops the inlet annulus for downstream components and helps to increase pressure recovery and other flow characteristics of the intake flow. These 3 engine intake components are depicted below in Figure 1-2, where the blue curve represents the diffuser wall, the red curve represents the inlet cone, and the black curve represents the inlet lip. This figure shows a 2D axisymmetric view of a standard subsonic inlet, where the full 3D view is achieved by rotating the curve about the line of symmetry. Only the inner walls of the diffuser are shown in this figure. To effectively design engine intakes, the design of the intake lip as well as the diffuser must be understood.
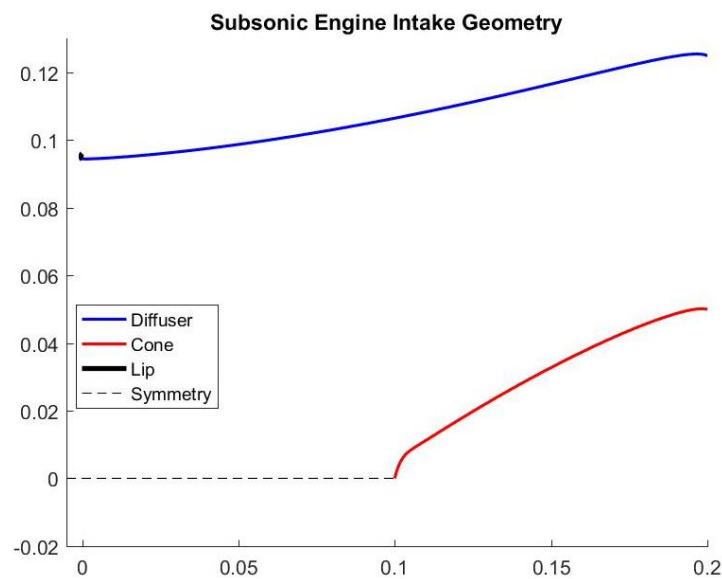
Figure 1-2: Overview of intake design components.

1.2.1: Design of Inlet Lips

In designing inlet lips, a superelliptical parametrization of the lip geometry is widely used for subsonic intakes [14-16]. The equation for the inlet lip is described below in Equation (1-1):

$$\left(\frac{x}{a}\right)^p + \left(\frac{y}{b}\right)^q = 1 \tag{1-1}$$

where x and y are the lip coordinates. In parametrizing the lip, it is important to pay attention to the fineness ratio and the contraction ratio, defined below. The fineness ratio defines the aspect ratio of the inlet lip. Larger fineness ratios will lead to longer and flatter inlet lips. The contraction ratio is used to define area contraction achieved by the inlet lips. These ratios are defined below in Equations (1-2) and (1-3).

$$Fineness\ ratio = \frac{a}{b} \tag{1-2}$$

$$Contraction\ ratio = \frac{A_{hl}}{A_t} = \frac{r_{hl}^2}{r_t^2} = \frac{(r_t + b)^2}{r_t^2} \tag{1-3}$$

The parameters a,b,A_{hl}, A_t are all defined in the figure below. A_{hl} is used to define the inlet area at the very beginning of the lip, while A_t is the area at the throat of the inlet lip. At the end of the inlet lip is where the intake diffuser will begin.
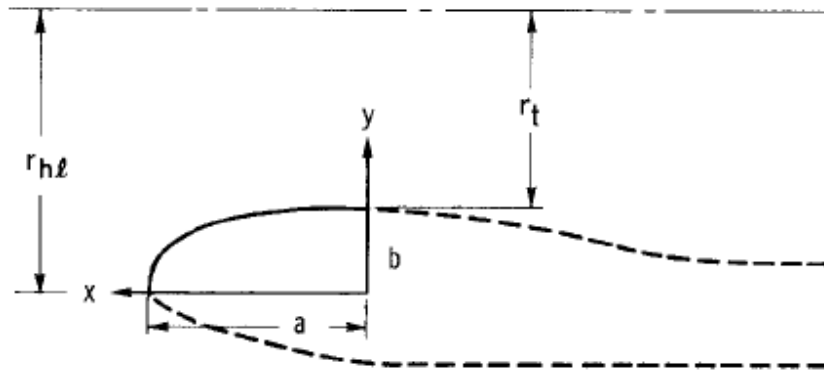
Figure 1-3: Inlet lip design parametrization [13].

Albers and Miller performed a study on the effects of different parametrizations on inlet performance, including varying the exponent of the superelliptical parametrization, varying the contraction ratio, and varying the fineness ratio. They found that the contraction ratio of the inlet lip has the largest effect on inlet performance in terms of flow Mach number distributions [15].

They found that large contraction ratios lead towards Mach number reduction upstream of the throat at off-design case due to high curvature in the lip. As a result, to ensure good off-design performance, smaller contraction ratios are preferable. In the study conducted by Albers and Miller this was quantitatively stated as $\frac{A_{hl}}{A_t} \leq 1.38$ [15]. The study also analyzed the effects of the fineness ratio on inlet performance by analyzing the average and local adverse Mach number gradients along the inlet lip wall. The results found that past a fineness ratio of 2 the inlet performance becomes insensitive to increases in the fineness ratio. Additionally, it was found that the optimal fineness ratio for subsonic intakes is between 1.5 and 2. Finally their study analyzed the effects of the exponent of the superelliptical equation (considering p=q). The analysis concluded that the optimal exponent depends on the fineness ratio, and that optimal performance is generally achieved with both the fineness ratio and the value of the exponents are near 2 [15].

A later study conducted experimentally also explores the effects of inlet lip geometry on overall intake performance. Figure 1-4 below shows how the experimental analysis was conducted. A single diffuser geometry was analyzed, while upstream of the diffuser varying inlet lips could be plugged in. Different angles of attack (as defined by α in the figure) were analyzed. The experiments revealed that large contraction ratios (between 1.46 and 1.56) in the lip yielded the best results in terms of total pressure recovery at design conditions for the inlet. However, at these large contraction ratios there was a significant drop-off in performance (in terms of pressure recovery) at off-design conditions [16].
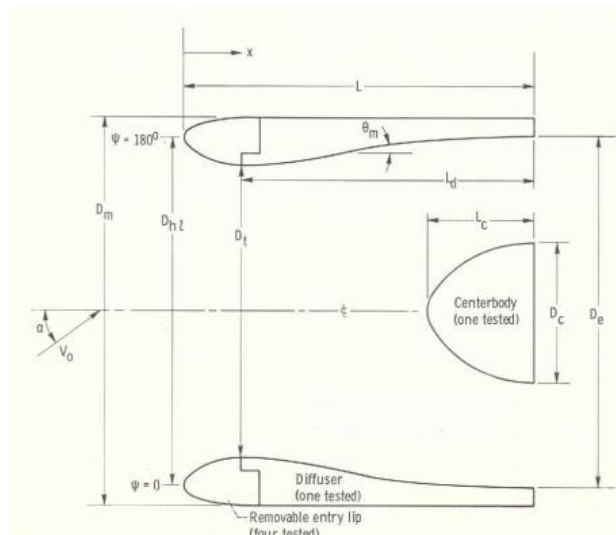
Figure 1-4: Experimental evaluation of diffusers [16].

The preceding studies of inlet lip design are focused on low speed engine intakes that are not in the high subsonic speed range of interest for future compact engines. These studies offer a good baseline and starting point for future anlaysis; however, since the Mach number that are studied differ drastically from the ones of interest, the findings will not necessarily apply to the high subsonic regime. With this being considered, the starting point for lip geometries in application to compact engines will be a fineness ratio of 2 with exponents of 2 since it was revealed that these values made the intake least sensitive to off-design conditions, which are an important consideration in UAV applications. Similarly, the contraction ratio of the intake will start out low to ensure optimal performance at off-design conditions, but the effects of varying these parameters will be considered in the overall intake design.

1.2.2: Design of Intake Diffuser

Many challenges exist in designing compact diffusers for engines operating in the high subsonic regime. Compact diffusers tend to lead to separated flow with secondary flow characteristics caused by circumferential and radial static pressure gradients dictated by flow separation [17]. Geometric relationships have been set forth to establish flow separation boundaries for compact diffusers [17-18] as done below in Equation (1-4):

$$\frac{A_2}{A_1} = 1 + \frac{2(sin\theta_{avg})L}{L_{ref}} \tag{1-4}$$

where θ_{avg} is the average angle of diffusion of the diffuser wall and the reference length refers to the inlet radius for annular diffusers. This relationship can be used to set the size of the intake given a desired intake area ratio.

Mayer et al performed 3D optimizations for highly compact off-set diffusers, and found that by optimizing for the length, the diffuser length could be shortened by up to 10% with small penalties in pressure recovery [19]. This study indicates that the equation above can be stretched when being applied to optimized inlet geometries. Hoyle et al performed a 2D optimization of air intakes and found that a local acceleration near the inlet of the diffuser helps prevent separation downstream in the diffuser [20] due to the local increase in Reynolds number. The added momentum to boundary layer helps prevents separation. This implies that the inlet lips should be

designed with a low fineness ratio, however, in UAV applications this is not desirable since high fineness ratios improve off-design performance.

Zhang et al performed an optimization for diffusers to investigate methods to minimize pressure distribution distortion and found that pressure distortions could be reduced by 70% [21]. However, the work was applied to an S-duct diffuser, so the results only demonstrate the potential for flow distortion minimization in optimizations.

Tormalm applied duct design to UAV technology in order to design compact highly diffusive ducts for UAVs [22]. The effects of inlet lips and aggressive diffusers were investigated in his work, and he found that at high speeds the pressure recovery of the intake compared well between CFD and experimental results. This implies that CFD can resolve trends in intake performance and that optimizations using CFD can be reliably applied to find intake designs for compact engine technology.

1.3: Off-Design Considerations

As off-design considerations become increasingly important several studies investigating off-design performance of engine intakes have been conducted. Tyler and Williamson experimentally explored the effects of non-uniform inlet flow on subsonic diffuser performance for a variety of different diffusers, including annular designs. They investigated a wide range of inlet flow distortions and found that the pressure recovery of an intake is highly dependent on inlet flow distortion [23]. Wolf and Johnston conducted an experimental investigation with similar goals. Their work concluded that diffusers with non-uniform velocity profiles are more likely to stall and have poor performance in terms of outlet velocity profile. They also found that diffuser performance is affected by the relative locations and variations of non-uniform inlet flow, revealing that the degree of non-uniformity is a key factor in off-design intake performance [24]. The considerations of non-uniform inlet flow are particularly important to consider in off-design analyses such as during angle of attack operations and takeoff conditions.

Kennedy et al explored the effects of high angles of attack on intake performance computationally and found that the performance of the intake decays with large angle of attacks [25]. Due to fan operation, the angle of attack of the aircraft differs from the intakes physical angle of angle (due to varying streamline curvature), making the intake performance more susceptible to performance issues at high angles of attack. NASA explored the ability of CFD to

resolve high angle of incidence cases by comparing to simulations to experiments. The investigation found that CFD does not resolves the pressure recovery factor up to angles of attack of 15 deg [26].

Low speed operation of compact, highly diffusive engine intakes also presents an issue to performance of the intake. During low speed applications, the capture area of the intake increases, which increases the streamline curvature and streamline angle of attack on the intake [27]. This increases the risk of separated flow during low speed applications [28]. The effects of the capture area are explored by Cantwell and are graphically depicted below in Figure 1-5. The increased capture area at low speeds (top graphic) enhances separation likelihood and reduces intake performance. This increased capture area plays a large role in takeoff operation of the intake as will be demonstrated in Chapter 4. The increased capture area at takeoff is due to stagnant flow upstream of the inlet having little momentum, making it easier for the turbofan downstream of the intake to suck the air in [27-28].
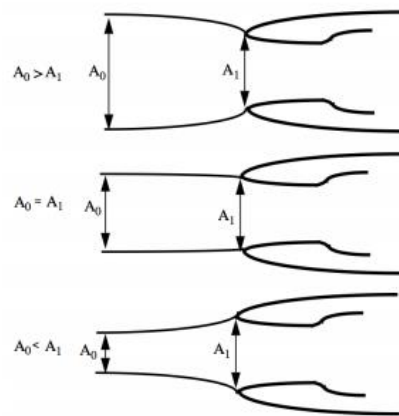
Figure 1-5: Capture area comparison for different aerodynamic conditions [27].

Reddy performed optimizations of subsonic intakes to evaluate the tradeoffs between cruise and takeoff conditions for intakes and found that designs made to improve takeoff performance adversely affected cruise performance [29]. This finding implies that improving takeoff performance of an optimized intake for cruise conditions will require some sort of variable geometry implementation. Majic et al analyzed the effects of morphing the nacelle for a turbofan and found improvements in turbofan performance at various flight conditions depending on the degree to which the inlet was morphed [30]. The pressure recovery at climb

conditions was boosted by nearly 7%, showing the potential gains implementing a variable intake geometry can have on an overall mission.

Klein summarized much of the work regarding intake design in terms of the effects of inlet flow quantities on diffuser performance. He concluded that increasing the inlet turbulence intensity or Reynolds number leads to a general increase in pressure recovery, while increasing the inlet shape factor (essentially the fineness ratio) leads to a decrease in pressure recovery of the diffuser [31]. These results establish that intake performance is dependent upon the inlet conditions of the intake. The computational domain used in the subsequent chapters will account for this and impose inlet quantities well upstream of the physical intake.

1.4: Overview of Relevant Physical Principles and Computational Tools

The bulk of this thesis is focused on computational analysis of engine intakes. The computational solvers will focus on resolving internal flows by solving the Navier-Stokes equations (continuity, x, y, and z momentum, and energy relations). The used computational model solves the Reynolds-averaged Navier Stokes form of the equations by decomposing flow quantities into a time-averaged quantity plus a fluctuating quantity. RANS solvers are known to be sensitive to the turbulence model chosen to resolve the flow. To determine which turbulence model to use, Anderson conducted a study for annular diffusers using various turbulence models [32]. The study found that k-ω-sst turbulence model resolved flows in annular diffusers better than other turbulence models by comparing CFD results to benchmark experimental diffuser data. This turbulence model is a 2-equation model with compressibility effects included. Based on Andersen's results, the k-ω-sst model is used throughout this thesis. Andersen concluded that the y+ value of the mesh must be kept below 20 to properly resolve intake performance (in this thesis it is maintained below 1, preventing the use of wall functions). Andersen also showed that 2D axisymmetric CFD results compare well with full 3D simulations and with the experimental data, so the computational analysis in this thesis is primarily done with 2D axisymmetric domains.

The solver used in the analysis described here is CFD++, a solver developed by Metacom Technologies. CFD++ can solve steady and unsteady compressible Navier-Stokes equations using RANS/URANS simulations and various turbulence models [33]. It can also handle a full range of Mach numbers, making it suitable for selection in transonic applications like the ones

discussed here; and furthermore, can handle all mesh topologies so that any meshing strategy can be used [33].

The optimizations performed utilize a multi-objective minimization approach to improve performance in multiple parameters. The package used, CADO, is primarily used for turbomachinery component optimizations, but can be adapted to optimize engine intakes. The package was developed at the von Karman Institute, and utilizes differential evolutionary algorithms and Darwinian evolution to evolve populations over time to create a pareto front [34]. The pareto front represents a family of designs within the design space that attains optimal performance in both objectives that are optimized for. Increasing performance in one objective along the pareto front leads to a decrease in performance of the other objective. CADO has been successfully implemented in a variety of applications. Overstate developed the software and implemented it to optimize a radial compressor for microgas turbines [35]. Overstate et al implemented CADO to optimize internal cooling channels for high pressure turbine blades [36]. CADO was also used by Juangphanich et al to design and optimize highly loaded turbine stages, while Andreoli et al optimized the tip cooling to improve rotor efficiency [37-38]. Previously, CADO was also used to optimize high speed engine intakes for pressure losses and flow distortion [6]. CADO has successfully been utilized in a variety of optimization problems related to turbomachinery and engine intakes, and as such is utilized in the optimizations within this thesis.

CADO operates on differential evolution (DE) algorithms, which are similar to genetic algorithms. The DE allows users to set numerical bounds on design parameters to reduce the design space. Before optimizing the geometries, CADO runs a design of experiments (DoE) to evaluate the full design space and create an initial database. From this database, the best candidates are selected as the initial population for the optimization. Then the differential evolution (DE) algorithm utilizes a parallel direct search method to create populations for each generation [39]. The DE creates new populations by randomly mutating the initial vector (previous population). Then crossover is introduced to increase diversity into the mutated population. This is done by mixing parameters of the new population with parameters from a different population [39]. This new population now contains several individuals based on the previous population, mutation, and crossover. The size of each population is reduced to the set population size by the DE using a nondominated sorting genetical algorithm (NSGA-II) [40]. In

this way the DE evolves the design space over time to develop a pareto front. In the present work, CADO is used to maximize intake flow diffusion and minimize pressure losses.

1.5: Problem Statement

Intakes in high-speed compact engines have many roles. Future engine technologies are becoming increasingly versatile in operation. Engines must be capable of at operating high-speed cruise conditions, high angle of attack conditions (ascent and descent trajectories), loiter conditions, as well as at take-off conditions. As engines become increasingly compact, the challenges in designing an intake capable of operating at these conditions becomes a significant design challenge. The focus of this research will be on the designing aerodynamically optimal engine intakes at the mission extremes; namely at high-speed cruise conditions and at take-off conditions.

Engine intake designs will first be optimized for high-speed cruise flight to investigate the relationship between geometric intake design and the aerodynamic performance of intakes. The intake design will be constrained by the physical dimensions of a turbofan which will be implemented into a real engine [1]. Then intake performance will be evaluated at the other extreme of engine operation: takeoff conditions. The challenges in designing a highly compact engine intake capable of large flow diffusion and of ingesting large massflows at takeoff will be investigated, and methods to design an intake optimized for both conditions will be discussed. Next the engine intake will be integrated into an overall engine model, and the performance of an optimized engine intake at various potential operating conditions will be evaluated to determine the off-design performance of an optimized intake. Finally, an experimental model and plan is presented for future validation of the intake analysis done in this work.

CHAPTER 2 : RESEARCH OBJECTIVES AND METHODOLOGY

To create a comprehensive methodology to design high subsonic speed engine intakes that can optimally operate at a variety of conditions, the research is broken down into 4 main objectives. First an aerodynamic investigation and optimization of engine intakes at high speed cruise conditions will be conducted, with a focus on maximizing diffusion, pressure recovery, and flow homogeneity. Then a similar investigation of intake performance will be conducted considering take-off conditions. The design trade-offs between these two very different conditions are explored, and methods to develop intakes that can work at both conditions are considered. Third, the assessment of the intake will be integrated into an engine analysis to assess the impact of intake performance on the overall engine. Finally, the numerical methods used to accomplish all this will be validated against experimental investigations. The objectives and research methodology are summarized below in Figure 2-1:
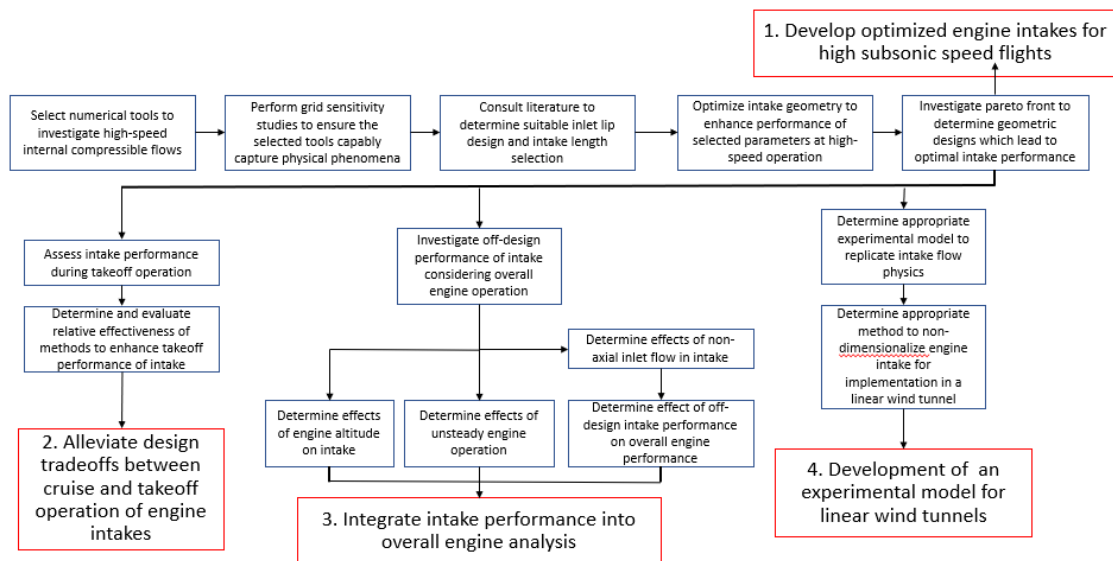
Figure 2-1: Summary of research methodology.

2.1: Objective 1—Development of Optimized Intake Geometries for High Speeds

In order to optimize engine intakes for high subsonic speeds first the aerodynamics of high-speed flights will be investigated numerically. This aerodynamic investigation is conducted by designing 2D intake profiles and evaluating them using 2D axisymmetric numerical

simulations in CFD++. The numerical solver uses Reynolds Averaged Navier Stokes (RANS) equations to resolve the flowfield. A mesh sensitivity study is performed to ensure the numerical results do not depend on grid resolution.

To achieve high speeds the inlet speed for cruise conditions is set to Mach 0.9. Additionally, the outlet area is fixed by downstream engine components. The inlet area for cruise conditions is set by isentropic equations to achieve the desired diffusion of the flow field. To investigate the aerodynamics of these high-speed intakes, several cases are run with different intake geometries. The effects of inlet lip geometries and intake lengths are analyzed in a preliminary analysis.

Using the results of this investigation, numerical optimizations are then performed. The preliminary investigation is used to set the length of the engine intake based on weight and size constraints, pressure losses, and flow distortion parameters. With the intake length set, the geometric shape of the intake is then optimized using a differential evolution optimizer that employs a genetic sorting algorithm. The optimization software utilized is CADO and was developed at the Von Karman Institute for Fluid Mechanics for Tom Overstate. CADO has been used in a wide range of turbomachinery applications to achieve optimal designs [6, 34-38]. The optimization strategy employs a multi-objective approach in order to minimize multiple objectives and develop a family of geometries that minimize the objectives. The optimizer is used to maximize flow diffusion and minimize total pressure losses in the intake. The results yield a family of related geometries along a pareto front. Along this pareto front, improving performance of one objective leads to a penalty in the other objective.

The optimization strategy is summarized below, with the various numerical tools utilized included. Seven design parameters are used to vary intake geometries, which are inputted into MATLAB to parametrize the intake geometry using Bezier curves. The computational domain is set up using ICEM, which is then solved with CFD++. The results are analyzed using Tecplot to determine relevant flow quantities, with particular attention paid to pressure losses and flow diffusion. Then the DE and NSGA-II algorithms are coupled to create new populations focused on minimizing the objectives. The optimizer evolves intake designs from population to population by introducing diversity to optimal geometries from a preceding population. Population size is set to 40 (over 25 populations) based on the recommendations set forth by Piotrowski and Crossley [41-42].
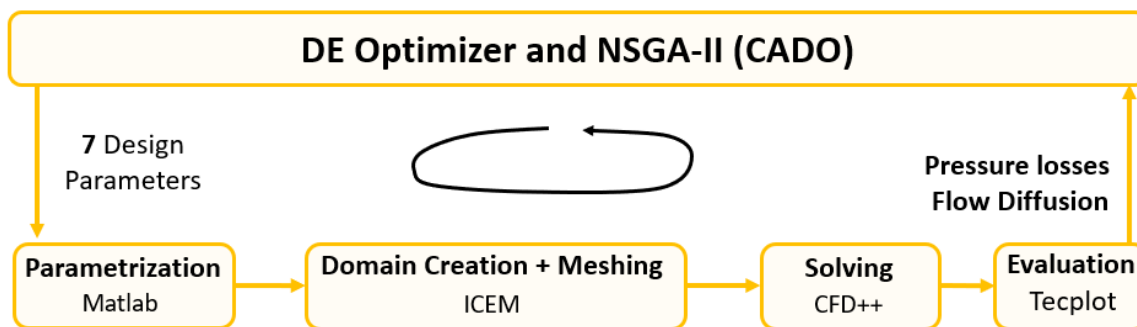
Figure 2-2: Optimization overview.

2.2: Objective 2—Assessment of Intake Performance at Take-Off Conditions

The optimized engine intake is analyzed at takeoff conditions (zero flight speed at sea-level). Due to increased capture area, the streamline curvature dramatically changes, resulting in poor performance. Takeoff performance is primarily measured by massflow ingestion. Due to large levels of separation at takeoff from aggressive streamline curvature, the massflow ingested by highly diffusive intakes can be much lower than desired. Methods to enhance the massflow ingestion are explored; these methods include inserting slots in the intake, sliding the inlet diffuser, sliding the intake cone, designing variable geometry intakes, and increasing fan suction. The goal of this section is to demonstrate typical levels of massflow ingestion enhancement by these various methods.

2.3: Objective 3 – Integration of Intake Performance into Engine Analysis

Next, the intake analysis performed needs to be integrated into engine analysis. This will be done first by considering the impacts of various engine operation on intake performance, and second by integrating off-design intake performance into an engine model using TMATS. The effect of non-axial inlet flow as well as non-design speed on intake performance is first considered. This generates a map of intake performance that depends on flight Mach number and angle of attack for the engine. Then the effects of unsteadiness in the engine are considered on intake performance. This is done by considering unsteadiness in turbofan downstream of the engine intake. To consider the wide range of applications for UAV missions, the effects of different altitude operation is also considered on intake performance. Finally, these results are used to create a map of off-design intake performance, which is inputted into an engine model to

determine thrust performance of an overall engine at various off-design conditions. This map is useful for mission analysis of future UAV applications to determine optimal speed for ascent and descent trajectories.

2.4: Objective 4 – Experimentally Validate Numerical Methods used for Intake Analysis

The optimized intake geometry is numerically evaluated. To validate the ability of CFD to accurately determine optimal intake geometries, an experimental model of the engine intake must be developed. To efficiently and easily test intake future intake geometries, the experimental model will be developed for a linear wind tunnel, which will allow for a variety of experimental conditions to be evaluated.

The experimental model is developed to convert an annular engine intake to a 2D profile based on the diffuser curvature and area ratio of the intake. The experimental model replicates relevant flow physics of the original intake; including shear stress distribution and enhancements in pressure losses and flow diffusion from baseline to optimized geometries. Then a method to non-dimensionalize intake flow parameters to test the proper conditions is developed. This allows for appropriate determination of the Reynolds number for experimental testing. This section develops a method for experimentally testing engine intake designs in a linear wind tunnel.

CHAPTER 3 : DEVELOPMENT OF OPTIMIZED ENGINE INTAKES FOR HIGH SUBSONIC SPEEDS

The focus of this chapter is on the anlaysis and design of compact engine intakes at high subsonic speeds. Specifically, the design process is applied to creating an engine intake for a micro-turbofan UAV engine. First the design constraints on the engine intake are considered to set 1D engine intake parameters. These design conditions and constraints serve to create a design space for the engine intake by setting diffusion requirements and sizing the inlet and outlet sizes of the intake. Then a suitable set of performance parameters are considered. Next the aerodynamics of high-speed engine intake performance are investigated, the intake is sized, and the lip is designed according to methods found in literature. Finally, the diffuser and fan cone geometry are optimized to minimize the relevant aerodynamic performance parameters using CADO.

3.1: 1D Design of Engine Intake

To start the design of engine intakes a 1D analysis of the intake is performed. This involves considering the design conditions and constraints set by the downstream engine components. Additionally, the overall intake is sized (inlet and outlet diameters), and a set of parameters is defined to evaluate the aerodynamic performance of the intake.

3.1.1: Design Conditions and Constraints

At cruise conditions, the engine will be operating at an altitude of 3000m and a Mach of 0.9. The turbofan downstream of the engine intake operates optimally at Mach0.45 and is designed for a channel radius of 0.125m with an inner channel radius of 0.05m. This sets the outlet area of the engine intake to 0.0491 m^2 according to Equation (3-1):

$$A_2 = \pi(r_{2,outer}^2 - r_{1,inner}^2) \tag{3-1}$$

where the area determines the outlet area of the intake. The small intake size represents a significant constraint for takeoff conditions due to massflow requirements. However, at cruise conditions, where flow diffusion is a significant design requirement, the reduced intake size

(diameter) is not a significant constraint. Rather, minimizing intake length will be a significant constraint as reduced length leads to increased curvature and increased separation; which results in reduced flow diffusion and increased pressure losses.

The next step in the design of the intake is to determine the desired area ratio for the intake. This is done based on isentropic equations and setting desired inlet and outlet speeds for the intake. For the considered example, the inlet speed that is desired is Mach 0.9, while the downstream fan desires flows at Mach 0.45. Then using isentropic flow equations, the inlet to outlet area ratio can be determined using a quasi-1D approach as defined in Equation (3-2):

$$\frac{A}{A^*} = f_1(M) = \frac{\left(\frac{\gamma+1}{2}\right)^{\frac{\gamma+1}{2(\gamma-1)}}\left(\left(1+\frac{\gamma-1}{2}M^2\right)^{\frac{\gamma+1}{2(\gamma-1)}}\right)}{M} \tag{3-2}$$

Since the choked area, A^*, is assumed constant by the 1D isentropic equations, the inlet to outlet area ratio can be determined using Equation (3-3):

$$\frac{A_{in}}{A_{out}} = \frac{A_{in}}{A^*}\left(\frac{A^*}{A_{out}}\right) = \frac{f_1(M_{in})}{f_1(M_{out})} = 1.44 \tag{3-3}$$

Since the outlet area is fixed by the fan, the area ratio fixes the inlet radius of the intake to 0.0953 m. This 1D analysis fixes the physical inlet to outlet area ratio of the engine intake. Then varying the diffuser geometry allows for analysis of how the diffuser geometry effects flow parameters like flow diffusion, separation, and pressure recovery without changing the area ratio.

3.1.2: Performance Parameters

Next, a suitable set of performance parameters needs to be defined to evaluate the aerodynamic performance of the intake. During cruise conditions at high speeds, the intake must be capable of considerably diffusing the flow speed, while delivering flow with minimal separation and pressure losses, as well as delivering homogeneous flow to the downstream engine components. To measure flow diffusion, the ratio of inlet to outlet Mach numbers is used (larger values means more diffusion occurred) as shown below in equation 3. The inlet Mach number is defined as the massflow averaged Mach number at the physical inlet of the intake, while the outlet Mach number is defined as the massflow averaged Mach number at the outlet of

the intake. Pressure losses are defined in terms of total pressure, as shown below, in equation 4. Minimal pressure losses ensure that maximal total pressure is delivered to downstream components, allowing for more power and work extraction from the turbine. The downstream engine components also desire minimal flow distortion (minimal boundary layer development and separation), which can be measured by taking the RMS value of the outlet Mach number, as shown below in equation 5. The flow distortion parameter essentially measures the radial variation in flow quantities at the outlet of the intake. The goal of the aerodynamic investigation is to discover diffuser and cone geometries that maximize flow diffusion while minimizing pressure losses, flow distortion, and separated area. The parameters are defined below in Equation (3-4) through Equation (3-7).

$$Flow\ Diffusion = \frac{M_1}{M_2} \tag{3-4}$$

$$Pressure\ Loss = 1 - \frac{P_{02}}{P_{0,freestream}} \tag{3-5}$$

$$FlowDistortion = \frac{\sqrt{\sum_i^N \rho_i u_i A_i \left(M_i - M_{avg}\right)^2}}{\dot{m}} \tag{3-6}$$

$$M_{avg} = \frac{\sum_i^N \rho_i u_i A_i M_i}{\dot{m}} \tag{3-7}$$

Another important constraint in high-speed flight is the weight of the engine intake. Especially for the considered application to micro-turbofan engines, the weight of the engine intake must be minimized since large weight leads to reduced engine performance; which affects mission range and maximum attainable speed. Since the inlet and outlet diameters of the intake are already fixed, the only way to minimize weight of the intake is to minimize intake length. To summarize the design requirements: the intake must minimize flow distortion, pressure losses, and length, while maximizing diffusion capabilities. Furthermore, the inlet and outlet areas of the intake are fixed, which represents a significant design constraint.

3.2: Geometry Parametrization, Computational Domain, and Mesh Sensitivity

The intake geometry is parametrized and generated in MATLAB using Bezier curves to ensure continuity in the first and second derivatives of the physical intake. The intake geometry created in MATLAB is a 2D profile of the intake, with the geometry being varied by control points as shown below in Figure 3-1. The blue curve represents the diffuser wall, while the pink curve is the fan cone wall. The first 3 and last 3 points of each curve are set to have the same radial height, to ensure that the inlet and outlet areas are met by the Bezier curves.
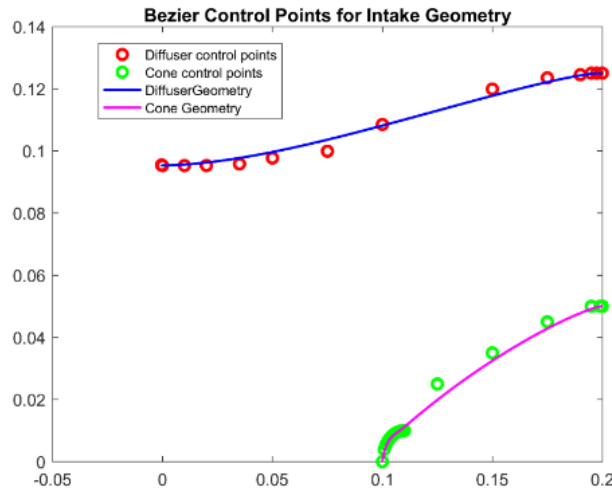
Figure 3-1: Intake geometry parametrization using Bezier curves.

The intake geometry is then imported into Ansys ICEM Mesher, where the computational domain is defined. Figure 3-2 below shows the computational domain used to run computational fluid dynamics (CFD) simulations. The domain used for simulations is 2D axisymmetric, where the line of symmetry is the x-axis. For cruise conditions, the selected altitude is 3000m where the static pressure is 70,120 Pa and the static temperature is 279 K. At the inlet (red line), total inlet quantities are imposed. At cruise, the desired flight speed for this application is Mach 0.9, so using isentropic flow equations the total pressure and total temperature are applied at the inlet as follows in Equation (3-8):

$$\frac{P}{P_0} = f_2(M_{in}) = \left(1 + \frac{\gamma - 1}{2} M^2\right)^{\frac{\gamma}{\gamma - 1}} \tag{3-8}$$

so $P_0 = \frac{P}{f_2(M_{in})}$ where P is simply the static pressure at 3000 meters. The total temperature is imposed similarly using Equation (3-9):

$$\frac{T}{T_0} = f_3(M_{in}) = \left(1 + \frac{\gamma - 1}{2}M^2\right)^{-1} \tag{3-9}$$

so $T_0 = \frac{T}{f_3(M_{in})}$ where T is the static temperature at 3000 meters. The inlet conditions are imposed upstream of the intake to avoid artificially imposing the Mach number at the inlet of intake. This is done because Klein showed that diffuser performance depends on inlet conditions, so imposing the inlet conditions upstream of the intake prevents artificially imposing diffuser performance [31]. Additionally, this allows for the streamline curvature to be solved for by the numerical solver, allowing for better resolution of the boundary layer and separation within the intake.
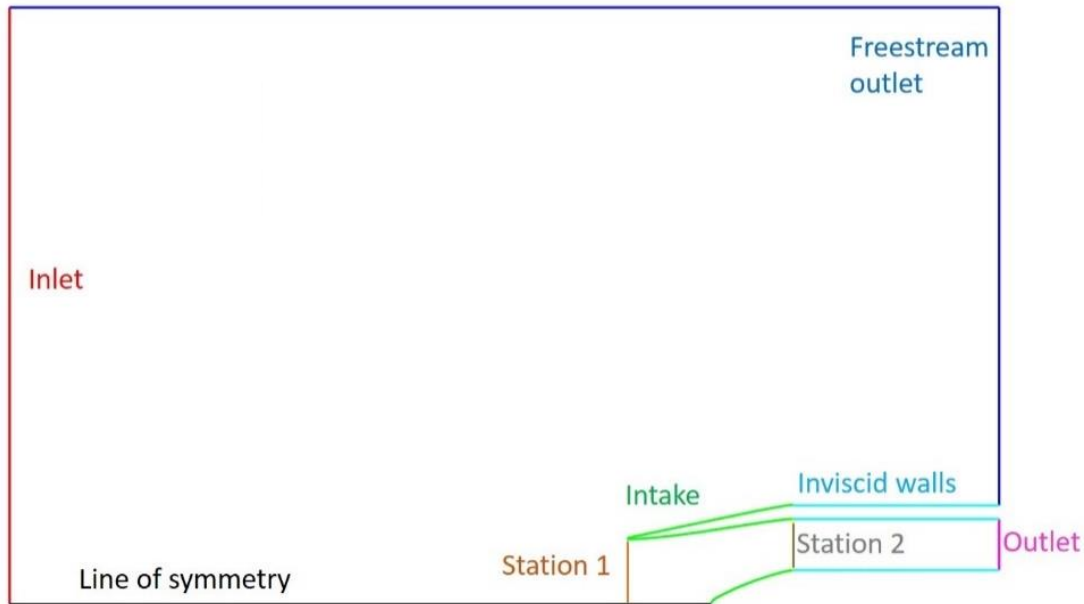
Figure 3-2: Computational domain for intake analysis.

The green lines represent the intake geometry that is parametrized and generated in MATLAB. These walls are solved as adiabatic viscous walls in the numerical simulations. The dark blue lines represent domain outlets, where the freestream static pressure is imposed. The gray line shows the end of the physical intake. This line represents where station 2 quantities are extracted, such as total pressure and Mach number at the intake outlet. However, the domain is

extended beyond this point so that nothing needs to be imposed at the actual outlet of the intake. Inviscid walls (turquoise) are used to extend the domain past the physical intake. The inviscid walls extend the domain, so that the imposed downstream boundary condition does not arbitrarily impose non-physical phenomena at the end of the intake. At the outlet downstream of the intake a static outlet back pressure is imposed based on the desired Mach number by the downstream fan. This back pressure is used to simulate the pressure from the fan. The back pressure is imposed using Equation (3-10) with the total pressure at the inlet:

$$P_{static,outlet} = f_2(M_{out}) * P_{0,freestream} \qquad (3\text{-}10)$$

The imposition of the back pressure in this manner imposes a Mach number at the outlet of the domain. Because of this, the outlet Mach number of the intake (at the gray line) does not vary significantly in the different simulations performed. Rather, the inlet Mach number for the physical intake (Mach number at the start of the green curves) varies from case to case. It is for this reason that the diffusion achieved by the intake is measured in terms of M_1 and M_2 instead of just M_2. The relevant flow quantities, such as outlet total pressure and outlet Mach number are extracted at station 2. Inlet quantities for the intake are extracted at station 1, not the inlet of the domain. This analysis allows for proper analysis of the intake's performance.

In ICEM, a structured mesh for each intake geometry is created. To ensure that the boundary layer is accurately captured, the y+ is maintained below 0.7 along the diffuser and cone walls. The mesh is then imported into CFD++ where the flow field is resolved using RANS simulations and the k-omega-SST turbulence model. The turbulence model is chosen based on the work of Andersen [32].

To ensure grid insensitivity, a mesh sensitivity study is run according based on the methods established by Celik [43]. The grid size is increased in every direction by a factor of 1.1 between each case. For each different mesh, relevant aerodynamic parameters such as massflow through the intake, total pressure loss, and outlet Mach number are compared to ensure a large enough mesh is used. The results of the grid sensitivity are shown below in Figure 3-3, with a final grid size of 87k being selected. The results show that by a grid size of 87,000, all relevant parameters have converged and increasing the mesh size doesn't impact the CFD results. This analysis ensures that the grid being used to analyze different intakes is large enough to properly resolve intake performance.
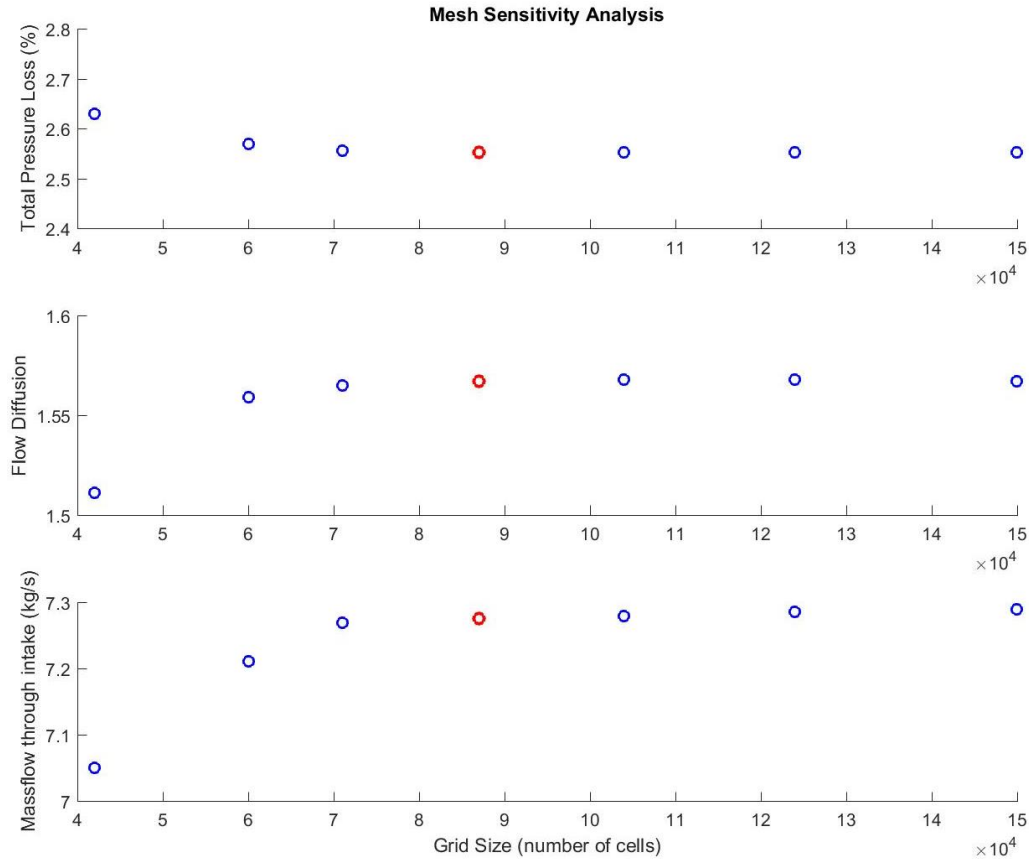
Figure 3-3: Mesh sensitivity study. Top to bottom: pressure losses, flow diffusion, massflow.

3.3: Sizing Intakes for High Speed Flights

To understand intake behavior at high speeds, the performance of several different engine intake designs was evaluated in the computational domain defined above. Before optimizing the geometry for aerodynamic parameters, the effect of inlet lips and intake length is evaluated. These evaluations are used to determine an appropriate length for the engine intake taking into consideration size and weight constraints. Once the lips and length of the engine intake are fixed, an aerodynamic optimization is performed on the intake geometry to investigate methods to minimize pressure losses and flow distortion while maximizing diffusion. These optimizations are used to generate a family of related designs that can be used to guide designer's in how to create intake geometries for compact, high-speed applications.

3.3.1: Lip Design for Intakes

A crucial step in designing intakes is the design of the inlet lips. Inlet lips are often parametrized according the super ellipse equation shown below. Additionally, the equations for relevant geometric parameters of the inlet lips are described below by Equations (3-11) through (3-13). A full description of these equations is found in section 1.2.1.

$$\left(\frac{x}{a}\right)^p + \left(\frac{y}{b}\right)^q = 1 \tag{3-11}$$

$$Fineness\ ratio = \frac{a}{b} \tag{3-12}$$

$$Contraction\ ratio = \frac{A_{hl}}{A_t} = \frac{r_{hl}^2}{r_t^2} = \frac{(r_t + b)^2}{r_t^2} \tag{3-13}$$

Important parameters for the superellipse include the fineness ratio (which is defined as the ratio of the major to minor chords of the ellipse) and the contraction ratio (which defines the ratio of area contraction achieved by the lips). According to Albers and Miller [15-16], to maintain good off-design performance the contraction ratio needs to be maintained below 1.38. Additionally, in their work they found that the optimal value for the exponents in the super ellipse and the fineness ratio is near a value of 2. To simplify the analysis of the inlet lips, the equation will be simplified to that of an ellipse (p=q=2) which is near the optimal value for the exponents found by Albers and Miller.

With the lips defined as an ellipse, the next step is to determine the desired fineness ratio of the lips. Fineness ratios between 1 and 10 are evaluated for flow distortion to determine an optimal fineness ratio for the lips. The diffuser geometry was kept constant in this case, with a length of 20 cm. The fan cone was neglected to amplify the effects of different lip geometries on intake performance. Figure 3-4 below shows the results for 5 different fineness ratios (with a contraction ratio of 1.2), where the outlet Mach number distributions are compared. The goal of this analysis is to select a lip shape that produces the least amount of flow distortion (lip shape had negligible effects on pressure losses and total diffusion in this study). The figures show that as the fineness ratio decreases, the flow distortion at the outlet is decreased. The lips serve to compress the flow, and a smaller fineness ratio results in a shorter lip, and therefore a more aggressive compression of the flow before the diffuser geometry starts. This flow compression

serves to keep the flow more attached as it travels through the intake, and thus, especially for cases where aggressive diffusion is required, it is best to design intake lips with small fineness ratios. As a result, a fineness ratio of 2 is selected for the intake and used throughout the rest of the analysis. Appendix A shows the radial distributions of the outlet Mach number for 3 selected cases to show the radial flow distortion for the different cases.
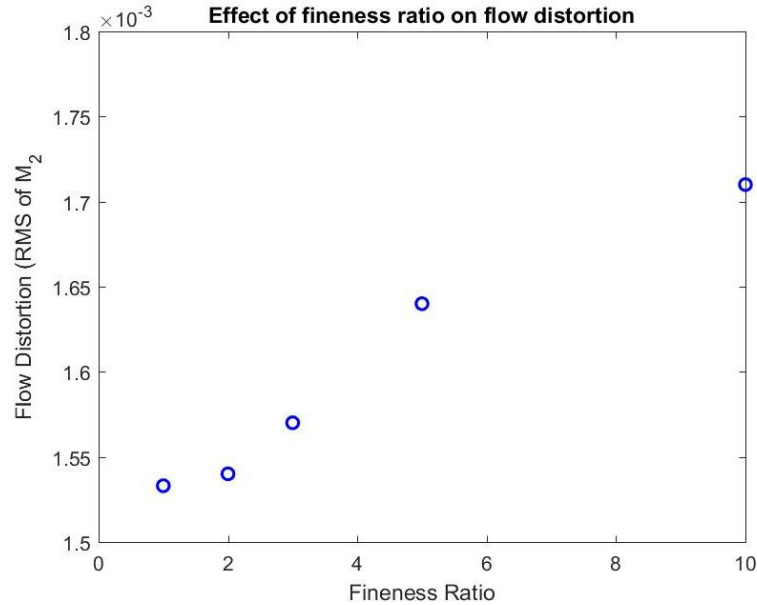
Figure 3-4: Effect of fineness ratio on intake flow distortion.

Contraction ratios between 1.1 and 1.4 are considered, with a fineness ratio of 2 applied to the inlet lips. The results in terms of outlet flow distortion are shown in Figure 3-5 below. As suggested by [17], larger contraction ratios tend to perform better at design points, while smaller ones perform better at off-design. Because larger contraction ratios tend to add more momentum to the flow, increasing the contraction ratio tends to help in preventing separation. However, at off-design conditions, when streamline curvature becomes more extreme, it is preferable to have less aggressive curvature in the intake. Because the off-design conditions for a UAV mission can be rather extreme, minimizing the contraction ratio is favorable. The results show that there is a dramatic drop-off in performance below a ratio of 1.2, so this is chosen as the ratio for the intake.
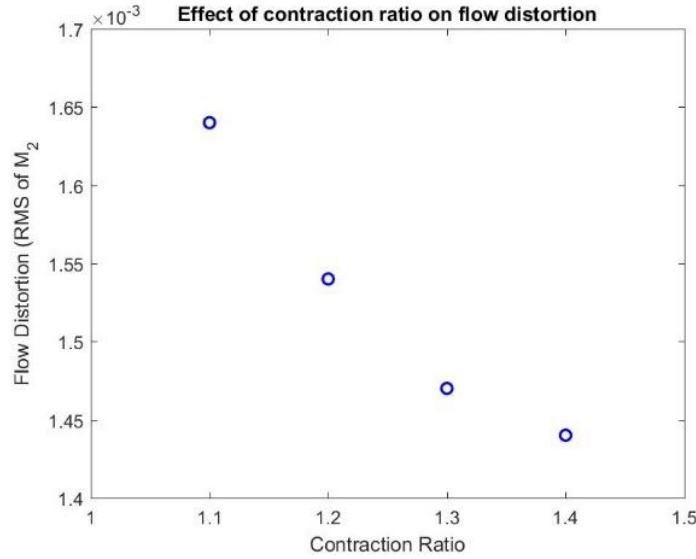
Figure 3-5: Effect of contraction ratio on intake performance.

For high subsonic speed flights, it has been shown that minimizing the fineness ratio improves flow distortion performance. The effects of the fineness ratio on total pressure losses and diffusion are mostly negligible (see Appendix A). Increasing the contraction ratio leads to improved performance in terms of flow distortion (and negligible reduction in pressure losses). However, because many applications for high-speed compact engine intakes requires robust off-design performance, the contraction ratio is kept small based off literature recommendations. Moving forward in the design of the intake, the lip geometry is parametrized as an ellipse with a fineness ratio of 2 and contraction ratio of 1.2.
Figure

3.3.2: Effects of Intake Length on High Speed Performance

The next step is to determine an appropriate length for the intake. Previous studies have applied Equation (3-14) to determining a reasonable size for intake length:

$$\frac{A_2}{A_1} = 1 + \frac{2L\sin(\theta_{avg})}{L_{ref}}$$

(3-14)

where the angle refers to the overall half angle of the diffuser [18]. The average angle of diffusion for a symmetric annular diffuser can be approximated in terms of the inlet and outlet radius and the intake length, which leads to Equation (3-15):

$$\frac{A_2}{A_1} = 1 + \frac{2L(r_2 - r_1)}{L_{ref}\sqrt{L^2 + (r_2 - r_1)^2}} \tag{3-15}$$

In the case of the present design, where the area ratio is fixed, the parameters A_2, A_1, r_2 and r_1 are all known. The radii represent the radius of diffuser inner walls, while the areas represent the inlet and outlet area for the annular intake. The reference length that is typically chosen for axisymmetric diffusers is simply the inlet radius. However, since a fan cone will also be used in the intake, the reference length definition is modified to account for the presence of the cone. The new reference length is defined in Equation (3-16).

$$L_{ref} = \frac{r_1 + (r_2 + r_{2,cone})}{2} \tag{3-16}$$

Here the cone radius represents the outlet cone radius, which is defined by the fan downstream of the intake. Using this definition of the reference length and plugging in the known parameters for area and radii, the approximate required length of the intake is 21 cm. Below this threshold, Kline [18-19] predicts that the intake will stall. This analysis does not extend into the high subsonic speed regime and does not account for optimized geometries.

To extend the analysis to high-speed, compact engine intakes, intakes with lengths varying from 15 cm to 30 cm are parametrized, and the effect of the length on relevant flow quantities such as flow distortion, diffusion, and total pressure losses is analyzed. The aspect ratio of the diffuser is stretched from case to case, so the local angle of curvature of 30cm case is exactly half the local angle of curvature of the 15 cm case. Each case uses the same fan cone geometry.

Each geometry is then evaluated for total pressure losses, flow distortion, and diffusive capabilities. Results are shown below in Figure 3-6 and Table 3-1, where intake axial length is plotted against the relevant flow quantities. In selecting the final length of the intake, there are a couple different factors that are considered. As the length is increased, the frictional effects of the intake are also increased, which plays a role in the pressure losses. Increasing the length allows for less extreme and more favorable curvatures in the diffuser, but these gains are offset by increased frictional losses. This can be seen in the figures below, where the flow distortion parameter does not significantly improve past a length of 20 cm. Figure 3-6a the total pressure losses as a function of length, where from 17.5 cm to 20 cm there is nearly a 7% decrease in the pressure losses. However, increasing the length past 20 cm leads to reduced reduction in pressure

losses, as increasing the length from 25 cm to 30 cm only reduces the pressure losses by 2%. A similar trend can be seen in Figure 3-6b where there is an 9% improvement in the diffusive capabilities when increasing the length from 17.5 cm to 20 cm, but just a 2% gain in diffusion when increasing the length from 20 to 25 cm.
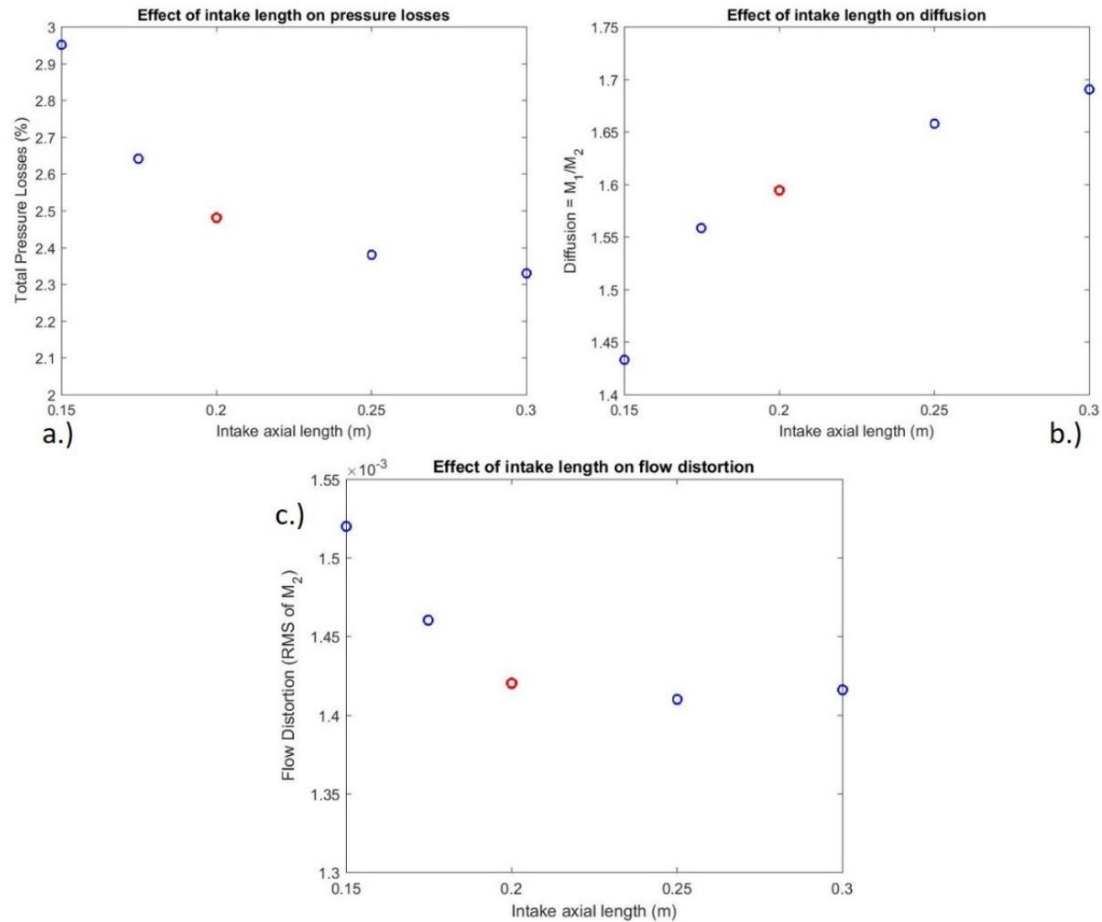
Figure 3-6: Effect of intake length on performance.

Table 3-1: Effect of intake length on performance.

Length (cm)	Pressure Loss (%)	Diffusion = $\frac{M_1}{M_2}$	Flow Distortion
15	2.95	1.43	0.00152
17.5	2.64	1.56	0.00146
20	2.48	1.59	0.00142
25	2.38	1.66	0.00141
30	2.33	1.69	0.00142

Increasing the intake length beyond 20 cm provides minimal performance enhancement. Furthermore, increasing the length of the intake leads to other penalties in the overall engine

performance, such as increased weight. From an overall engine perspective, minimizing weight of the intake leads to improved engine performance. Going from an intake length of 20 to 25 cm results in weight increasing by approximately 25% which dwarfs the enhancements in pressure recovery, diffusion, and flow distortion. Therefore, a length of 20 cm is selected to balance the aerodynamic performance of the intake with a desire for minimal inlet weight.

An intake length of 20 cm offers reduced weight relative to longer designs, while offering potential for optimizations of the diffuser and cone geometry to further improve aerodynamic performance. To determine the appropriate length of a high-speed engine intake, the equations set forth by Kline [18] offer a simple, quick, and accurate method to determine the necessary length. To reduce the length beyond this point, analysis of the intake in terms of diffusion and pressure losses can be conducted. However, due to the potential for intake stalling at off-design, care should be taken when shortening the intake length beyond the limit established by Kline. In this case, the intake length is shortened by less than 5% of what is suggested by Kline.

3.3.3: Validation of 2D Approach

The analysis done thus far has been in a simplified 2D, axisymmetric domain rather than a full 3D domain, as suggested by Andersen [32]. Before optimizing the intake geometry, it is important to verify that the 2D axisymmetric domain accurately reflects the full 3D physics. This is done by simply creating a 3D computational domain with the same boundary conditions and comparing the 2D and 3D results. The flow diffusion, pressure loss, and flow distortion parameters match to 2 significant figures as shown in Table 3-2 below. The radial profiles at the outlet of the intakes also compare well, as seen by the flow distortion matching within 0.2%. Based on this comparison, optimizations of the intake geometry will take place using a 2D axisymmetric domain, which greatly reduces the computational time of simulations.

Table 3-2: Comparison of 2D axisymmetric to 3D results.

Parameter	2D results	3D results
Flow Diffusion $= \dfrac{M_1}{M_2}$	1.59270	1.59271
Total Pressure Loss (%)	2.4831	2.4830
Flow Distortion	0.001425	0.001421

3.4: Aerodynamic Optimization of Intake at High Speeds

Now with geometric parameters such as intake length and lip geometry determined, geometric effects of diffuser and cone design on intake performance is investigated to create optimal intake geometries. For high speed flight one of the most relevant flow quantities is total pressure loss through the intake. Minimal total pressure losses ensure that the downstream components can operate at design conditions during cruise and allows the turbine to extract maximal power. Flow diffusion is also a relevant aerodynamic parameter for high speed cruise operation. The turbofan downstream of the intake operates best at a speed well below the cruise speed, so the intake must be capable of diffusing the flow to a desired Mach number. The equations used to define these parameters are defined by equations 3-3 and 3-4.

These flow quantities are driven by different geometric parameters. Pressure losses are primarily driven by separation phenomena, which is primarily driven by local curvature of the diffuser. Diffusion performance, while coupled to separation phenomena, is primarily driven by the respective area diffusion achieved by the diffuser and cone, which is controlled by boundary layer development [17]. To investigate intake designs that simultaneously achieve optimal performance in both aerodynamic parameters, a differential optimization used to minimize pressure losses and maximize flow diffusion is performed.

3.4.1: Optimization Set-Up

As in the preceding analysis of the intake, the intake geometry is parametrized in MATLAB using Bezier curves. The number of Bezier control points controlling the intake geometry is reduced to 7. This reduces the number of free parameters in the optimization and more directly impact the intake geometry by varying each control point. Figure 3-7 below shows the updated parametrization of the intake. Red points reflect design parameters that are varied radially by the optimizer, whereas blue points represent fixed points that are used to control the area ratio. The lip shape also remains fixed in these simulations and is not depicted in the figure. The 7 varying control points (4 for the diffuser, 3 for the cone) represent the free parameters in the optimization. The optimization methodology and routine are fully discussed in Chapter 1.4 and revisited in Chapter 2.1.
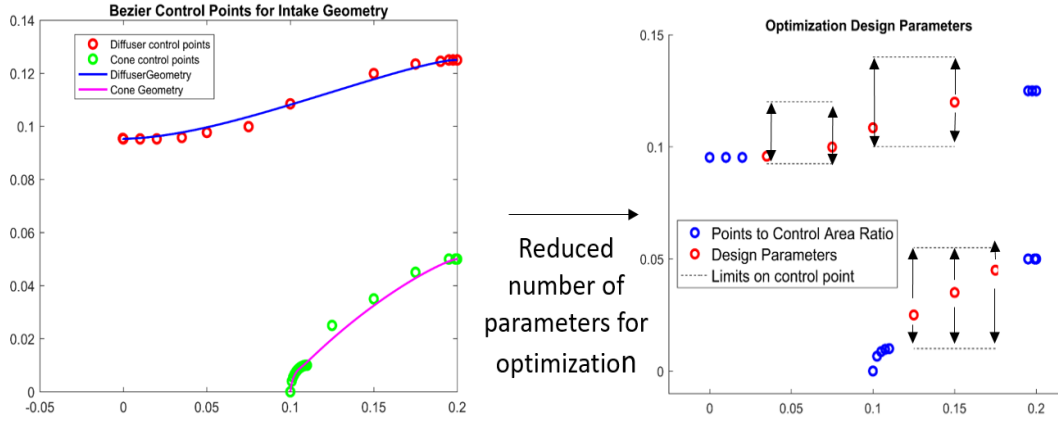
Figure 3-7: Reduced intake parametrization for optimization.

3.4.2: DoE Results and Discussion

An initial design of experiments is performed with 128 individuals evaluated to observe the extremes for each free parameter. The DOE results are shown below in Figure 3-8, where the x-axis represents the pressure losses as a percent, the y-axis represents the flow diffusion, and the contour represents various quantities. In these figures, the goal is to minimize pressure losses and maximize flow diffusion, so designs in the upper left quadrant of the graph represent designs with optimal performance.
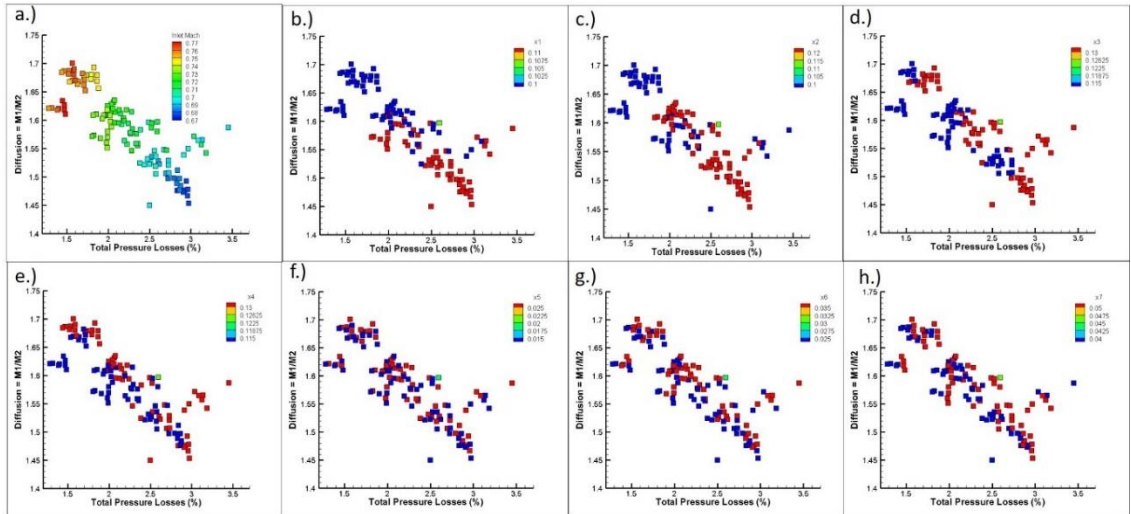
Figure 3-8: DoE results.

In Figure 3-8the contour represents inlet Mach number at the beginning of the intake (station 1). The station 2 Mach number is primarily controlled by the static back pressure

imposed at the domain's outlet. As a result, M_2 does not vary as much as M_1 from design to design, and it is necessary to calculate the ratio of M_1 to M_2 to determine flow diffusion performance. The contour does show a direct relationship between flow diffusion and inlet Mach number; however, the parameters are perfectly related as can be seen by the fact that there are cases with M_1=0.77 that achieve less diffusion than cases with an M_1=0.74. For a more detailed analysis of the relationship between M_1 and flow diffusion, please see the Appendix B.

From Figure 3-8b-h the effects of the different geometric parameters on intake performance can be seen. Parameters x_1-x_4 represent the control points for the diffuser, sorted by axial location. Similarly, parameters x_5-x_7 represent the control points for the cone geometry. Figure 3-8b-c show that the performance of the intake is related almost directly to the initial opening of the intake. The red points show control points that cause a large local curvature early in the diffuser geometry. Parameters x_1 and x_2 occur before the cone, so by opening the diffuser early in the intake geometry there is a clear penalty in the achievable flow diffusion and pressure recovery. Figure 3-8c-h show that the remaining geometric parameters lead to a variety of performances, depending on the values of x_1 and x_2.

The figures show a large spread in pressure losses and flow diffusion performance of various intakes. The DOE shows that the free parameters x_1 and x_2 appear to be directly related to intake performance. As a result, when launching the optimization, the allowable range in the x_1 and x_2 parameters is reduced, to allow the optimizer to better optimize the other geometric parameters. Then, the initial population size was trimmed down to 80 from 128, as shown below, and the optimization routine is launched.
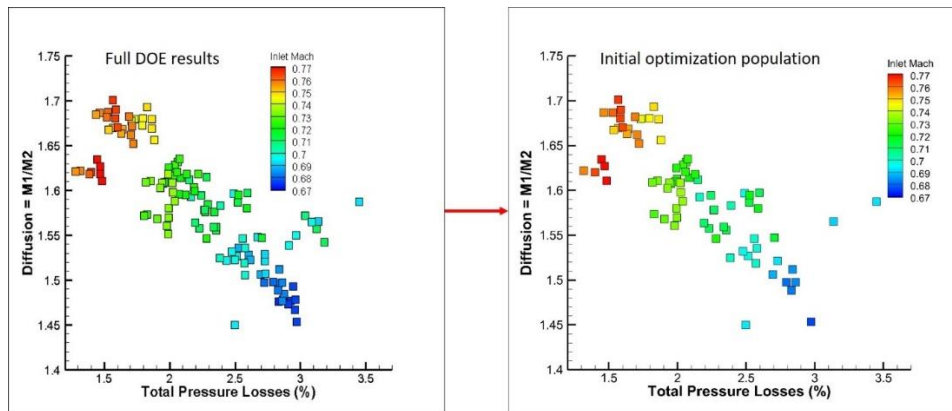
Figure 3-9: Reduction of DoE.

3.4.3: Optimization Results and Discussion

The optimization routine is launched to minimize pressure losses and minimize $\frac{M_2}{M_1}$ (which will maximize flow diffusion). The optimization is run over 25 populations, each with 40 individuals. Overall 1000 different individuals are evaluated by the optimizer. The full optimization results are shown below in Figure 3-10, where the x-axis again represents total pressure losses (%), y-axis is the flow diffusion, and the contours represents the inlet Mach number (left) and flow distortion (right). The results show a reduction in pressure losses by over one percentage-point and increase in flow diffusion of over 10% from the DoE.
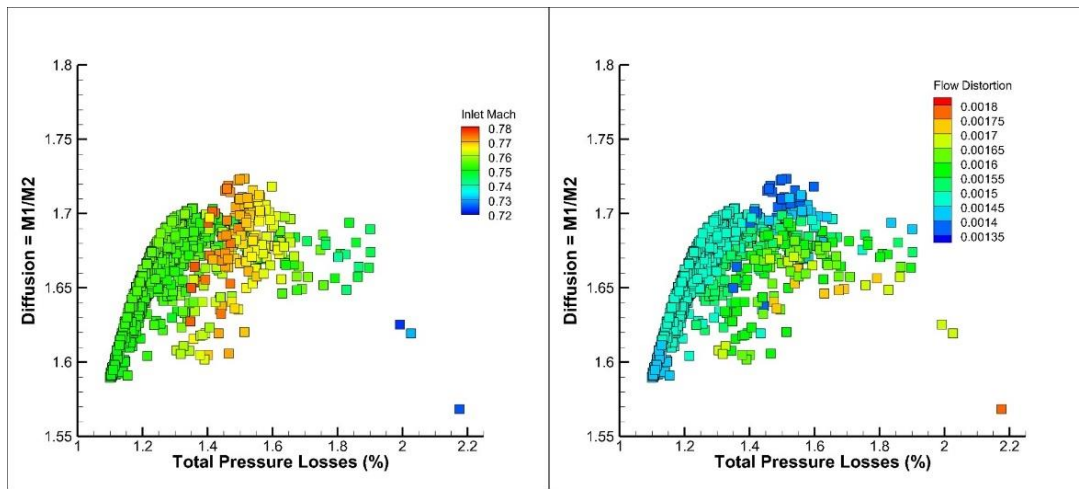
Figure 3-10: Optimization results.

Figure 3-11 below show how various free parameters effect performance of the intake. Free parameters x_3-x_6 are charted to show how the second half of the diffuser geometry and the first half of the cone geometry effects intake performance.
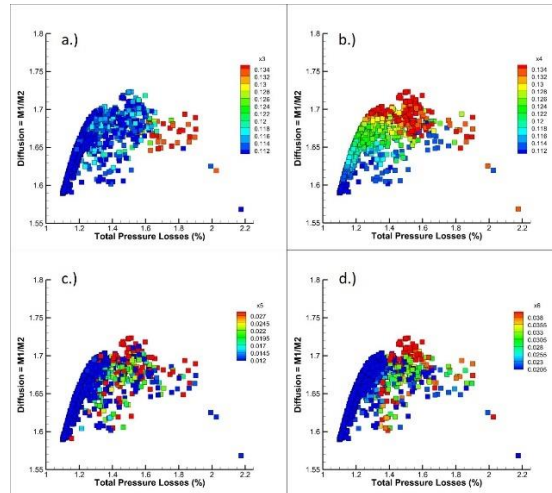
Figure 3-11: Effect of select free parameters on intake performance.

Figure 3-11b shows that increasing the value of x_4 (final radial location of the diffuser) leads to enhanced flow diffusion, but also increases pressure losses. This is due to the sudden curvature increase caused by large values of x_4 creating some separation towards the end of the intake. This leads to pressure losses in the intake. Flow diffusion, on the hand, is enhanced by this sudden increase since there is a rapid area change near the outlet, allowing for a reduction in outlet Mach number. The relationship between x_4, M_2, and pressure losses are shown more clearly below in Figure 3-12.
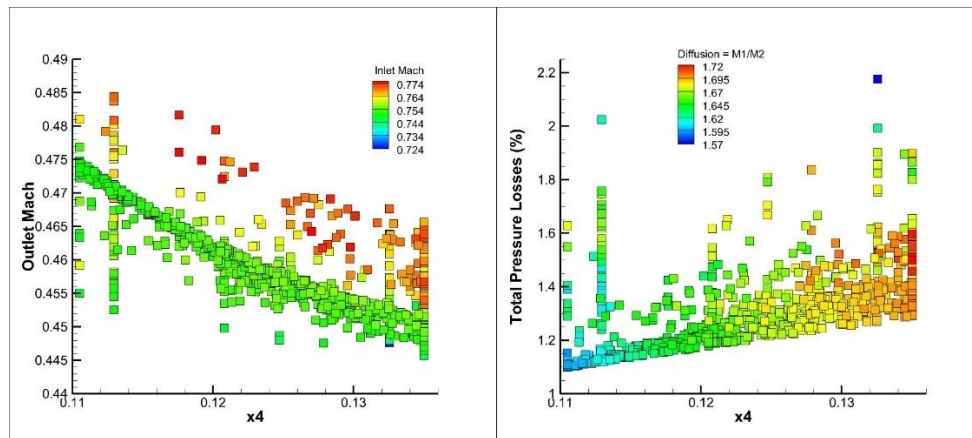
Figure 3-12: Optimization results for M_2 vs x_4 vs total pressure losses.

The linear relationship between x4 and the outlet Mach number is depicted here and holds for most designs. Additionally, the contour, representing the inlet Mach number, shows that there is no significant relationship between the inlet Mach number and parameter x4. This

helps explain how along the pareto front, there is a group of intake curves that see an enhanced flow diffusion performance caused by reduction in M_2 without significantly impacting M_1. This means increasing x4 enhances flow diffusion. However, Figure 3-12 (right) shows that the opposite is true for pressure losses. In general, increasing x_4 enhances pressure losses.

3.4.4: Investigation along Pareto Front

To fully understand the design implications revealed by the optimization, the effects of free parameters on intake performance are investigated along the pareto front. The pareto front represents a region of the plots along which any increase in the performance of one objective (pressure losses or flow diffusion) negatively impacts the performance of the other objective. The results along the pareto front are shown below, where the contour represents the inlet Mach number. The pareto front represents a region where the flow diffusion increases from 1.56 u to 1.73 (over a 10% increase in the diffusive abilities) while the pressure losses range from 1.15% up to 1.6%. The pareto front shows a much larger increase in flow diffusion performance relative to total pressure losses, implying that unless there is a significant constraint on the pressure loss performance, it is ideal to choose a design towards the upper region of the pareto front. The baseline geometries that were analyzed had pressure losses of roughly 2.5% and flow diffusion values of 1.55. This optimization allows for the pressure losses to be cut in half, and for the flow diffusion performance to be improved by over 10% over baseline geometries. The pareto front is shown below in Figure 3-13. The left figure shows the contour of the inlet Mach number, whereas the right contour shows the flow distortion. Along the pareto, there is a direct relationship between diffusion and flow distortion (improving diffusion also improves flow distortion).
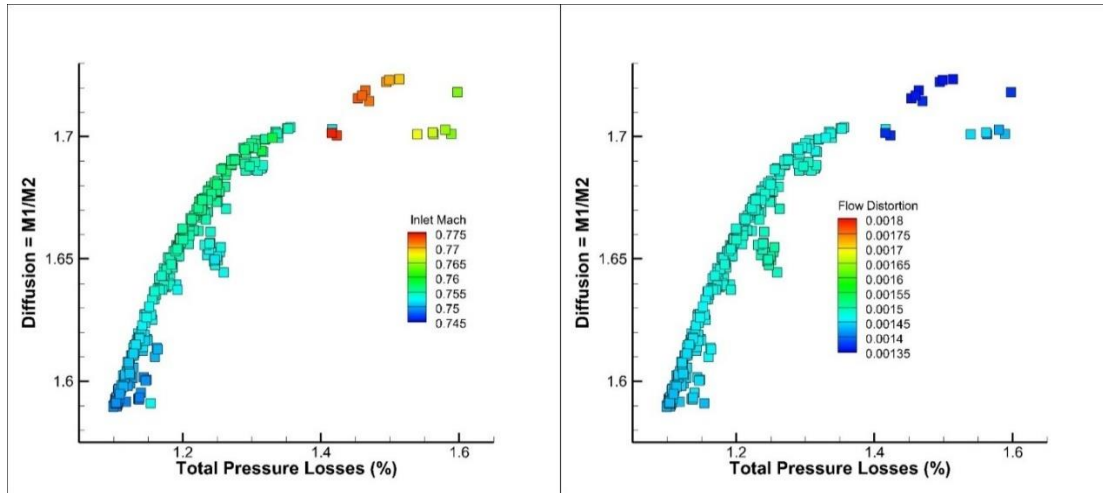
Figure 3-13: Pareto front from optimization.

Along the pareto front, the free parameters with the greatest impact are x_3-x_5, depicted below in Figure 3-14. X_3 and x_4 represent the control points of the diffuser geometry in the second half of the diffuser, once the cone geometry begins. Parameter x_5 represents the first control point of the cone, which helps determine how aggressive the contraction due to the cone will be. In each case, increasing the radial location of the control point leads to increased diffusive capabilities, while reducing the control point radial location reduces pressure losses. These figures can be used to set design bounds for control points in future compact engine intake designs, so that a full optimization does not need to be performed; however, to fully understand how to design optimal engine intakes, other geometric parameters need to be considered.
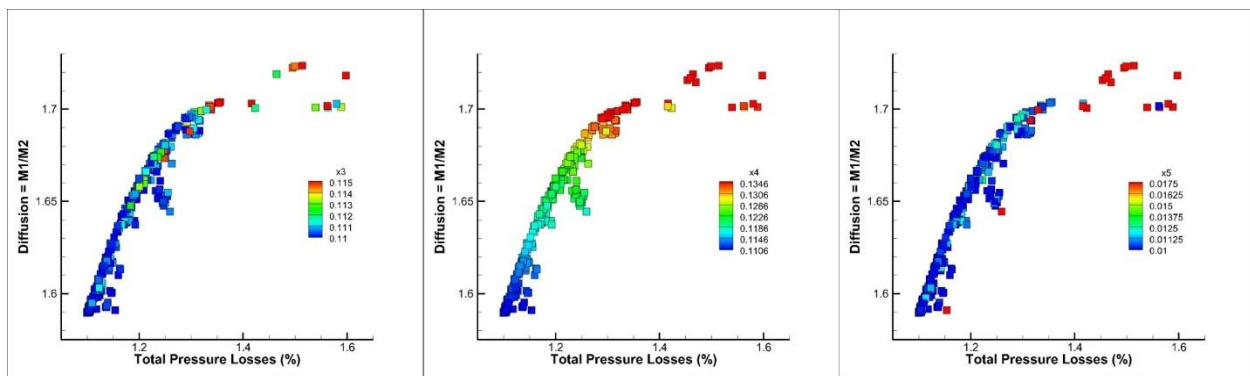
Figure 3-14: Effect of free parameters along pareto front.

The intake geometry is dependent on each free parameter, so solely varying one will not dramatically affect the performance, since the Bezier curve generating the intake geometry

depends on each control point. To more clearly show how to design compact engine intakes for high-speed cruise flight, the first derivative of the diffuser (which drives local separation phenomena) and the area ratio of the intake (which drives diffusion) needs to be evaluated. Five cases along the pareto front are selected and geometrically shown below. The performance of each case is also summarized in Table 3-3 below.
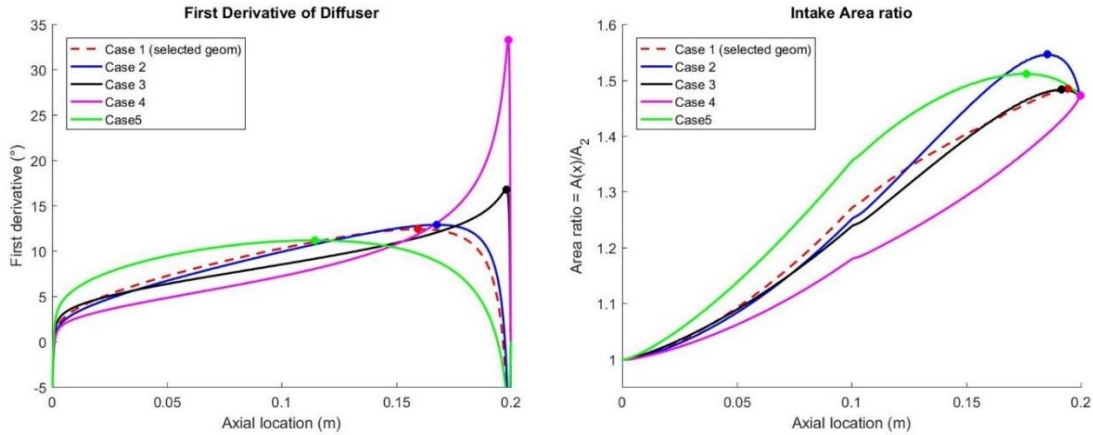
Figure 3-15: Geometric comparison of 5 cases along the pareto front.

Table 3-3: Results along pareto front.

Case	Flow Diffusion	M_1	% Pressure Loss	Flow Distortion
1	1.72	0.77	1.50%	1.36e-3
2	1.69	0.76	1.29%	1.47e-3
3	1.66	0.75	1.30%	1.51e-3
4	1.59	0.75	1.15%	1.43e-3
5	1.71	0.76	1.62%	1.44e-3

The figure also depicts the location of the peaks in first derivative of the diffuser and overall area ratio. Comparing cases 1 and 2, the first derivatives of the diffuser are roughly identical, however the aerodynamic performance of the two cases differs. Looking at Figure 3-15(right) the differences in performance can be attributed to the difference in cone geometry (seen by the difference in area ratio in the second half of the intake). This implies that having an area compression near the outlet of the intake, achieved by aggressively contracting the cone wall near the outlet, leads to decreased pressure losses. Comparing cases 1 and 2 to cases 3 and

4, the primary geometric difference is that cases 1 and 2 have lower values of peak curvature whereas cases 3 and 4 have higher peaks that are very close to the outlet. This shows that keeping the max first derivative value around 10-15° while shifting the peak away from the outlet increases the diffusive ability of the intake. However, this occurs at a cost in the pressure losses. Shifting the peak too far away from the outlet, as in case 5, results in significant pressure loss penalties, while no gain occurs in flow diffusion.

Based on the data presented in Table 3-3 above and in the figures, to optimize for flow diffusion and pressure losses, a moderate peak angle of curvature near 75% of the axial span is required. Shifting the peak away from the outlet in small amounts will improve flow diffusion a small amount while incurring pressure losses. Shifting the peak towards the outlet on the other hand, leads to moderate reduction in pressure losses at the cost of flow diffusion. Based Figure 3-15(left), it is clear that a zone of area compression near the end of the intake leads to reduction in pressure losses as nearly all optimized geometries have a compression zone near the intake outlet. Figure 3-16 below shows the normalized shear stress plots for each of the 5 cases to further investigate the differences between each geometry.
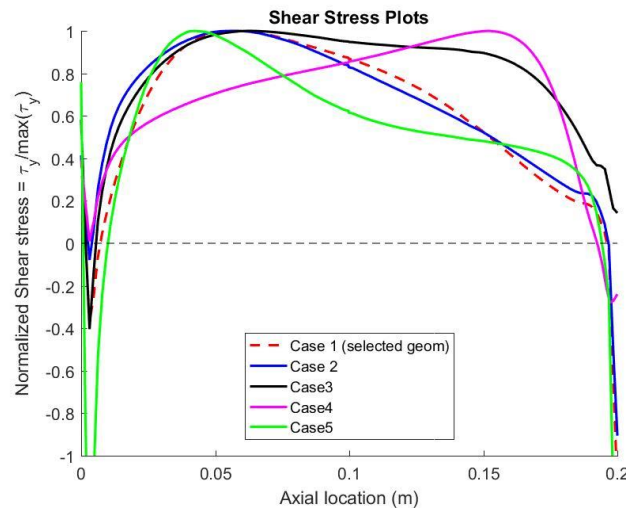
Figure 3-16: Shear stress comparison of cases along the pareto front.

Here cases 3 and 4 show that they are the least likely cases to separate. This is due to the peak curvature being pushed to the outlet of the intake. With small curvatures until the very end of the intake, the flow is unlikely to separate, and only separates in case 4 due to a radically large peak angle of curvature. To minimize separation phenomena the peak angle should kept below 20° and shifted near the outlet. Cases 2-4, which have the lowest values in pressure losses, are

the cases with maximal diffuser opening in the presence of the cone. This can be seen in Figure 3-15(left) by looking at the area under the diffuser derivative curve. This implies that aggressive curvature diffusion in the presence of the cone results in cases that are less likely to separate and as a result have lower pressure losses. However, this is balanced by the already discussed need to shift the peak in curvature away from the outlet, which results in geometries with less diffuser opening in the presence of the cone. Reducing the diffuser opening allows for increased flight speed, and increased flow diffusion.

Case 1 is chosen as the final optimized geometry due to its high diffusive capability relative to other optimized geometries. The pressure loss difference between case 1 and the lowest pressure loss case is 0.35%; while the gain in diffusion is over 10%. Considering the relatively large gain in diffusion, Case 1 is selected as the final geometry. The geometry for case one is shown below, as well as the Mach number contour for the case in Figure 3-17.
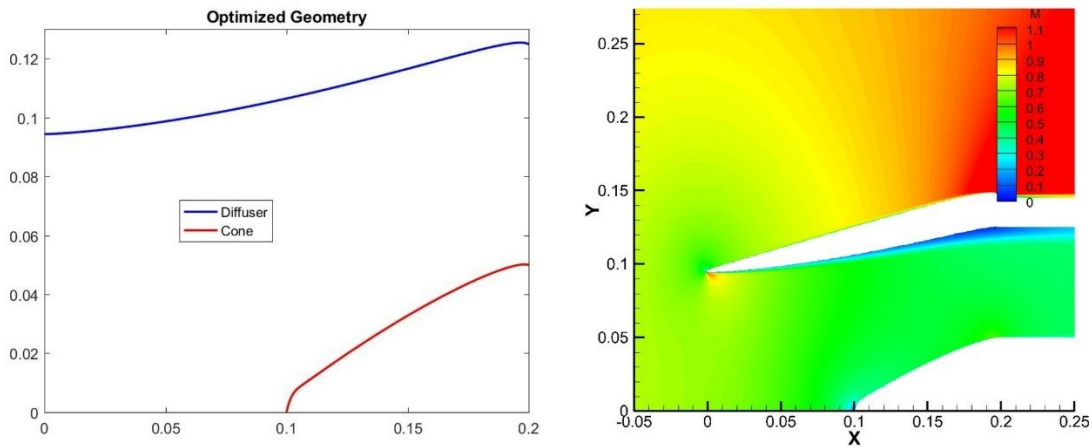
Figure 3-17: Optimized geometry. Left shows the parametrized geometry, right shows the Mach number contour.

3.4.5: Variable Area Analysis

To validate the fixing of the area ratio in the intake analysis, a new DoE is performed, adding the inlet area of the intake as a free parameter. This allows the DOE to vary the area ratio of the intake to assess whether increasing the area ratio (allowing for increased diffusion) or decreasing the area ratio (which will help reduce the pressure losses) is possible. This analysis is done considering the already constrained length and outlet radius. The results from the DoE are shown below in Figure 3-18.
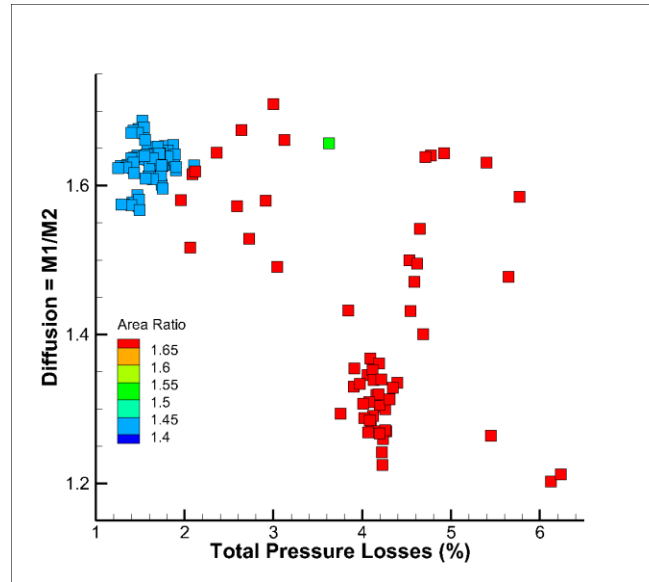
Figure 3-18: DoE for variable area ratio geometries.

It is clear from the DOE that increasing the area ratio beyond 1.45 in order to achieve more diffusion results in intake designs that are infeasible. This is primarily due to large curvatures found in the intake, causing separation which increases the total pressure losses and significantly reduces the achievable flight speed. Going back to equation 10 in section 3.3.2, the reason becomes clear: to achieve an area ratio of 1.65, the necessary length is much greater than 20 cm. The only way to improve the flow diffusion performance would be to increase the length of the intake, which results in significant weight increases. Designers of engine intakes must be aware of this trade-off; the optimized results shown here can only be improved by increasing the length of the intake and doing so would incur other engine penalties.

3.4.6: Design Recommendations for Compact, High-Speed Intakes

To design an optimal, compact, engine intake first the design constraints need to be defined; in this case the outlet area ratio as well as the desired cruise flight speed, and desired outlet speed. Then the design of the inlet lips should be considered, with Fineness ratios near 2 and contraction ratios near 1.2 being found suitable for this application. Then the intake length should be selected by the designer, considering the study conducted by Albers and Miller [15]. It was found that by redefining the reference length for turbofan engines, their results can be extended into the high-speed turbofan domain. Finally, to design an optimal intake geometry, the design of the diffuser and cone walls needs to be considered. The results of the optimization

performed above suggests there are some contradicting geometric parameters for optimal intake designs. To reduce pressure losses and separation, a compression zone near the outlet of the intake is desirable. Along these lines, it is desirable to have a somewhat large peak in curvature (15-20°) near the outlet (at greater than 90% of the axial span). Pushing the peak value above this value induces separation and results in increased pressure losses. To improve flow diffusion a smaller peak curvature (closer to 10-15°) that is close to 75% of the axial span is desired. This helps minimize boundary layer development at the outlet, which increases the area for diffusion. Shifting the peak curvature in further upstream in the intake design will lead to small increases in flow diffusion with penalties in pressure losses. And reducing the peak location past 70% of the axial span results in no performance gains as both flow diffusion and pressure losses are penalized. So, to design an optimal, compact engine intake for a particular diffuser length, with the cone length set to 50% of diffuser length, the following design criteria should be considered:

1. Peak angle of curvature of roughly 15° (between 12-15°)
2. Peak angle of curvature occurring near 75% of diffuser axial span, or 50% of cone axial span (between 70-75% axial span of diffuser)
3. An area compression zone near the outlet to help reduce separation and minimize pressure losses (obtained through aggressive cone compression near the domain outlet as well as the diffuser itself compressing the flow)
   o The area compression should not happen before 90% of the axial diffuser span
4. Inlet lips designed elliptically, with a fineness ratio near 2 and a contraction ratio near 1.2
5. Intake length sized according to the following criteria:

   o $\frac{A_2}{A_1} = 1 + \frac{2L(r_2 - r_1)}{L_{ref}\sqrt{L^2 + (r_2 - r_1)^2}}$

   o $L_{ref} = \frac{r_1 + (r_2 + r_{2,cone})}{2}$

These design recommendations are made for cases in which minimizing pressure losses and maximizing flow diffusion are the primary aerodynamic objectives.

3.5: Validation of Design Recommendations

To ensure that the above design recommendations are in fact suitable for different applications, the design recommendations will be applied to a different set of conditions. To

ensure that the design meets necessary criteria, the pressure losses must be kept below 1.75%
(max value of the pareto front for the previous application). The new design will be for an intake
operating in at a speed of Mach0.75 rather than Mach0.9. This is selected because most subsonic
applications will not operate so close to the sonic point. Additionally, the outlet radius
constrained to be 0.15m rather than 0.125m to assess the design recommendations for slightly
large intakes. Because the diffusion required in this case is smaller than the diffusion required in
the previous case, the flow diffusion parameter will be scaled according to Equation (3-17):

$$Corrected\ Flow\ Diffusion\ = \frac{M_{domain,outlet}}{M_{domain,inlet}} * \frac{M_1}{M_2} \tag{3-17}$$

where the domain values help normalize the flow diffusion. The domain values are those
imposed in the simulations by the boundary conditions. For the inlet of the domain these values
are M0.9 in the normal case and M0.75 in the validation case. The outlet Mach number is set
using isentropic flow equations as a function $P_{0,inlet}$ and $P_{s,outlet}$ and is imposed to M0.45 in both
the original simulations and in the validation case. The optimized geometries achieved corrected
flow diffusion between 0.8 and 0.85, so the validation design should have a value above 0.8.

Based on the isentropic area ratio equations discussed previously, the area ratio for the
intake is 1.37. Then using equations 10 and 11, the length of the intake is determined to be 0.15
m (with the cone radius maintained at 0.05m). The inlet lips used in the previous design are
maintained and applied to this design. Next the geometry is parametrized in MATLAB according
to design recommendations 1-3 above. The intake geometry is displayed below in Figure 3-19.
The peak angle of curvature is 14.7° occurring at roughly 70% of the diffuser axial span. The
area compression near the outlet of the intake can be seen.
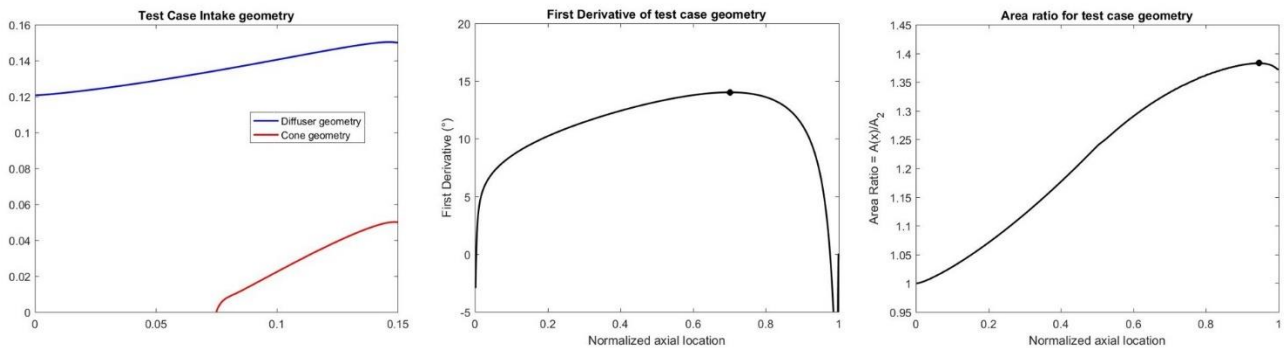
Figure 3-19: Test case geometry.

Just as in the previous simulations, the intake is meshed in ICEM with a y+<0.7 and simulated in CFD++. The boundary conditions for the case are set up using the same approach as before. The domain inlet is set up for M0.75, the area ratio for the intake is designed to diffuse flow to M0.45, and the domain outlet is set to obtain M0.45. The results are summarized below, with the table showing the performance of the new test case against results from the pareto front from the optimization. Figure 3-20(left) shows the Mach number contour for the intake at cruise conditions, where qualitatively the results are similar to the optimized geometry results shown in Figure 3-17. Figure 3-20 (right) compares the shear stress distributions of the original optimized design and the test case. There is more separation in the test case, however the separation occurs early in the geometry and just like in the optimized case, reattachment occurs within 10% of the axial span.

Table 3-4 compares the test case against cases along the pareto front. The corrected flow diffusion is similar to the values found along the original pareto front, as are the total pressure losses and the flow distortion values. The design recommendations posted above will hold across a wide range of high subsonic speed compact engine intake design problems.
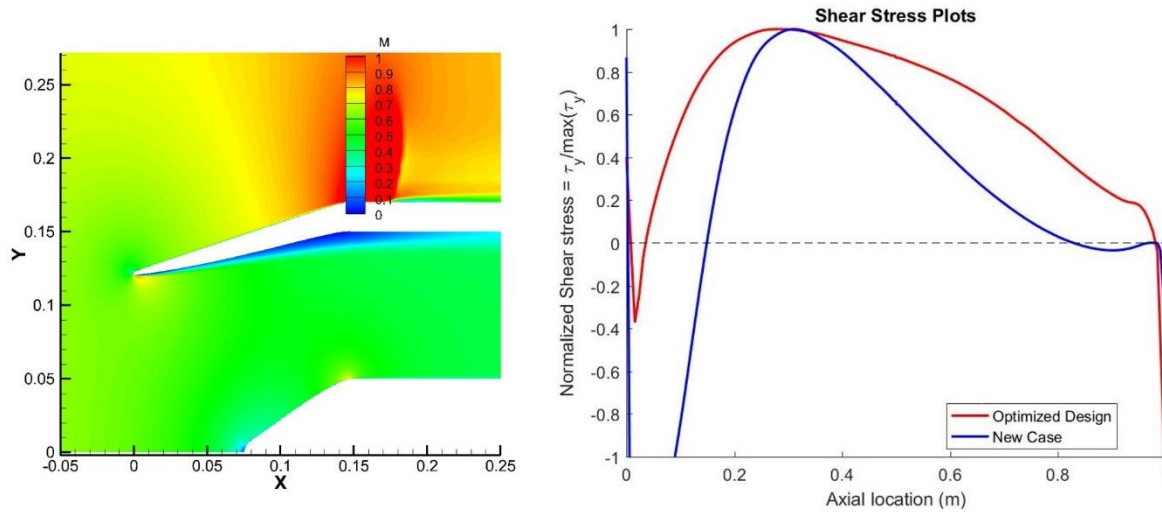
Figure 3-20: Results for the new test case. Contour and shear stress comparisons shown.

Table 3-4: Comparison of new test case to pareto front.

Case	Flow Diffusion	Corrected Flow Diffusion	% Pressure Loss	Flow Distortion
1	1.72	0.86	1.50%	1.36e-3
2	1.69	0.85	1.29%	1.47e-3
3	1.66	0.83	1.30%	1.51e-3
4	1.59	0.80	1.15%	1.43e-3
5	1.71	0.86	1.62%	1.44e-3
New Case	1.35	0.81	1.23%	1.25e-3

3.6: Summary of Aerodynamic Investigation

In this chapter, a methodology for designing engine intakes for high-speed cruise flight based on aerodynamics was presented. The design methodology is summarized by the flow chart below, which starts by determining the intake size. The size of the intake can be reduced from what is found in literature based on optimal engine intake design. Then the inlet lips must be designed keeping in mind the application. For applications where off-design performance is important, the literature suggests maintaining low contraction ratios (below 1.36) and a fineness ratio of 2. In this chapter, the contraction ratio was set to 1.2 to enhance off-design performance, and a fineness ratio of 2 was chosen.
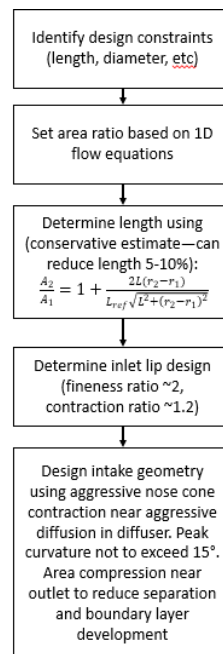
Figure 3-21: High subsonic speed engine intake design methodology.

Results from the high-speed optimization reveal that the intake geometry can be parametrized and created using a Bezier curve while ensuring a maximum angle of curvature between 10-15° while keeping the peak curvature value in regions with aggressive cone contractions. This helps adjust streamline curvature and minimize pressure losses. Furthermore, an area contraction near the outlet of the intake helps to minimize boundary layer development and increase flow diffusion performance. The flow distortion parameter was shown to be related to the diffusive capability of the intake, so maximizing intake geometries for diffusive capability also minimizes flow distortion in the outlet of the intake. The primary phenomena driving intake performance are boundary layer development and separation. Separated, or detached flow, leads to larger pressure losses. Furthermore, the true flow area is reduced, which results in reduction in diffusive capabilities. Designing intakes to minimize boundary layer development will results in optimal intake performance.

CHAPTER 4 : ASSESSMENT AND ENHANCEMENT OF INTAKE PERFORMANCE DURING TAKEOFF OPERATION

Optimizing engine intakes for aerodynamic performance at cruise conditions is just one piece of the design puzzle. Future high-speed engine intakes must be capable of operating at a variety of conditions. Takeoff conditions represent the opposite end of the spectrum in terms of intake performance; while at cruise conditions the focus is on delivering uniform flow with minimal losses at an appropriate speed, takeoff performance is generally driven by the amount of massflow ingested. Massflow ingestion is typically a cycle requirement given by downstream engine components. During takeoff for turbofan applications, the flight speed is 0, which means that all air ingested is due to fan suction. This often creates an aerodynamic challenge for the engine intake which manifests in terms of large separation bubbles due to increased capture area at takeoff. In this chapter, the limitations at takeoff of a compact intake capable of large flow diffusion will be investigated, and solutions to the issues will be proposed.

4.1: Aerodynamic Tradeoffs between Cruise and Takeoff

Engine cycle requirements are the primary driver behind takeoff design requirements. As an example, in the turbofan engine that the optimized intake is being applied to, takeoff requirements for the engine are 6.7 kg/s. Compact high-speed engine inlets need to have a large outlet to inlet area ratio to effectively diffuse flow, must have a small outlet area to maintain compactness, and must have relatively aggressive diffuser curvatures to remain compact. These design constraints lead to intake designs with small inlet areas that are sensitive to separation at off-design conditions.

Many future applications of these engine intakes will be in turbofan applications where large amounts of power (and therefore massflow) are required at takeoff. Due to the small inlet areas, there is a limited amount of massflow that can pass through compact engine intakes with large area ratios. Furthermore, at takeoff, where flow is ingested through fan suction, the capture area of the intake increases, leading to aggressive streamline curvature. High speed intakes are already sensitive to separation issues, and the increased capture area exacerbates this issue;

ultimately leading to poor takeoff performance. To illustrate this, the optimized geometry for cruise conditions is evaluated at takeoff conditions.

4.1.1 Takeoff Computational Domain

The computational domain is set up similar to the cruise simulations. The same mesh as in the cruise simulations is used. The inlet total quantities are simply atmospheric conditions, while the static pressures applied to the freestream outlets are also atmospheric (P=101325 Pa, T = 293K). The back pressure applied to the outlet downstream of the intake is determined by suction created by the fan. For takeoff conditions this boundary condition is dictated by the fan design, and in this application can range from 75000-85000 Pa.

Due to high levels of separation, the takeoff optimization does not converge well as a steady simulation. The simulations are run for 5000 iterations before global convergence is achieved, and the global residuals are low (below 1E-5). This is demonstrated below in Figure 4-1 where the residual plot for a steady takeoff simulation is shown. In the first 2000 iterations the solver has trouble accurately resolving the flowfield, showing that for takeoff simulations extra iterations are required. Once the solver does start to achieve convergence, flow quantities such as massflow, total pressure losses, and surface static pressure distribution.
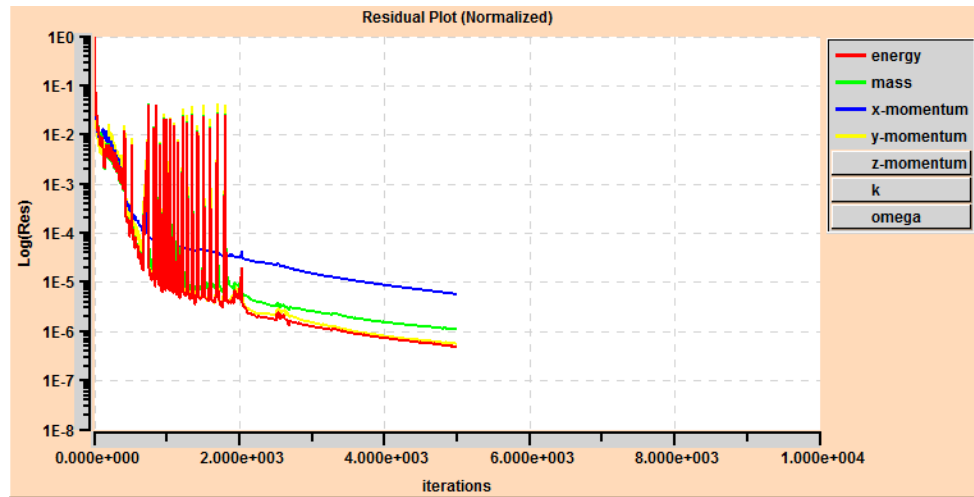
Figure 4-1: Convergence history for takeoff simulations.

4.1.2: Assessment of Optimized Geometry at Takeoff Conditions

Figure 4-2 below shows the performance of the optimized geometry at takeoff conditions for back pressures ranging from 85,000Pa down to 75,000 Pa. It is clear from these figures that massive separation occurs at takeoff. Decreasing the fan back pressure leads to negligible reductions in the separation bubble as illustrated by Figure 4-2 a-c below. However, the increased suction by the fan does manage to improve the acceleration of the flow in the intake. Carefully looking at the streamlines (taken at the same upstream location), it is clear that reducing the back pressure allows for more flow to enter intake. The massflow with a back pressure of 85,000 simulations is 3.59 kg/s; and improves to 4.37 kg/s when the pressure is reduced to 75,000 Pa. This is well short of the takeoff requirement of 6.7 kg/s that this particular intake is being applied too. To ensure that the takeoff performance of the intake will be adequate, the extreme condition, where the suction due to the fan is 85,000Pa will be considered moving forward to assess the full range of intake operation.

a.) (85000 Pa) b.) (80000 Pa) c.) (75000 Pa)
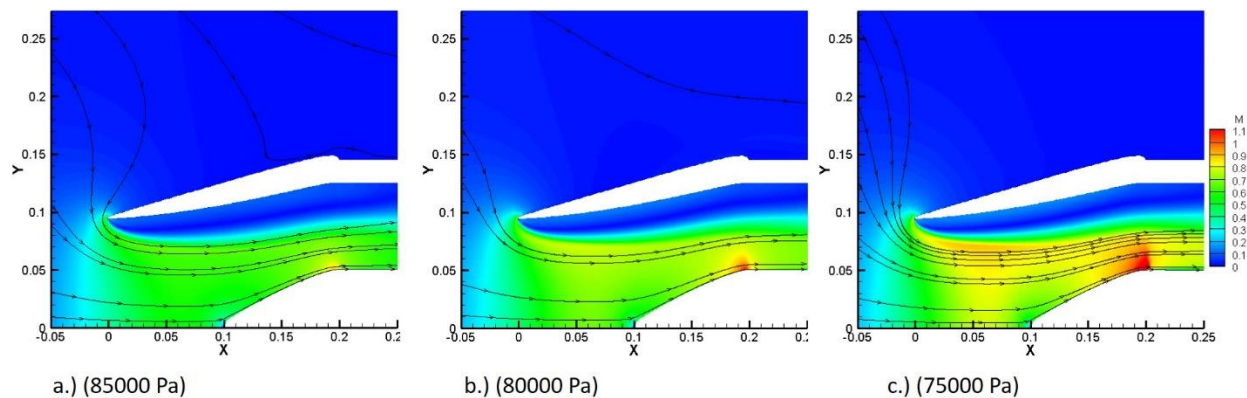
Figure 4-2: Mach number contours for optimized geometry at takeoff.

As mentioned previously, the cause for this separation is the difference in capture area and streamline curvature between cruise and takeoff conditions. Figure 4-3 below illustrates the difference in capture area between cruise and takeoff conditions. The increased capture area at takeoff is caused by fan suction which needs to suck in large quantities of air. This leads to flow entering the intake at extreme angles, causing separation. This separation dramatically reduces the effective area of the intake, which negates is ability to ingest large massflows. The streamlines shown in the figure below are taken at the same locations at the inlet of the domain.
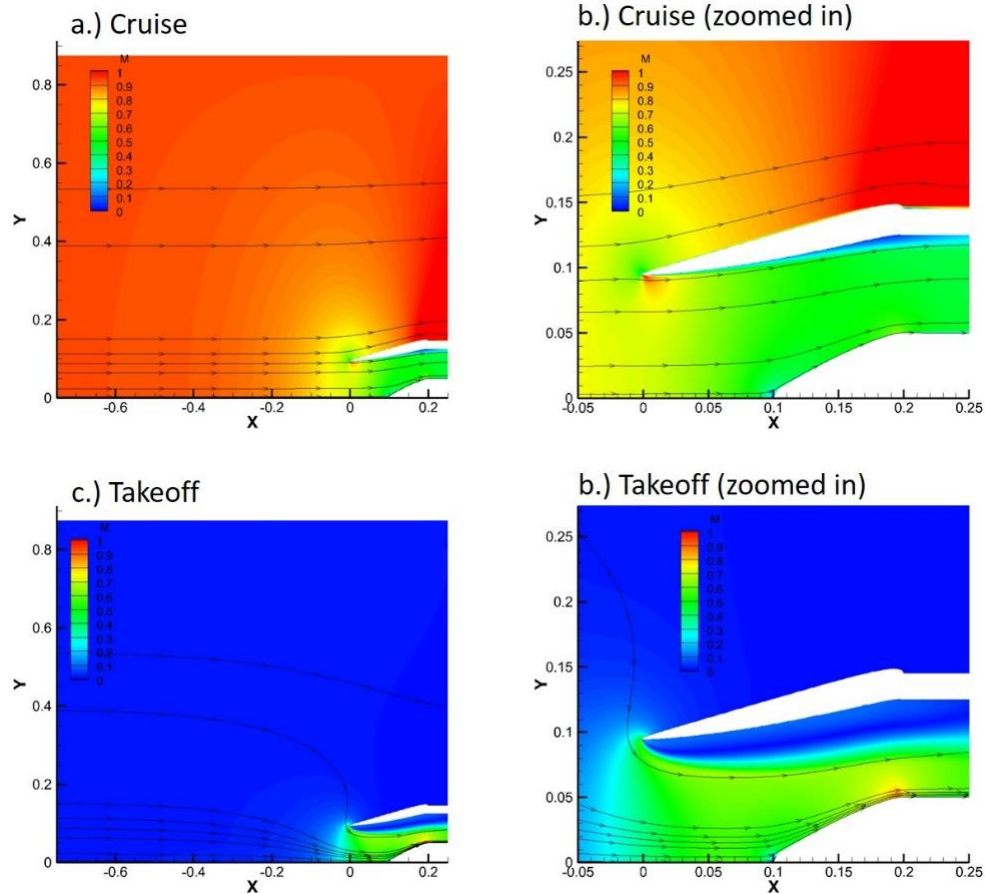
Figure 4-3: Comparison of capture area between cruise and takeoff.

Cruise operation is vital to intake performance; however, takeoff operation is an aerodynamically separate challenge that also needs to be addressed for engine intake design. Cruise performance often dictates engine operability since it effects mission duration, mission length, and fuel consumption. Therefore, methods to improve takeoff performance need to be developed so that future engine intake design can focus on optimal cruise performance without being hampered by takeoff constraints.

4.2: Variable Area Intake for Takeoff

In cases where drastic improvements of takeoff performance are required, a variable area intake design may be suitable. By designing an intake with a variable geometry, the inlet area can be increased, leading to increased massflow ingestion at takeoff conditions. To demonstrate

this, a design of experiments is launched with the inlet area being an added parameter (similar to section 3.5). The intake area ratio varies from 1.1 to 1.5, and the results are shown in Figure 4-4.
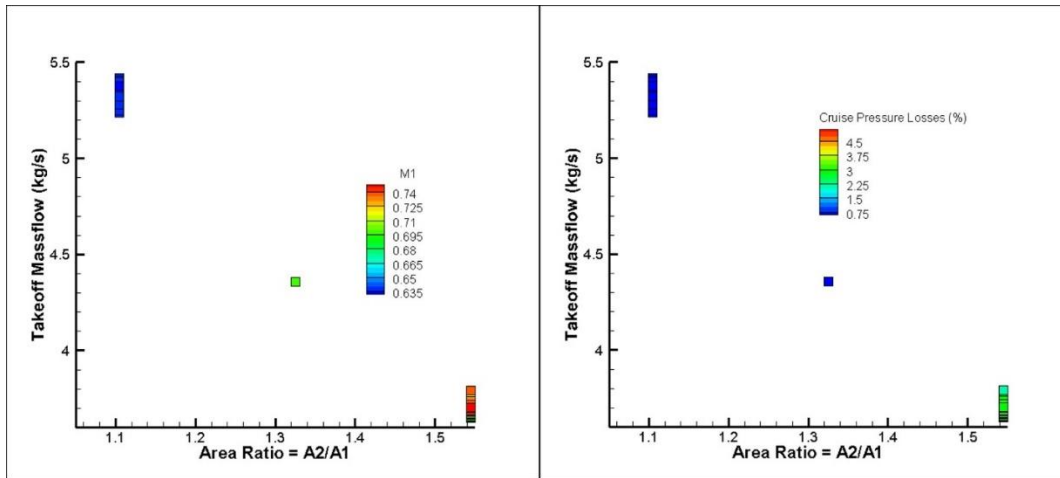
Figure 4-4:Effect of area ratio on takeoff massflow.

The relationship between the inlet area (controlled by area ratio) and massflow at takeoff is clearly shown. Additionally, the sacrifices involved with increasing the inlet area can be seen by looking at the contours. Increasing the inlet area leads to increased pressure losses (right) and decreased flow speed (left) at the inlet of the intake during cruise operation. The increased pressure losses (increased by a factor of 2) would lead to a decrease in engine performance at cruise conditions. Additionally, the reduced inlet speed shows that for the fan to operate at optimal conditions, the maximum inlet speed achievable by the intake at cruise conditions is greatly reduced. The optimal Mach number for cruise conditions is reduced by over 15% in increasing the potential massflow that can be passed at takeoff. Further complicating the issue, the massflow requirement was still not met despite the reduced intake area ratio and inlet speed. These results establish the need to design a variable intake geometry to avoid designing an intake that operates optimally only at cruise or takeoff conditions.

4.2.1: Variable Area Intake Optimization Set-Up

To design a variable area intake, the second half of the engine intake will be kept constant. Then the front half of the engine intake can be designed out of a flexible material or in a manner that allows for the geometry to be varied. An optimization routine is performed,

considering only the front half of the diffuser geometry to be variable. The new parametrization is shown below in Figure 4-5. Seven parameters are used to vary the front part of the diffuser geometry using a Bezier curve. The first 3 control points are controlled by the area ratio parameter, which set the overall area ratio (first 3 points all have the same radial location). The next 6 control points are used to create the rest of the diffuser geometry, with reducing amounts of freedom to force the curve to form with the second half of the diffuser.
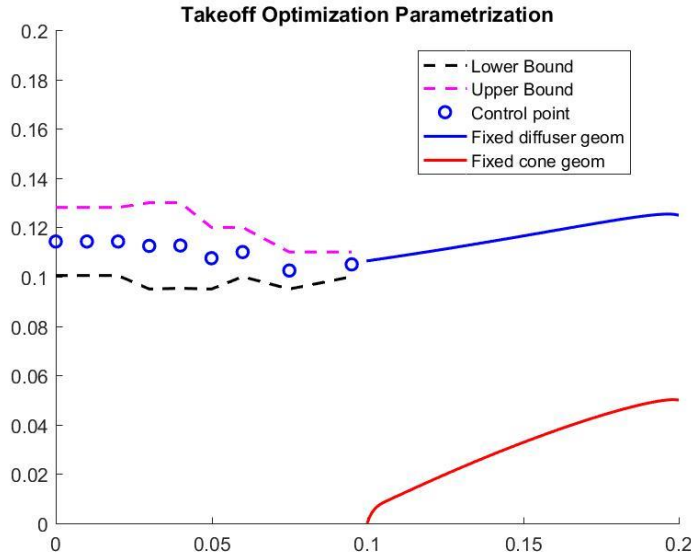
Figure 4-5: Geometric parametrization for variable geometry intake optimization.

4.2.2: Optimization Results

The goal of the optimization is to maximize the massflow ingested at takeoff conditions while minimizing the amount of geometric change required. The geometry change is simply measured by the radial change in intake position required at each point along the intake curve. The equation defining the radial change is defined below in Equation (4-1).

$$Radial\ change = \frac{\sum abs(R_{new} - R_{orig})}{\sum R_{orig}} * 100 \qquad (4\text{-}1)$$

This is a simple metric used to compute the feasibility of intake design. Large geometry changes will require the front half of the intake to be designed out of a highly flexible material capable of adopting different shapes. The more the intake geometry changes, the more difficult it will be to design such an intake with reliable accuracy. This is a significant concern for cruise conditions.

The optimization results are shown in Figure 4-6. The result of the optimization shows that a large change in intake geometry is required for the intake to ingest enough massflow. Furthermore, the optimization results show that increasing massflow is directly related to the inlet area of the intake, and that the radial change of the intake parameter is simply a byproduct of the inlet area varying. This is clearly shown by the left image where the contour represents the intake area ratio.
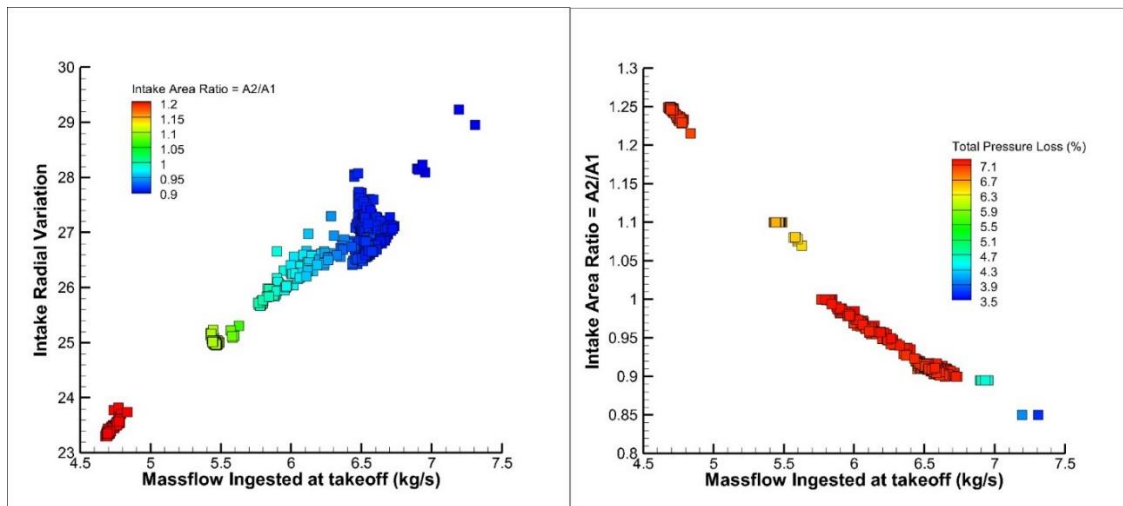
Figure 4-6: Takeoff optimization to minimize geometric change and maximize massflow.

The contour in the right figure reveals that the pressure losses at takeoff conditions are not directly related to the massflow ingested. The plot reveals drastically increased pressure losses during takeoff operation, but there are cases with a total pressure loss of ~6% that ingest only 5 kg/s while geometries with a pressure loss of 7% are capable of ingesting 6.5 kg/s. To assess the viability of a variable geometry diffuser, an individual design that passes the required 6.7 kg/s with the least amount of radial variation is chosen. This design is then superimposed on top of the original optimized geometry and shown below in Figure 4-7a. Figure 4-7b shows the Mach number contour of the takeoff geometry. Due to the streamline curvature, there is initially separation in the intake. However, the front half of the intake geometry at takeoff acts to compress the flow, which helps the flow reattach. The takeoff geometry then has two benefits: not only is the intake area increased, allowing for more massflow to enter, but also, the separation bubble is reduced, further increasing the massflow suction possible at takeoff conditions.
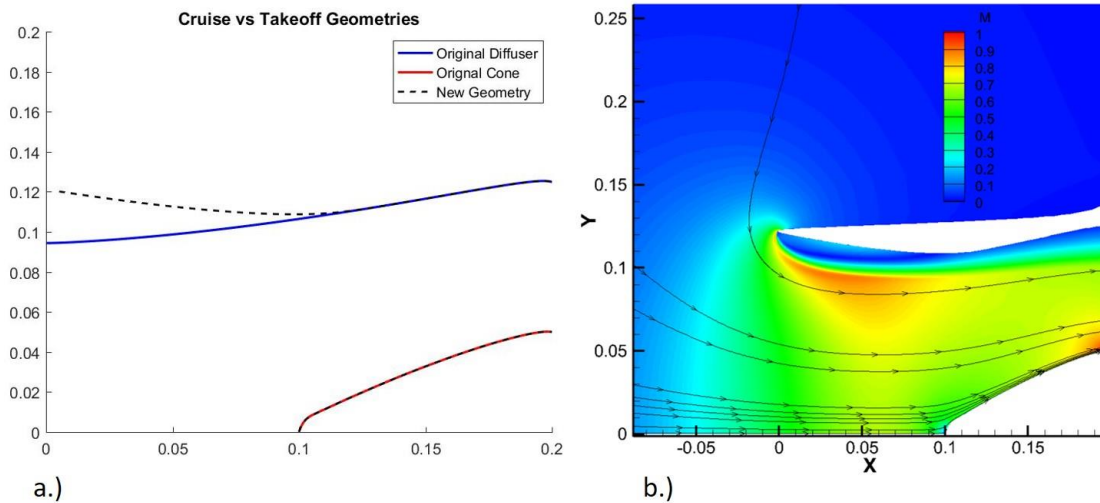
Figure 4-7: Variable intake geometry and Mach number contour.

4.2.3: Methods to Design a Variable Intake Geometry

Mechanically designing a variable geometry intake is a challenge unto itself. There are two potential methods to design an intake that can vary from the blue curve to the dashed one as shown above in Figure 4-7a. The first method is to design the front half of the intake out of a flexible material, and then placing a ring in the front half of the intake. During cruise conditions the ring will contract to decrease the inlet area and bring the diffuser to the optimized shape from Chapter 3. Meanwhile, during takeoff operation, the ring will expand to increase the inlet area and create an initial compression region to help reattach flow. The ring will only need to actuate half of the diffuser geometry, simplifying the design a bit. However, this solution could lead to issues in terms of repeatability of compressing the diffuser to the cruise geometry. This could lead to issues with attaining the optimized performance at cruise conditions. Similar solutions have been explored for future hypersonic applications [44].

A second method to varying the intake geometry is to design the front half of the diffuser in a chainmail-like manner. This allows for the geometry to be easily adjusted from configuration to configuration and opens avenues for variable geometries during ascent, descent, or even loiter operations as well. Designing part of the intake in this manner allows for the intake geometry to be variable to a large degree. The chainmail-like idea can best be visualized by imagining a series of metal pieces hinged to one another. This allows each part of the intake to move relative to the next part of the intake, allowing for a geometry that can be varied greatly.

4.3: Alternate Methods to Enhance Takeoff Performance

Designing variable area intakes represent a significant challenge. As discussed in the previous section, the design either requires a flexible material to be used or a complex chain-mail like design. In many cases, these methods will not be necessary. Rather only small increases in takeoff performance may be required. There are several potential ways to increase the massflow ingested at takeoff conditions that are far simpler than designing a variable geometry intake. Some of these methods are briefly explored here.

4.3.1: Sliding Nacelle

Sliding the intake diffuser, or nacelle, extends the length of the intake. Doing so gives the flow increased distance to diffuse, which can help to reduce the separation bubble and increase the massflow ingested. To evaluate this, the diffuser of the intake is shifted upstream 4cm, with a wall extending the intake. Appendix C shows gives more details on what the transformed geometry looks like. Figure 4-8 shows the results of this geometry, with the massflow ingested decreasing slightly to 3.58 kg/s. When the back pressure is reduced to 75,000 Pa the massflow is 4.33kg/s. Sliding the intake diffuser resulted in small penalties in intake performance. The separation bubble is shown to increase in size, resulting is small decreases in massflow ingested. This is due to increased frictional effects caused by lengthening the diffuser by sliding it upstream. Furthermore, the contraction by the cone is now shifted further downstream from the inlet lips, causing decreased intake performance. The most aggressive diffusive portions of the diffuser are now shifted further away from the cone, which increases separation and reduces massflow ingestion. Rather than sliding the nacelle, it seems logical that sliding the cone could result in improved takeoff performance.
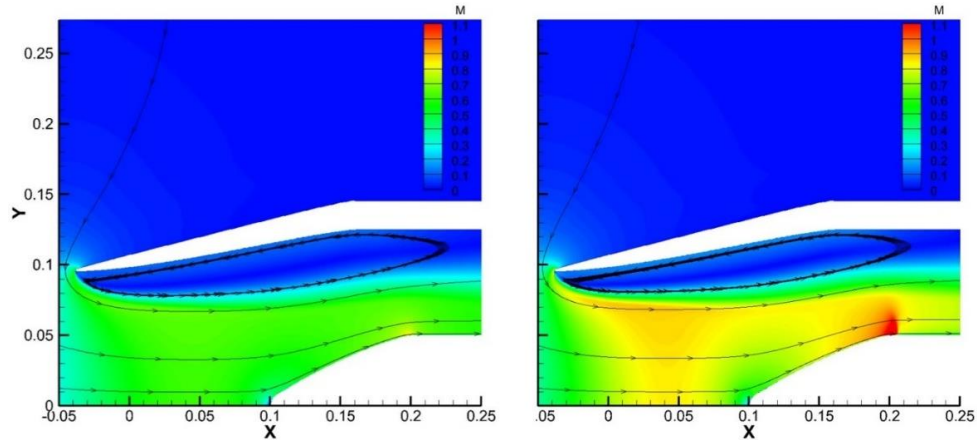
Figure 4-8: Mach number contours for sliding nacelle. Left shows 850000 Pa back pressure, right shows 75000 Pa.

4.3.2: Sliding Cone

Sliding the intake cone is another potential method to improve takeoff performance. Sliding the cone to the beginning of the intake will help change the streamlines of the flow by causing flow contraction near the inlet of the intake. Appendix C shows how this is done. Sliding the cone can keep the flow attached, which will in turn improve performance by reducing the separation bubble and increasing the massflow ingested. To evaluate the effectiveness of this method, the intake cone is slid 10cm and 13 cm in separate simulations. Sliding the cone upstream 10 cm starts the cone at the same place as the diffuser, while sliding it 13 cm upstream allows the cone to change the flow path upstream of the intake. Figure 4-9 below shows the Mach number contours for these cases. Figure 4-9a shows the original geometry, while Figure 4-9b shows the results with the cone slid 10 cm, and Figure 4-9c shows the cone slid 13 cm. Sliding the cone 10 cm results in a performance improvement in the massflow of roughly 5% (improving to 3.75 kg/s). However, sliding the cone 13 cm results in a decrease in terms of massflow performance, down to 3.25 kg/s.
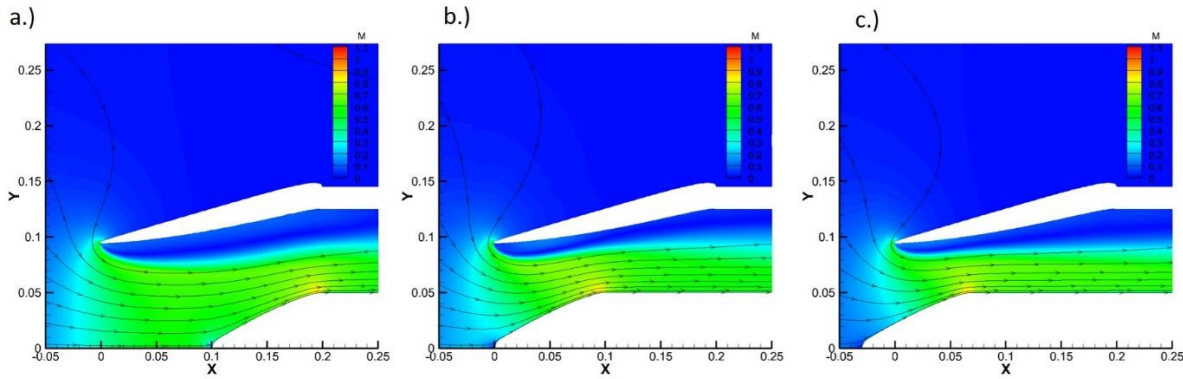
Figure 4-9: Sliding cone results. Left to right: original, 10 cm, 13 cm.

Comparing a.) to b.), the contour shows a reduction in the size of the separation bubble. In particular, the detached flow region near the inlet of the intake is significantly reduced. This occurs primarily due to the cone changing the streamline curvature at the inlet, causing flow compression in addition to the flow separation at the inlet. The flow compression aids in reducing the separation phenomena, leading to decreased size of the separation region, thus increasing the massflow ingested. Comparing c.) to a.) and b.), there is even more reduction in the separation region near the inlet. However, when the cone is slid past the start of the diffuser as in c.), there are negative effects in the downstream portions of the diffuser. Namely, the cone curvature does not compress the flow near middle nor exit of the diffuser. This results in increase separation in the latter stages of the diffuser. This increased separation region is clearly seen when comparing b.) to c.). This accounts for the reduction of massflow when the cone is shifted upstream of the diffuser. Furthermore, shifting the cone upstream in the geometry leads to increased frictional effects, which also play a minor role in the massflow ingestion.

4.3.3: Slots in Intake

Designing slots along the inlet walls is another method to enhance the intake performance at takeoff conditions. Opening in downstream portions of the engine intake provides more area for the fan to suck in flow, thus enhancing massflow ingestion. Unlike the proposals in the previous sections, this method does not directly impact the streamline curvature, so the separation bubble at the inlet of the intake is largely unaffected. Rather, by opening a slot, there is increased massflow simply due to increased air flow availability. To evaluate the potential for this method two separate evaluations were considered.

First, a small slot along the diffuser wall is opened. The slot is 0.25 cm in width. This evaluation is done to evaluate the effectiveness of adding multiple slots along the intake geometry, since the slot is very small. The takeoff massflow was increased to 3.75 kg/s at a back pressure of 85,000Pa. This represents an increase of roughly5%in the takeoff massflow performance. Adding several small slots along the diffuser walls gives more area for fan suction, and by adding several slots, takeoff performance can be easily enhanced.

Making slots along the intake walls can be difficult. Instead, a large slot downstream of the intake can also be considered. In the current architecture, the fan is located 5 cm downstream of the intake. So, a 5 cm slot is opened between the exit of the intake and the inlet of the fan to allow the fan the capability to suck in flow that bypasses the intake. This large slot allows for great enhancement of the takeoff massflow and offers a relatively simple mechanical implementation. The results of the simulation are shown below in Figure 4-10. Now the takeoff massflow is increased dramatically to 5.41 kg/s. This large enhancement indicates that when significant massflow enhancements are necessary, a large slot between the intake and the fan can be designed. The streamlines in the figure below indicate that this method is effective at sucking in large flows that bypass the intake. This is necessary for large improvements since the streamlines at takeoff conditions cause large separation which cannot be significantly reduced since the streamline curvature is extreme.
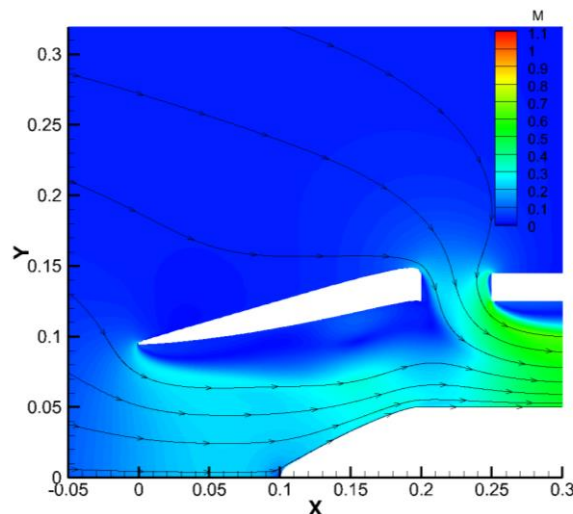
Figure 4-10: Mach number contour for large slot in inlet engine architecture.

4.3.4: Increasing Fan Suction

A final method to improve the performance of the intake at takeoff conditions is to stretch the operating limit of the fan downstream of the intake. For example, significantly reducing the back pressure of the fan will lead to increased suction, allowing for increased massflow ingestion. Reducing the fan back pressure to 65000 Pa results in the massflow ingested increasing to 5.25 kg/s, which represents significant improvement in the performance at takeoff. However, the flow also starts to become choked as shown in Figure 4-11 below, and decreasing the back pressure further results in no gain in massflow ingestion. Appendix C shows the contours for back pressures ranging from 50,000Pa up to 85,000Pa for more reference.
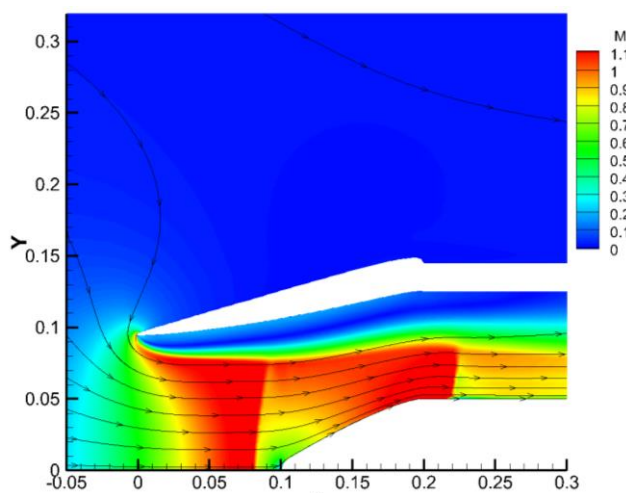
Figure 4-11: Mach number contour for reduced fan back pressure.

4.4: Conclusions and Recommendations for Future Designs

In this chapter, the aerodynamic differences between cruise and takeoff operation is demonstrated. The challenges of designing a compact engine intake capable of operation at these extreme engine conditions are fully addressed and solutions are proposed. It is clear that when designing engine intakes, the size of the engine must be analyzed for takeoff conditions where large massflows are required. Due to turbofan suction, large separation occurs, so numerical studies need to be performed to fully understand how to size the engine intake. However, cruise operation often dictates engine operability, because cruise operation controls mission duration, mission length, and overall fuel consumption. Therefore, in high speed applications where flow diffusion is critical, methods to enhance takeoff performance without sacrificing cruise operation must be evaluated.

Several avenues to improve the takeoff massflow ingestion are explored in this chapter. The simplest solution is to increase suction due to the fan. Depending on the application, this has limited effects, as once the flow becomes choked, it is impossible to increase the massflow. The effective area is reduced when the flow is choked by large separation. Many applications require either more massflow than the fan is capable of sucking in before choking or have a fan that cannot operate at low enough pressures. The effects of sliding the intake diffuser and cone could be considered in these applications. Sliding the nacelle results in penalties in takeoff performance due to increased friction and decreased compression from the cone. However, sliding the cone provides small boosts in the massflow performance. Furthermore, the results presented suggest that there is an optimal distance to slide the fan cone, which is something that future designers can take advantage of. Slots are another possible solution; and are easily implemented. In the 2D simulations, a small slot within the intake walls proved favorable, suggesting that if small enhancements are needed, several slots can be made in the diffuser walls. For larger enhancements, a passage between the fan and the intake can be opened, resulting in large massflow enhancements.

The massflow ingested during takeoff operations is directly related to the area of inlet flow for the fan. The methods above attempt to increase this area by opening increased area for suction or by changing the streamlines to reduce separation and thus enhance the area. A final method to enhance the massflow ingestion is by designing a variable area inlet. Designing part of the diffuser out of a flexible material allows the intake to adapt various configurations during operation. This method has the advantage of being able to adapt multiple geometries, so the applications are not limited to enhancement simply during takeoff conditions. Furthermore, the inlet area can be greatly increased without modifying the diffuser wall, resulting in only part of the diffuser needing to be adjustable. The table below summarizes the different methods explored in this chapter and shows the enhancements achieved by each. The enhancements show future designers what avenue to explore depending on the massflow enhancements they need for their applications.

Table 4-1: Summary of proposed takeoff enhancements.

Design	Fan back pressure = 75 kPa	Fan back pressure = 85 kPa	Fan back pressure = 65 kPa
Nominal Optimized Design	4.37 kg/s	3.59 kg/s	5.25 kg/s
Variable Area Intake Design	7.65 kg/s (+75.7%)	6.74 kg/s (+87.7%)	Not evaluated
Sliding Nacelle (3.75 cm)	4.33 kg/s (-0.9%)	3.58 kg/s (-0.3%)	Not evaluated
Sliding Cone (10 cm)	4.59 kg/s (+4.9%)	3.75 kg/s (+4.5%)	Not evaluated
Sliding Cone (13 cm)	3.93 kg/s (-10.1%)	3.25 kg/s (-9.5%)	Not evaluated
Small Slot in intake	4.55 kg/s (+4.1%)	3.75 kg/s (+4.5%)	Not evaluated
Large slot between intake and fan	6.31 kg/s (+44.4%)	5.41 kg/s (+50.7%)	Not evaluated

CHAPTER 5 : INTEGRATION OF INTAKE INTO OVERALL ENGINE ANALYSIS

With the engine intake designed for cruise conditions and methods to improve takeoff challenges addressed, the next step in engine intake analysis is to analyze overall intake effects on engine performance. This will be done by assessing the intake at off-design conditions (reduced speeds and non-axial inlet flow), assessing how the intake performs at unsteady conditions (variations in fan suction), and to assess how the intake performs at different Reynolds numbers (various altitudes). Then the off-design engine performance will be integrated into an engine model to assess the impacts of off-design intake operation on overall engine performance.

5.1: Effects of Flight Speed and Non-Axial Inlet Flow on Performance

Assessing intake performance at off-design conditions helps determine ascent and descent trajectories. Additionally, during operation of any mission, even at cruise, the flow may not be perfectly axial. So, an off-design assessment is necessary to determine how the intake will react to non-optimal flow conditions. Based on previous numerical and experimental studies, the scope of this analysis is limited to $\pm\,10°$ for inlet flow [27-28]. The off-design speeds considered range from M0.3 to M0.7. To assess off-design performance the primary parameter used is the pressure recovery factor, defined below in terms of total pressure losses (all mass-flow averaged quantities). Flow diffusion and separation parameters will also vary with regards to varying the speed and angle of attack, but the engine performance will be primarily affected by the pressure recovery, which is defined in Equation (5-1).

$$Pressure\ Recovery = 1 - Pressure\ Loss = \frac{P_{02}}{P_{0,freestream}} \qquad (5\text{-}1)$$

To properly assess the angle of attack, the domain is converted to a 3D domain. This is done by simply rotating the domain about the line of symmetry to create a 3D domain and mesh, where the y+ is maintained below 0.6 everywhere. Figure 5-1 shows the 3D mesh. Then each off-design speed (M0.3, M0.5, and M0.7) is simulated at different angles of attack between 0 and 10°. Non-axial inlet flow conditions are also considered at the design speed of M0.9.
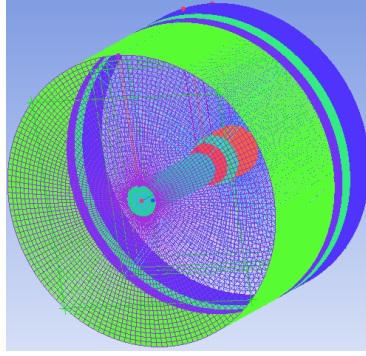
Figure 5-1:3D mesh used for off-design analysis.

The results for off-design cases at a M0.9 are shown below. The cuts represent an axial cut at the mid-plane of the intake (z=0). The streamlines for each case are taken at the same upstream location. Looking at the zoomed in figures, the separation bubble in the intake increases in size as the angle of attack is increased. In the cases with -7.5° and -10° angles of attack, almost no flow is passed through the upper half of the intake. Furthermore, at the increased angles of incidence, unsteadiness due to the separation bubble is noticeable. Figure 5-2 below shows transient simulation results for Mach0.9, -7.5°. The case is run full unsteady and compared to the results of the steady simulations to ensure that the steady results capture the desired trends in pressure recovery. The time averaged total pressure differs from the steady simulation total pressure by less than 0.01%.
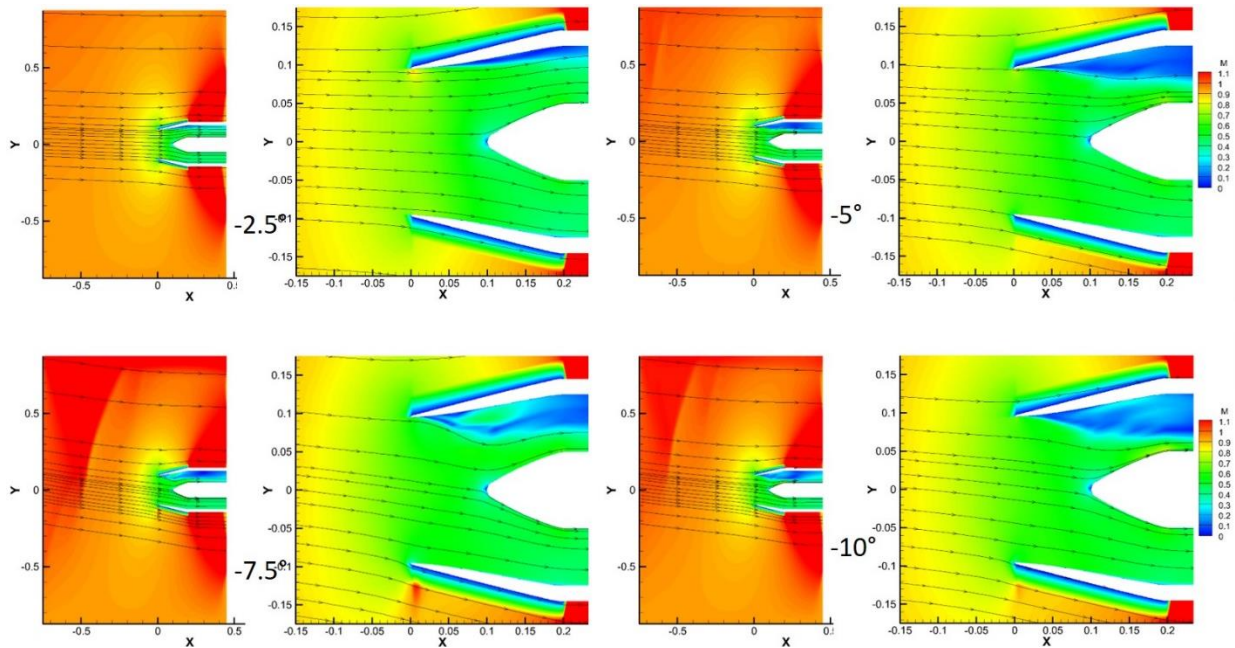
Figure 5-2: Mach number contours for off-design Mach0.9 cases.
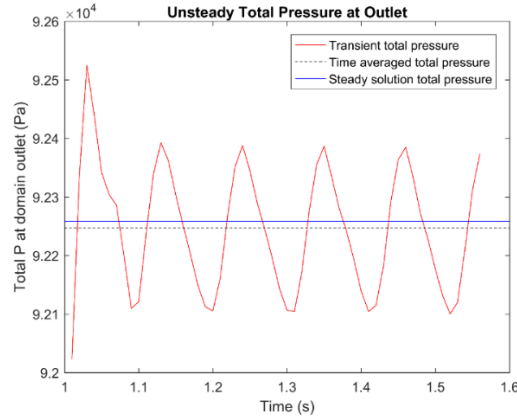
Figure 5-3: Time history of unsteady total pressure. Steady solution matches time-averaged value.

Figure 5-4a show the intake performance map as a function of speed and angle of attack. The pressure recovery of the intake increases significantly with reduced speed, which can be explained by the decreased suction generated by the fan. This causes less extreme flow diffusion, minimizing separation, and helping to eliminate pressure losses. The effects of increased speed on intake performance are particularly clear at high angles of attack, where the increased fan suction results in more extreme inlet streamline curvatures when compared to lower speeds. At low speeds of M0.5 the pressure losses are roughly 4%, however, at high speeds of M0.9 the losses increase to over 15%. At high speeds, non-axial inlet flow has a significant impact on intake performance. The full effects of this on the overall engine will be further explored in section 5.4.
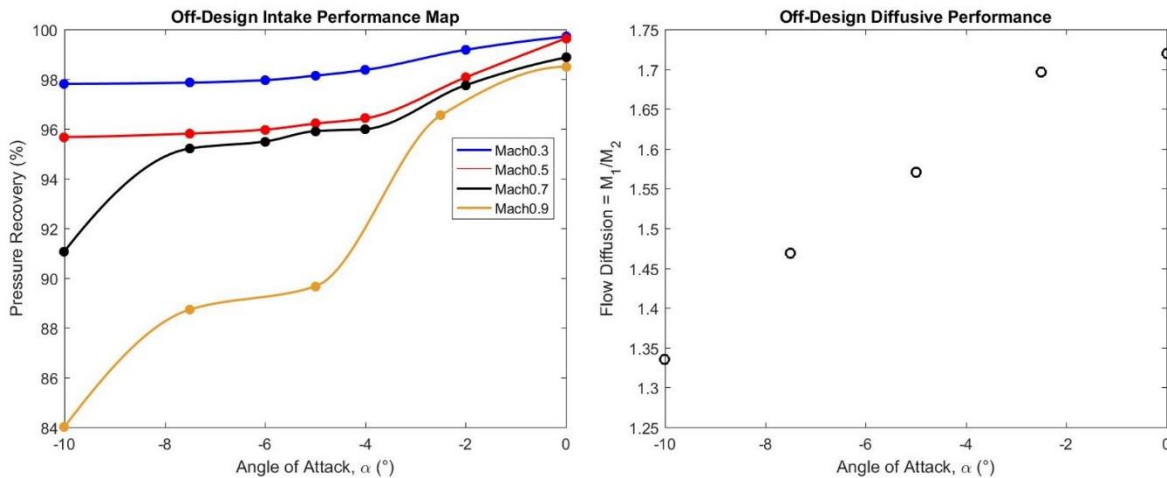
Figure 5-4: Off-design performance of intake. Left shows the pressure recovery of the intake. Right shows the achievable flow diffusion for non-axial flow at cruise speed.

The dramatic drop-off in intake performance at high-speeds and high angles of attack effects more than just the pressure recovery. Figure 5-4b shows the flow diffusion performance of the intake as a function of the angle of attack for M0.9 cases. Small variations in the angle of attack result in small effects in flow diffusion; but beyond 2.5° intake diffusion is significantly impacted.

During ascent and descent operations, a significant reduction flight speed is favorable for intake performance. When the intake is not operating at axial conditions, the performance of the intake is very sensitive to flight speed, so decreasing flight speed at off-design conditions is desirable. The difference in performance from M0.5 to M0.7 at high angles of attack suggests that M0.5 is the fastest flight speed suitable for off-design performance within the intake.

The simulations performed here all occur at cruise altitude of 3000m. In section 5.3 the effects of altitude and Reynolds number on intake performance will be investigated.

5.2: Unsteady Intake Performance

The analysis performed on the intake so far has focused on steady evaluation of the intake. However, during operation, even during cruise, there will always be a component of unsteadiness in the operation of the intake. The unsteadiness can come from the operation of the turbofan, flight speed, or flight altitude. No operation is truly steady. Because of this, it is important to analyze the effects of unsteadiness on intake performance.

5.2.1: Setup for Unsteadiness Investigation

To evaluate the effects of unsteadiness on intake performance, the unsteadiness of the fan is considered. The back pressure imposed by the fan is kept at the same mean value as from the steady simulations, but is varied given a frequency and amplitude according to Equation (5-2).

$$P_{back}(t) = P_{back,ss} + A * P_{back,ss} * \sin(2\pi f t) \tag{5-2}$$

Here 'A' represents the amplitude variation as a percentage, and f represents the frequency of the oscillations. Six different cases are evaluated, with amplitude oscillations ranging from 2.5% to 5% and frequencies ranging from 10Hz to 25Hz. The transient simulation is set-up with a time-

step of 0.01s, so the chosen frequencies are set to be low enough that aliasing is avoided in the computations. The same 2D domain and mesh from previous studies are used, with the only change being the back pressure due to the fan. The simulation is run for a global time of 12.5s to ensure that the results converge, and the final 3 second of data are used for analysis.

5.2.2: Effects of Fan Unsteadiness on Intake Performance

Increasing the amplitude of the oscillations leads to reduced intake performance. Figure 5-5 below shows the effect of the amplitude on pressure recovery and flow diffusion for a frequency of 25 Hz. The oscillations show clear reductions in performance as the amplitude of the fan oscillations increases. Figure 5-5 below helps summarize these reductions. Increasing the unsteady amplitude from 2.5% to 5% increases the reductions in the diffusion and pressure recovery parameters by a factor of 2.
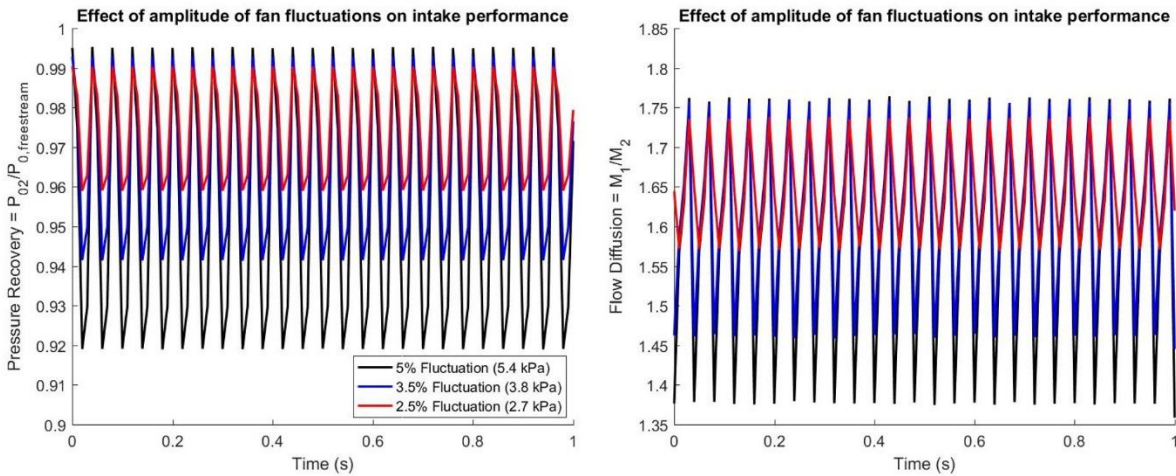
Figure 5-5: Effects of fan unsteadiness on intake performance (amplitude). Left shows pressure recovery, and right shows flow diffusion.

Figure 5-6 below summarizes the impact of the frequency of the oscillations. The results are shown for the 3.5% amplitude case. Increasing the frequency of the oscillations leads to an increased impact on the pressure recovery of the intake. The reduced frequency case shows dampened pressure recovery effects; but no such dampening is seen in the flow diffusion performance of the intake. Furthermore, the decreased frequency cases exhibit smaller reductions in intake performance than their higher frequency counterparts.
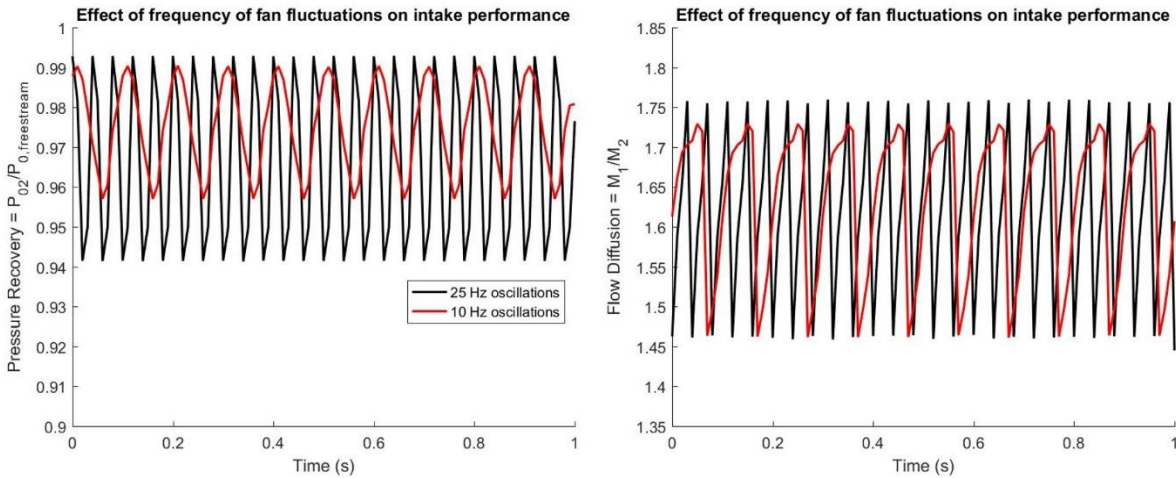
Figure 5-6: Effects of fan unsteadiness (frequency).

The intake is shown to be susceptible to unsteadiness, and intake performance clearly declines with increased unsteady effects. In turbofan applications this becomes a concern, as small variations in fan operation can reduce the intakes diffusive and pressure recovery capabilities. Table 5-1 below summarizes the results of the unsteady analysis, where increased amplitudes result in large decreases in intake performance. The frequency of the unsteadiness plays a similar role, but to a lesser extent. Reduced frequency noise helps dampen the oscillations, particularly in pressure recovery.

Table 5-1: Effect of fan unsteadiness on intake performance.

Amplitude of Oscillation (% of nominal fan back pressure)	Frequency of Oscillation (Hz)	Simulation Reduced Frequency = $f_{oscillation}$ * $t_{time,step\ simulation}$	Time-averaged flow diffusion	Time-averaged pressure recovery
2.5%	25	0.25	1.63 (-5.23%)	0.974 (-1.12%)
3.5%	25	0.25	1.61 (-6.40%)	0.967 (-1.83%)
5.0%	25	0.25	1.58 (-8.14%)	0.955 (-3.05%)
2.5%	10	0.1	1.65 (-4.07%)	0.976 (-0.91%)
3.5%	10	0.1	1.62 (-5.82%)	0.975 (-1.02%)
5.0%	10	0.1	1.61 (-6.41%)	0.969 (-1.62%)
Steady-state (0)	0	0	1.72	0.985

5.3: Effect of Altitude and Reynolds on Intake Performance

In many cases separation is highly sensitive to Reynolds number. In subsonic applications separation within the intake guides overall performance in terms of pressure losses and flow diffusion. The Reynolds number is defined as the ratio of inertial forces to viscous forces. Essentially, increasing the Reynolds number means adding energy to the mainstream flow, making the flow more difficult to disturb. Conversely, reducing the Reynolds number increases the impact that friction plays on the flow. As a result, reducing the Reynolds number leads to increased boundary layer development due to friction, and often increases the likelihood for separation. Separation increases the risks of pressure losses and reduces the effective area of the intake since the flow will follow a path that is not physically imposed by the intake geometry. This leads to potential for reduced flow diffusion and increased pressure losses at low Reynolds numbers.

5.3.1: Setup for Reynolds Investigation

To investigate how the intake performs at different Reynolds numbers, the intake is simulated at various altitudes. The static pressure and temperatures at these altitudes are used to impose a domain inlet of M0.9, and an outlet of M0.45 at the exit of the fan. These conditions are imposed in the same manner as in Chapter 3, using isentropic flow equations and static to total pressure ratios to obtain the desired inlet and outlet Mach numbers. Table 5-2 summarizes

the different boundary conditions used below, as well as the freestream dynamic viscosity for each case (using Engineering Toolbox).

Table 5-2: Boundary conditions used to study effect of altitude on intake.

Altitude (m)	Freestream P_s (Pa)	Freestream T_s (K)	Inlet P_0 (Pa)	Inlet T_0 (K)	Outlet P_{back} (Pa)	Freestream Dynamic Viscosity ($N \frac{s}{m^2}$)
0	1.01e5	294	1.78e5	343	1.56e5	1.82e-5
1000	8.99e4	282	1.58e5	328	1.38e5	1.76e-5
2000	7.95e4	275	1.39e5	321	1.22e5	1.73e-5
3000 (cruise)	7.01e4	269	1.23e5	313	1.08e5	1.69e-5
4000	6.17e4	262	1.08e5	305	9.50e4	1.66e-5
5000	5.40e4	256	9.48e4	98	8.32e4	1.63e-5
10000	2.65e4	223	4.65e4	260	4.08e4	1.46e-5
15000	1.21e4	217	2.12e4	252	1.86e4	1.42e-5
20000	5.53e3	217	9.70e3	252	8.51e3	1.42e-5
25000	2.55e3	221	4.47e3	258	3.93e3	1.45e-5

5.3.2: Impact of Reynolds Number on Intake Performance

The optimized geometry from Chapter 3 is evaluated at each of these conditions to assess the impact of Reynolds number (and altitude) on intake performance. Table 5-3 shows the performance of each case in terms of pressure losses, flow diffusion, and Reynolds number. The Reynolds number is calculated at the inlet of the intake for each case, and is computed as shown in Equation (5-3), where the dynamic viscosity is computed according the Sutherland's Law.

$$Re = \frac{\rho * u * d}{\mu} = \frac{inertial\ forces}{viscous\ forces} \qquad (5\text{-}3)$$

Table 5-3: Intake performance at various altitudes.

Altitude (m)	Reynolds Number/1e6= $\frac{\rho * u * d}{\mu}$	Flow Diffusion= $\frac{M_1}{M_2}$	Total Pressure Loss (%)
0	3.78	1.718	1.499%
1000	3.62	1.717	1.499%
2000	3.28	1.718	1.500%
3000 (Cruise)	2.82	1.720	1.501%
4000	2.65	1.721	1.499%
5000	2.41	1.718	1.500%
10000	1.41	1.709	1.503%
15000	0.67	1.696	1.505%
20000	0.31	1.677	1.504%
25000	0.14	1.661	1.505%

The results show that the overall total pressure losses remain largely unaffected by the Reynolds number. This can be explained by Figure 5-7, which depicts the normalized shear stress distributions for 4 selected cases along the diffuser wall. There is no significant difference in separation until the altitude is increased dramatically, and therefore the Reynolds number is decreased dramatically. On the left side of the figure it is clearly shown that each case is above zero in the middle 80% of the axial span. This leads to similar boundary layer development regardless of Reynolds number. It is only when the altitude is increased to 25 km, and the Reynolds number is decreased to below 0.25×10^6 that there is a significant change in the shear stress distribution (green curve in Figure 5-7a). Even at this decreased Reynolds number, the majority of the flow remains attached and unseparated. As a result, the massflow averaged pressure losses vary in very small amounts since the change in the boundary layer is minimal from case to case.
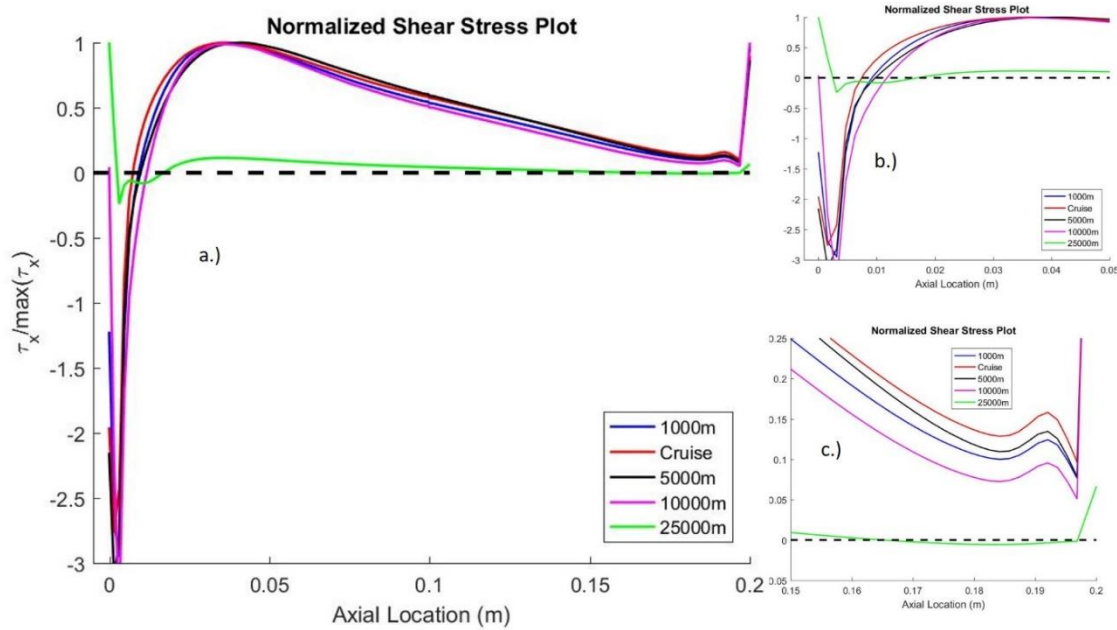
Figure 5-7: Shear stress comparisons at various altitudes.

However, Table 5-3 does reveal dependence between Reynolds number and flow diffusion. Looking at Figure 5-7b, the flow in each case starts out separated near the lip before becoming attached within the diffuser. The shear stress plots show that the reattachment point for each case is slightly different. As the Reynolds number is decreased, the flow attachment point is shifted downstream, leading to slightly more separation near the inlet for lower Reynolds number cases. Furthermore, looking at Figure 5-7c the lower Reynolds number cases have some separation near the outlet of the intake, while the higher Reynolds number cases remain attached throughout the geometry. These plots collectively show increased boundary layer development with reduced Reynolds number, which increases the changes for separation to occur in the geometry. That this boundary layer development and separation effects the diffusion more than the pressure losses may seem counterintuitive. However, by looking at the contour plots in Figure 5-8 with streamlines shown below, this phenomenon can be explained. Increased boundary layer development leads to the mainstream flow at the outlet having a reduced area. This reduces the effective area that the outlet of the intake has. The diffusion of the intake is primarily controlled by the area, so a small increase in the boundary layer development leads to reduction in the outlet area. The right figure, taken at a lower Reynolds number than the left, shows increased boundary layer development. This causes a reduction in diffusive capabilities,

which is particularly noticeable at low Reynolds numbers, where separation near the outlet of the intake occurs. This separation leads to the effective outlet flow area being impacted significantly, resulting in the large changes in diffusive capabilities shown for low Reynolds numbers in Table 5-3.
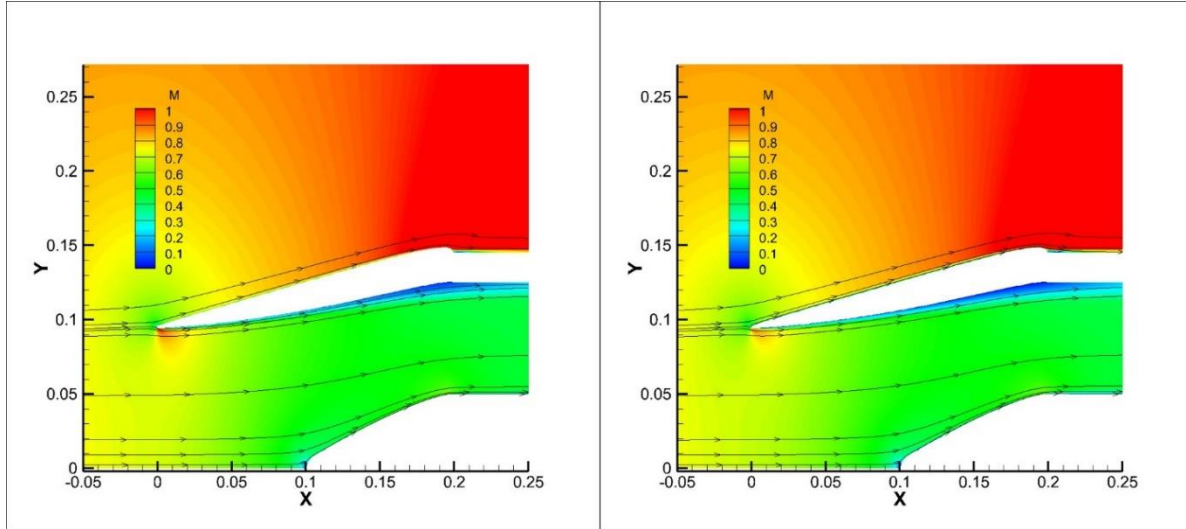
Figure 5-8: Mach number contours showing the difference in capture area for different altitudes. (Left) is a higher Reynolds number case.

Figure 5-8 above also shows streamlines taken at the same upstream location. For larger Reynolds numbers, there is a slightly larger capture area. This can further help explain the differences in diffusion performance. An increase in the capture area can be thought of as an increase in the inlet area of the intake. The diffusion of the intake is inversely related to the area ratio of the intake. So, increasing the inlet area increases diffusive capability, just as decreasing the outlet area (through increased boundary layer development) will decrease diffusive capabilities. Across all cases, there is not significant separation, so the increased boundary layer development primarily effects flow diffusion rather than pressure losses through the area mechanism discussed here. Equation (5-4) below summarizes the relationship between effective area and flow diffusion.

$$Flow\ Diffusion = \frac{M_1}{M_2} \alpha \frac{A_2}{A_1} \tag{5-4}$$

Below, Figure 5-8Figure 5-9 shows graphically shows the flow diffusion performance as a function of Reynolds number on a semilog. As described above, at very low Reynolds

numbers, the diffusion parameter suffers greatly due to increased boundary layer development. However, it is important to note that all the flow diffusion values are relatively large and would be near the Pareto front generated in Chapter 3. The Figure also shows that past a certain Reynolds number, there is no performance gain in in the intake. In fact, the optimal Reynolds number for the intake appears to be near the optimized cruise conditions. This indicates that the optimization of engine intakes is sensitive to the Reynolds number they are optimized at. The figure shows less than a 5% variance from optimal conditions in flow diffusion past a Reynolds of $2x10^6$, which indicates that all of the design recommendations given in Chapter 3 will still allow for the design of a near optimal intake if the Reynolds number for cruise conditions is greater than the given value.
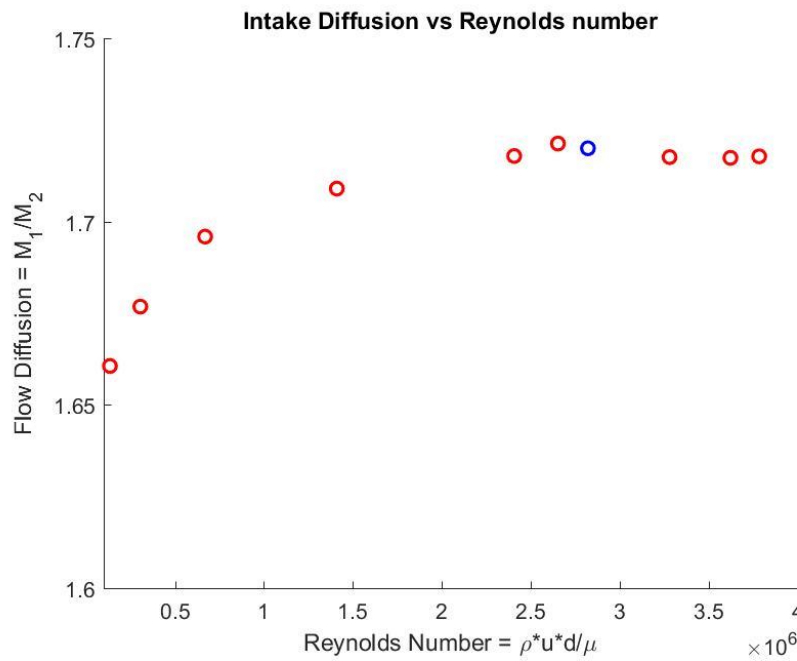
Figure 5-9: Reynolds number effect on intake flow diffusion.

5.3.3: Conclusions of Investigation

Based on Table 5-3, the results of this investigation show that the Reynolds number primarily affects the flow diffusion performance of the intake. This is because the optimized engine intake exhibits minimal separation across all Reynolds numbers. With little separation occurring, the total pressure losses of the intake remain largely unaffected by the Reynolds number. The Reynolds number does affect the boundary layer development, as demonstrated in Figure 5-8 above. The boundary layer increases with decreased Reynolds numbers due to an

increased impact of viscous forces (primarily friction), which effectively reduces the outlet area of the intake. Diffusion is primarily controlled by the effective area, so small reductions in outlet area will lead to penalties in flow diffusion which are not necessarily seen by the total pressure losses. Furthermore, the capture area of the intake varies slightly, and at high Reynolds numbers there is an increased capture area, leading to an increased effective inlet area. This serves to increase the intake area ratio which also promotes flow diffusion.

Furthermore, Figure 5-9 above shows that the intake itself operates optimally at a certain Reynolds number. Increasing the Reynolds number beyond the optimal value leads to slightly reduced performance. The performance is still near optimal conditions, but this is noteworthy because it implies that the intake optimization in Chapter 3 is sensitive to the Reynolds number; which suggests that the optimized intake geometry depends on the Reynolds number it is being applied too. The design recommendations put forth in Chapter 3 still apply to applications with higher Reynolds number, as the performance penalties are insignificant; however, for lower Reynolds number applications these recommendations may not hold.

5.4: Effect of Off-Design Performance on Engine

Now that a map of the optimized intake at off-design conditions has been created, it is possible to investigate the effects of off-design intake performance on overall engine performance. In this section, the effects of non-axial inlet flow and off-design intake speeds will be investigated. The altitude considered is the desired cruise altitude (3000m). The map generated in Section 5.1 for 3000m at off-design conditions will be used to evaluate the impact of the intake on engine performance.

To do this, a compact engine capable of application to UAV designs needs to be selected. The AMT Olympus is selected based on its intended use in UAV applications and on the availability of data [45]. The engine itself is a turbojet rather than turbofan engine, but methods to convert a turbojet to turbofan are currently being developed [1] making this a suitable choice of engine. The characteristics of the AMT Olympus are summarized below in Table 5-4. The engine has a single spool, single stage compressor, single stage turbine configuration.

Table 5-4: Summary of AMT Olympus.

Quantity	Value
Pressure Ratio	4
Max Shaft Speed (RPM)	108000
Mass Flow Rate (kg/s)	0.45
Fuel Consumption (kg/min)	0.64

5.4.1: Development of Engine Model in TMATS

An engine model can then be built using the Toolbox for the Modeling and analysis of Thermodynamic Systems (T-MATS) which is a tool for engine modeling developed by NASA [46]. The toolbox is integrated into Simulink for use in engine modeling applications. The toolbox uses thermodynamic relationships to quickly and reliable calculate engine performance and develop models for engine components. To focus on the intake performance, standard toolbox performance maps for the turbomachinery components downstream of the intake are used. Then the intake performance map generated in Section 5.1 is inputted into the engine model as a simple relationship where the pressure recovery of the intake is a function of Mach number and the angle of attack:

$$P_{rec} = f(M_{domain,inlet}, \alpha) \tag{5-5}$$

This allows the engine model to integrate the off-design performance of the intake into the overall engine analysis.

The model then uses thermodynamic relationships to evaluate the rest of the engine, using the general configuration shown below in Figure 5-10. The model takes as input the pressure recovery of the intake and the flight speed and outputs gross thrust. The ambient pressure is converted to a total pressure for the compressor based on the Mach number, isentropic relationships, and the pressure recovery of the intake. Then the torque in the compressor and turbine are matched, and the massflow and fuel rate are iterated on to achieve the imposed shaft speed. As part of this iteration, the inlet flow is part of an inner loop that is iterated on to match the massflows and torque. The fuel flow is controlled by an external controller in the engine model in order to maintain constant shaft speed. This model is developed

for steady conditions to evaluate off-design intake performance on overall engine thrust performance.
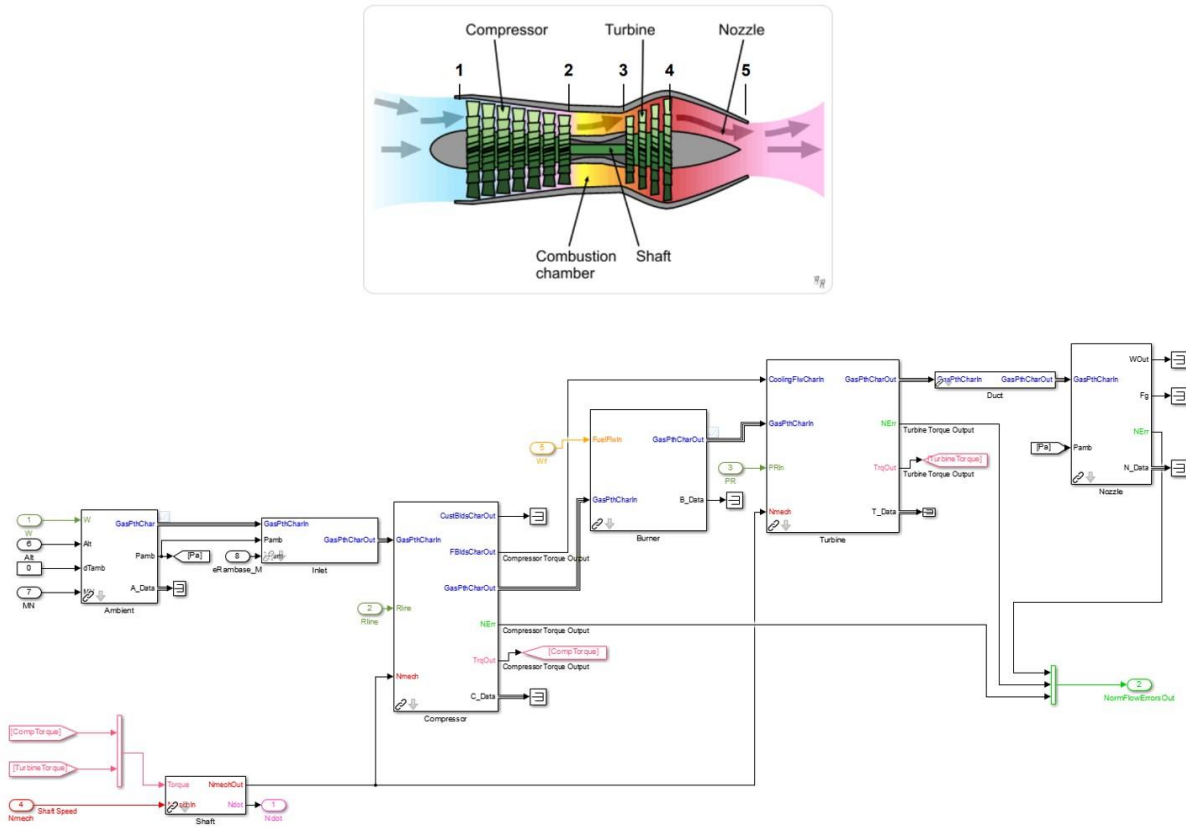
Figure 5-10: TMATS engine model overview.

5.4.2: Off-design Performance of the Engine

The pressure recovery values from section 5.1 are inputted into T-MATS and the gross thrust produced by the engine is calculated under steady conditions. Below the inputted pressure recovery map is shown, along with the normalized gross thrust produced by the engine. The gross thrust is normalized by axial flow at a speed of Mach0.3. Unsurprisingly, at axial, or near axial conditions, an increase in speed leads to an increased amount of thrust generated. This is due to the increased flight speed allowing for increased massflows and increased total pressure for the turbomachinery components; which ultimately leads to enhanced performance. However, at non-axial flow conditions, the impacts of poor intake performance can be seen on the overall engine. The desired flight speed of Mach0.9 becomes unfavorable compared to reduced speeds beyond angles of attack greater than 4°. However, reduced speeds of Mach 0.7 perform well at

angles of attack up to 8°. For applications where the angle of attack will exceed this value, a significant speed reduction is necessary.
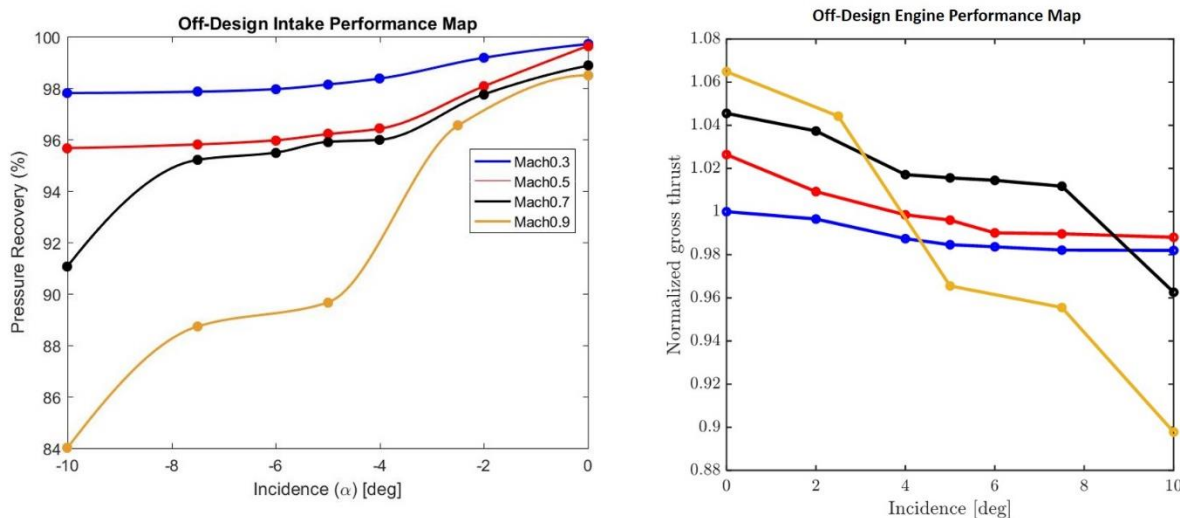
Figure 5-11: Off-design engine performance map.

Analyses such as this reveal the importance of designing intakes capable of performing at off-design conditions. Inlet lip curvature significantly impacts off-design performance [14-16], but as demonstrated here, for high speed applications the lip design alone does not off-set off-design challenges. When designing engines and engine intakes, a full mission analysis needs to be performed to determine the critical operational points. Ascent and descent operations require high angles of attack, to which the engine intake is extremely sensitive. These conditions have different requirements than high-speed cruise flight or takeoff conditions.

5.5: Conclusions of Off-Design Investigations

In this chapter various off-design operations of the engine intake were considered and analyzed. Literature suggests that intake performance is highly susceptible to non-axial inlet flow conditions. To investigate the effects of non-axial inlet flow, the engine intake was evaluated for various angles of attack at different speeds to determine intake performance at these conditions. The results revealed that lower speed operation is always beneficial in terms of pressure recovery for the intake. The benefits are amplified when the inlet flow is highly non-axial, as the pressure recovery of the intake decays rapidly past angles of attack of 5° for speeds above Mach 0.5. This shows future designers that high speed applications are extremely sensitive to axial operation,

and that maintaining axial inlet flow is necessary for good intake performance at high speeds. The effects of non-axial intake performance and off-design speed is also considered in an overall engine model. The engine model shows that at low angles of attack, the value of increased speed outweighs the decreased intake pressure recovery at high speeds. Figure 5-11 shows this by showing increased thrust generation at high speeds and low angles of attack. However, if the inlet flow is expected to be highly non-axial, it is preferable to reduce the speed, as high-speed intake performance at high angles of attack perform poorly enough to hamper the thrust generation of the engine.

The effects of turbofan unsteadiness are also investigated in this chapter. As future intake designs will be implemented into turbofan configurations, consideration of the unsteady back pressure generated by the fan is important. It is shown that the time-averaged performance of the intake is highly susceptible to both the amplitude and frequency of back pressure fluctuations generated by the fan. Reducing both amplitude and frequency leads to increased intake performance. As a result, future turbofan implementations of intakes need to account for back pressure unsteadiness and overall engine design should focus on damping turbofan fluctuations.

The performance of the intake varies at different altitudes and Reynolds numbers. The performance of intake flow diffusion declined with decreasing Reynolds number (and increasing altitude). This is due to the viscous forces beginning to dominate the flow physics, making the boundary layer easier to perturb. Increased boundary layer development effects the effective area of the intake, reducing flow diffusion. The importance of considering the altitude of cruise operation is clearly demonstrated by the Reynolds number investigation conducted in this chapter, as Figure 5-9 shows that the optimized geometry performance only holds at certain Reynolds numbers. Decreasing the Reynolds number past $2*10^6$ leads to decreased intake performance, making the design recommendations in Chapter 3 less meaningful.

CHAPTER 6 : EXPERIMENTAL MODEL FOR ENGINE INTAKES IN LINEAR WIND TUNNELS

Up to this point, the analysis has been purely numerical. The next step in the analysis of future compact high-speed engine intakes is to develop an experimental model for these intakes. The experimental model will be useful in validating and calibrating the numerical tools which are used to develop intakes. In this chapter, an experimental model for the intake designed in Chapter 3 is developed for operation in a linear wind tunnel. The methodology discussed in this chapter will help future designers determine how to appropriately non-dimensionalize testing conditions and how to replicate complex annular geometries in simplified 2D channels. An equivalent 2D profile will be mounted in a linear wind tunnel with full optical access along 2 windows, and a third window free for probes to be inserted. The testing here is focused on cruise conditions rather than takeoff since experimentally simulating the suction created by the fan at takeoff represents a new challenge.

6.1: Linear Wind Tunnel Operation

The experimental model will be implemented into the linear wind tunnel at the Purdue Experimental Turbine Aerothermal Laboratory (PETAL). The wind tunnel is designed to operate at wide ranges in Mach and Reynolds number; each of which can be varied independently through the use of a sonic throat downstream of the test section. The wind tunnel is designed with windows allowing optical access, making optical measurement techniques such as particle image velocimetry (PIV) and oil flow visualization possible. The dimensions of the wind tunnel test section are shown below in Figure 6-1. Upstream of the test section is a settling chamber, designed to reduce boundary layer development and make the inlet flow axial. Downstream of the test section is the sonic throat which allows for independent variations in the Mach and Reynolds numbers. In the experiments proposed here, the sonic throat will be used to choke the flow. The area of the throat will be set using flow relations to obtain the desired Mach number at the inlet of the intake. A full overview of the wind tunnel operation and design can be found in [47].
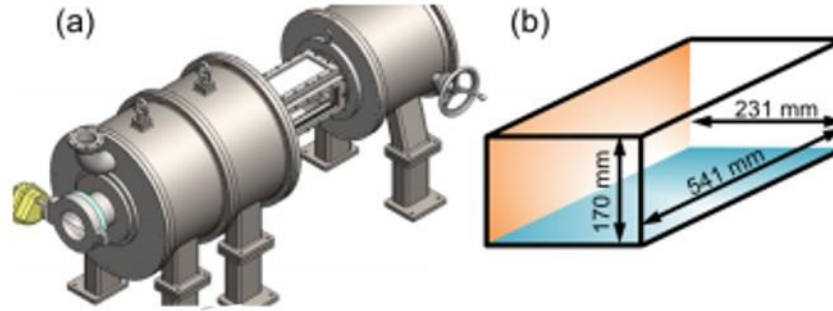
Figure 6-1: Linear wind tunnel with optical access.

6.2: Design of Test Article

To implement the intake into the wind tunnel and achieve the desired Mach number, the design must be scaled down. In this case, the design area must be scaled down by a factor of ¼. To implement the intake into the linear wind tunnel, the annular geometry must be converted into a channel profile. In doing so, the overall area ratio of the intake must be respected since flow diffusion is primarily controlled by the area ratio. Equation (6-1) summarizes the scaling performed.

$$\frac{A_{1,intake}}{A_{2,intake}} = \frac{A_{1,model}}{A_{2,model}} \tag{6-1}$$

By scaling the overall areas down by a factor of ¼, and respecting the overall intake area ratio, the inlet height of the experimental model must be 3.03cm and the outlet height must be 4.47cm. However, the question of how to convert the 3D annular intake design into a 2D channel profile remains. To help answer this question, potential experimental models will be proposed and evaluated by comparing numerical results from the model to the original geometry across optimized and baseline geometries. This will ensure that the selected model not only accurately replicates the physics of the original intake, but that it also differentiates between good and bad intake designs.

6.2.1: Methods to Replicate Intake Flow Physics

As discussed previously, intake performance depends on two separate geometric parameters: the curvature of the diffuser, and the effective area of the flow. During cruise

operation, the effective flow area is primarily determined by the diffuser and cone. This leads to two different ways to implement the intake geometry into the wind tunnel. The first method is to respect the curvature of the diffuser (first and second derivative of the diffuser wall is maintained) and scale the length down to meet the overall intake area ratio. The second method is to convert the intake geometry into a 2D profile that maintains the same area ratio as the intake along the curvilinear path. The two different geometries that can be considered are shown below in Figure 6-2 along with the original intake geometry. Figures a and b compare the wind tunnel profiles of the two different methods to the original geometry. Figures c and d show how the first derivative and area ratios for each case compare. The area ratio method shows a greater max angle of diffusion, meaning it is possible that this method will have increased separation throughout the profile. The diffuser method shows less area contraction at the end meaning it could have increased pressure losses and flow diffusion, as well as increased outlet separation.
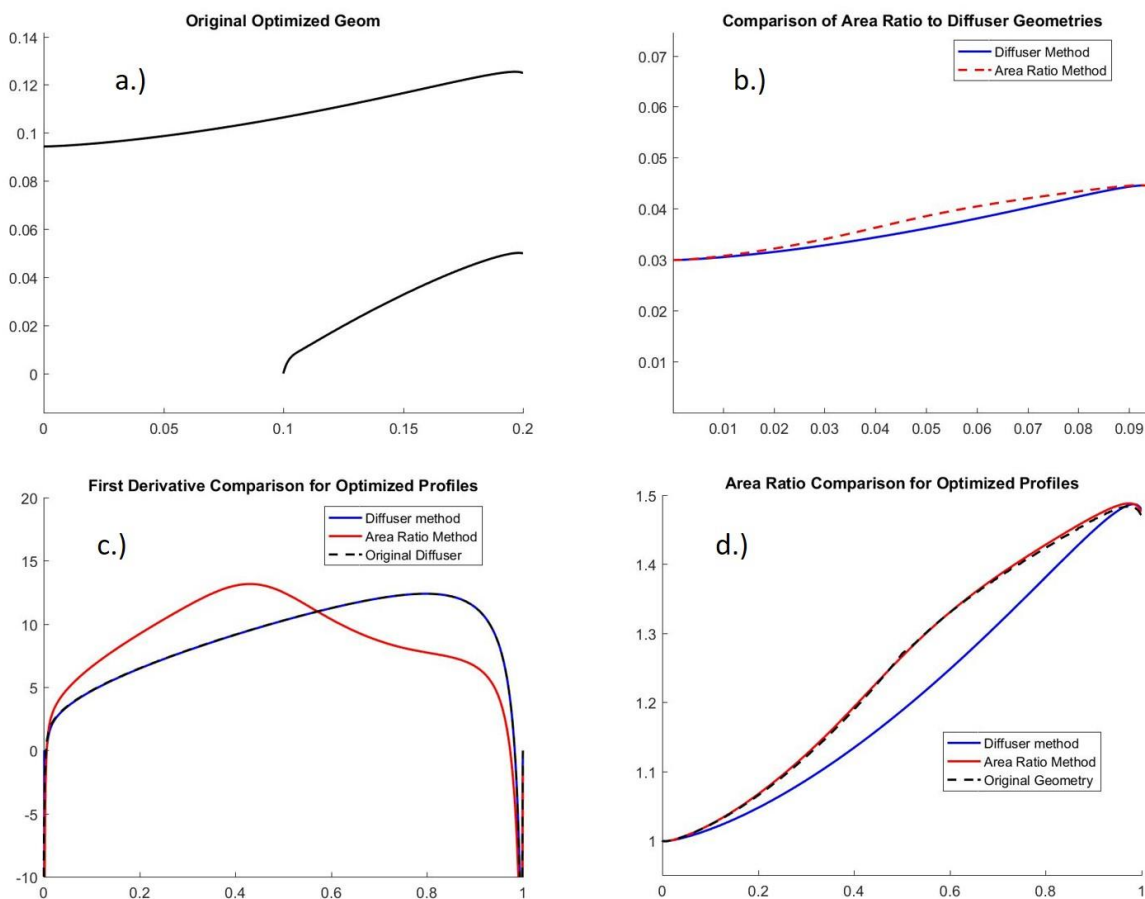

Figure 6-2: Experimental models proposed.

With these two methods considered, the geometries are imported into a new computational domain designed to replicate experimental test conditions. Three different cases are considered:

1. The diffuser method, with the lip of the diffuser modelled from the stagnation point on the lip. The length of the diffuser is scaled down so that the appropriate inlet to outlet area ratio is obtained.

2. The diffuser method, with a bump placed directly upstream of the diffuser. The bump is sized to have the same height as the stagnation point diameter (0.25mm). This simplifies the machining of the piece while still simulating the separation experienced by the lip

3. The area ratio method, with the area ratio of the lip respected as well. This geometry is scaled to have the same length as cases 1 and 2, so that the overall average angle of diffusion is the same between all 3 cases.

Upstream of the test article, an acceleration ramp is designed to accelerate the flow to the desired inlet Mach number. Then between the ramp and the start of the test piece, there is 2 cm of a flat plate. For case 2, the flat plate is 0.25mm beneath the start of the test article. Downstream of the test article is a long flat region to allow for probes to be inserted and measure flow quantities slightly downstream of the test article. This domain is imported meshed in ICEM with a y+<0.6, and imported into CFD++, and analyzed in 2D. The domain is depicted below, where all walls are considered adiabatic, the inlet has a massflow/length imposed, and the outlet has atmospheric conditions imposed. The outlet area is reduced to simulate the area that the downstream sonic throat will be set at. The domain imported into ICEM is shown below in Figure 6-3.

Figure 6-3: Computational domain for experimental model.

The total temperature imposed at the domain inlet is simply ambient (298 K). The massflow that is imposed during the experimental conditions will be done in order to achieve the desired Reynolds number at the inlet of the test article. Section 6.2.2 details how the Reynolds number is defined. The area of the sonic throat is set to simultaneously choke the flow and to

achieve the desired Mach number at the test piece inlet. In this case, the desired Mach number 0.75, which corresponds to the massflow averaged inlet Mach number at the intake lips during cruise operations as defined in Chapter 3. Each of the three methods discussed above are simulated in this domain. The Mach number contours for each case using the optimized geometries are shown in Figure 6-4.
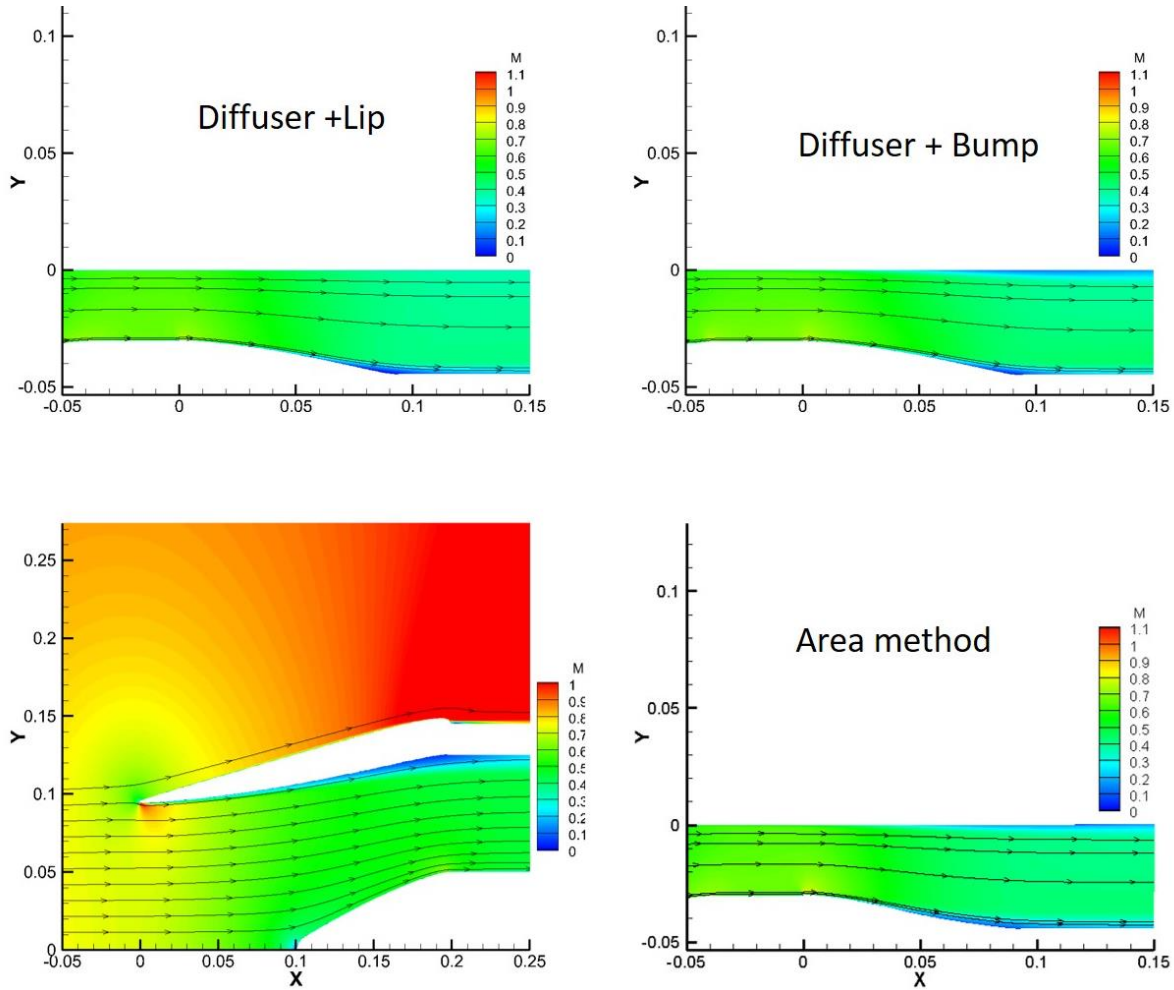
Figure 6-4: Experimental model contours.

Strictly from the contour plots, it is difficult to differentiate between the model options. A comparison of the isentropic Mach number (normalized static pressure distribution) and shear stress distributions is summarized below in Figure 6-5 to help distinguish between the three proposed options. Looking at a.), the normalized static pressure distributions for the 3 cases compare well with the nominal simulation. However, the area method distribution has a sudden increase in the isentropic Mach number around 40% of the diffuser span. Looking at the first

derivative for the area method, this increase corresponds to the sudden decay in the first derivative at the same location. This increase is not found in the diffuser methods, nor in the nominal simulations. Furthermore, b.), which shows the shear stress distributions for every case, shows that the diffuser methods replicate the shear stress distribution better than the area method. The local minima for each case occur very early in the geometry, followed by a local max, and then a steady decay. Near the outlet of the diffuser there is a jump in the shear stress caused by the diffuser contraction at the outlet. The diffuser methods replicate this trend, while the area method does not. Near 40% of the span, the area method shear stress starts to level off instead of gradually decaying as in the nominal simulations.
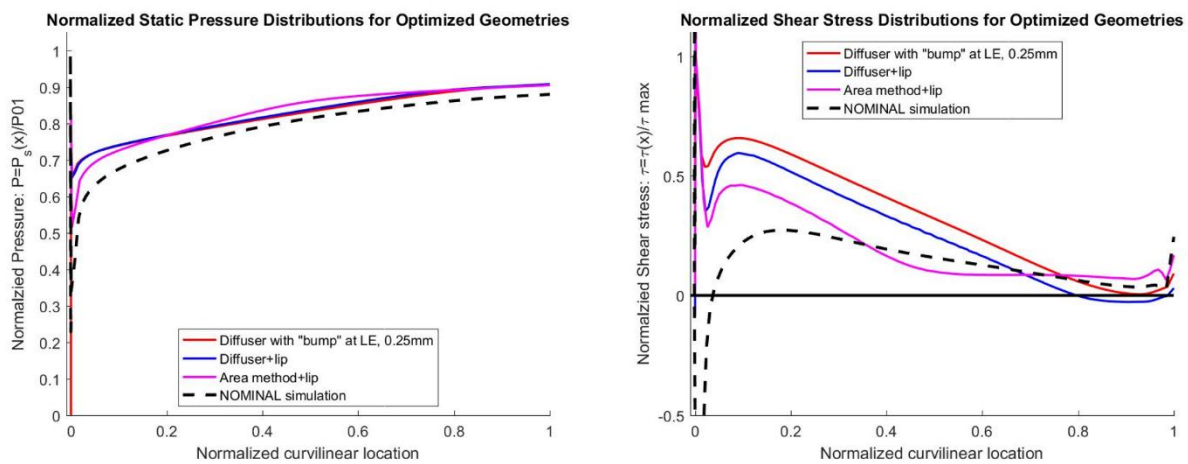
Figure 6-5: Static pressure and shear stress distributions for optimized geometry experimental models.

In the nominal simulations, there is a small amount of separation at the intake lips, which is not replicated by any of the methods proposed here. However, the methods all replicate the sudden drop in shear stress, and the corresponding increase. The shear stress plots also reveal that decoupling the area ratio effects from the diffuser effects of the intake is impossible. The nominal simulation reaches a local minimum near the outlet of the diffuser, without separating. The contraction in the diffuser near the outlet causes a spike in the shear stress, preventing separation. The area contraction near the outlet, which is more aggressive in the real simulations than in the diffuser simulations, also serves to help prevent separation. This can be observed by noting that the diffuser methods both separate before the diffuser contraction reattaches the flow.

Figure 6-6 below show the same plots for the baseline geometry. Once again, slight differences are noticeable in the isentropic Mach number trends between the area method and the nominal simulations. The differences are even more noticeable when looking at the shear stress trends. Again, the diffuser method replicates the general trends from the original simulation (an early local minimum, followed by a sudden increase, then a gradual increase in shear stress, followed by a jump near the outlet). The area method does not replicate the same trend, with the differences owed primarily to the differences in local curvature. Once again, however, the effects of the area ratio are noticeable. The nominal simulation manages to reattach at the outlet of the diffuser, due to the cone helping change streamlines and reattach the flow. However, the diffuser only methods don't have the cone helping, so they never reattach.
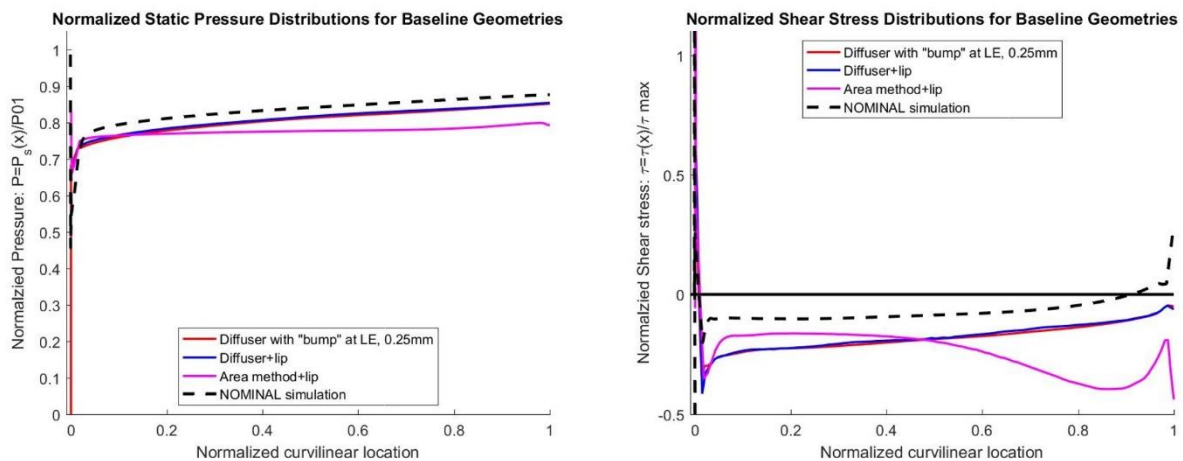
Figure 6-6: Static pressure and shear stress distributions for baseline version of experimental models.

When determining which method to choose, it is also important to consider how well the experimental models replicate the performance parameters of interest. Table 6-1 summarizes how each experimental model performs in terms of flow diffusion and pressure losses and compares the percent improvement from baseline to optimized geometries. The area ratio method predicts accurately the optimized profile flow diffusion; however, the improvement from baseline to optimized is well over-predicted. Meanwhile, the diffuser methods predict the improvements from baseline to optimized profile diffusion well, but the actual flow diffusion achieved in the optimized geometries is significantly reduced from the optimized. None of the 3

methods predict the improvement in pressure losses from baseline to optimized accurately, although they all predict significant improvement in pressure losses.

Table 6-1: Summary of experimental models.

Case	Flow Diffusion (Baseline)	Flow Diffusion (Optimized)	% Pressure Losses (Baseline)	%Pressure Losses (Optimized)
Nominal Simulations	1.44	1.72 (+19.4%)	2.67%	1.50% (-43.9%)
Diffuser+Lip method	1.37	1.67 (+21.9%)	1.95%	0.69% (-64.6%)
Diffuser+Bump method	1.39	1.65 (+18.7%)	2.05%	1.46% (-28.8%)
Area ratio method	1.18	1.69 (+43.2%)	2.41%	0.87% (-63.9%)

Based on the data presented above, case 2, the diffuser with a bump at the inlet of the profile, is selected. This case modelled the shear stress and static pressure distributions of the original geometry very accurately. Furthermore, the model predicts the enhancements in flow diffusion from baseline to optimized geometries. The overall pressure losses also compare favorably between this model and the original simulations. Furthermore, machining a scaled down version of the diffuser lip represents a challenge that can easily be removed by modelling the lip as a bump upstream of the diffuser to help trigger separation.

6.2.2: Definition of Reynolds Number

As demonstrated in Chapter 5, intake performance is sensitive to the Reynolds number. When going from simulations at high altitudes to a scaled down, ground level experiment, it is important to replicate the correct Reynolds number. In high subsonic speed applications with aggressive diffusion, the characteristic length defining the Reynolds number can be defined in several different ways. The diffusion rate of the geometry will affect performance of the intake, so it is desirable for the characteristic length to account for this. Correctly defining the characteristic length will allow for the experimental model to replicate the physics of the original intake.

If the characteristic length does not depend on the diffusion rate of the intake, the Reynolds number for the nominal simulations depends on the diameter. In the wind tunnel profile, the characteristic length can depend on either the inlet height of the diffuser part or the ratio of channel area to perimeter. This presents two potential Reynolds number definitions. If,

however, the characteristic length depends on the diffusion of the intake, then the outlet dimensions of the intake need to be considered when converting from the nominal simulations to an experimental model. Then, the characteristic length can depend on the change in diameter for nominal simulations and the change in channel height for the experimental model. This creates 2 more cases to consider. A final factor effecting the performance of the intake is the diffusion rate and curvature. Since these are the primary factors affecting performance, it is reasonable to define a characteristic length that accounts for these properties. The change in area per axial length is an appropriate method to measure this Reynolds number. Below, the 5 potential Reynolds number cases are summarized.

1. $Re_{cruise} = \frac{\rho*u*d_1}{\mu} = 2.77E6.$ $Re_{wind\ tunnel} = \frac{\rho*u}{\mu} * \left(\frac{h_1*width}{2h1+2width}\right)$

2. $Re_{cruise} = \frac{\rho*u*d_1}{\mu\backslash} = 2.77E6.$ $Re_{wind\ tunnel} = \frac{\rho*u}{\mu} * (h_1)$

3. $Re_{cruise} = \frac{\rho*u}{\mu} * (d_2 - d_1) = 8.85E5.$ $Re_{wind\ tunnel} = \frac{\rho*u}{\mu} * \left(\frac{(h_2-h_1)*width}{2(h_2-h_1)+2width}\right)$

4. $Re_{cruise} = \frac{\rho*u}{\mu} * (d_2 - d_1) = 8.85e5.$ $Re_{wind\ tunnel} = \frac{\rho*u}{\mu} * (h_2 - h_1)$

5. $Re_{cruise} = \frac{\rho*u}{\mu} * \left(\frac{A_2-A_1}{length}\right) = 9.4E5.$ $Re_{wind\ tunnel} = \frac{\rho*u}{\mu} * \left(\frac{A_2-A_1}{length}\right)$

Each of these cases is simulated in CFD++ by simply varying the inlet massflow to achieve the desired Reynolds number (the sonic throat is choked, so the massflow rate will not affect the inlet Mach number). The results of the simulations are shown below in Figure 6-7 and Table 6-2. The figure shows the shear stress distributions for the optimized geometries, which are the same across all models regardless of the Reynolds number. This shows the dependence of the shear stress on the diffuser curvature. The Table shows the flow diffusion performance between the baseline and optimized geometries at each Reynolds number case. As discussed in Chapter 5, the pressure losses are relatively independent of the Reynolds number, and the variations in these cases are negligible, so the flow diffusion parameter is used to determine the correct Reynolds number. The Table shows that Case 5 best predicts the improvement from the baseline to optimized geometries, suggesting that the correct definition of the characteristic length depends on the diffusion rate. Equation (6-2) summarizes the characteristic length used to define the Reynolds number.
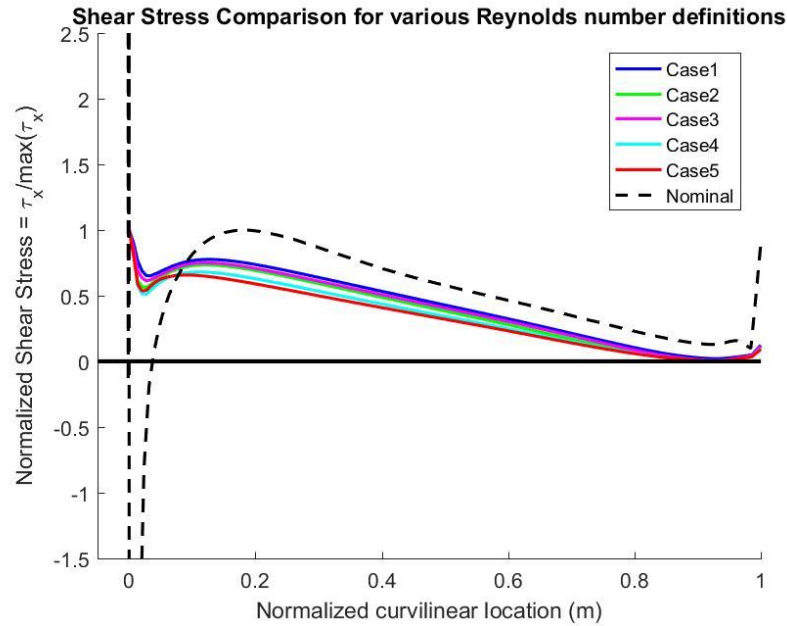
Figure 6-7: Shear stress distribution for different Reynolds number definitions.

Table 6-2:Summary of different Reynolds number definitions.

Case	Flow Diffusion (Baseline)	Flow Diffusion (Optimized)
Nominal Simulations	1.44	1.72 (+19.4%)
Case 1	1.33	1.67 (+25.6%)
Case 2	1.33	1.66 (+24.8%)
Case 3	1.33	1.66 (+24.8%)
Case 4	1.37	1.65 (+20.9%)
Case 5	1.39	1.65 (+18.7%)

$$d_{characterisitc} = \frac{\Delta Area}{length} \qquad (6\text{-}2)$$

It is logical that the Reynolds number for an intake should be defined in terms of its diffusion rate and somewhat dependent on the curvature. When creating an experimental model, it is necessary to account for parameters which effect intake performance. As demonstrated in previous chapters, the intake performance is dependent on curvature and diffusion. Therefore,

the Reynolds number which defines the intake should depend on these parameters. To experimentally replicate the Reynolds numbers at high speed cruise flights, the diffusion of the intake per unit length should be accounted for.

6.2.3: Final Experimental Configuration

With the Reynolds number defined and the experimental model selected, the experimental set-up has been defined. This section showed that for linear wind tunnel experiments, the best way to test an annular engine intake is to replicate the diffuser curvature. The overall area ratio of the intake must be respected so that the overall diffusion performance of the experimental model can be compared to the normal design. Replicating the curvature rather than the area ratio along the diffuser walls allows for better prediction of the boundary layer, and as a result better models the intake. However, in a linear wind tunnel experiment, neglecting the cone and the effective area ratio along the experimental profile means that some loss of information will occur. The cone serves to compress the area near the outlet of the intake, and adjusts flow streamlines to reduce the likelihood of separation. As a result, the experimental model will not perfectly replicate the intake performance.

When converting from the cruise operation to an experimental model, the Reynolds number must account for the area diffusion and the curvature. To do so, the characteristic length must be defined as the change in area of the model to the length of the model. This accounts for the diffusion rate of the intake as well as the curvature. Defining the inlet Reynolds number in terms of the overall diffusion rate allows the model to accurately replicate the flow physics for the intake. Below the experimental model geometry is shown. Equation (6-3) shows the Reynolds number definition for experiments in the wind tunnel. This Reynolds number defines how to convert from cruise operation to a scaled down, linear wind tunnel experiment.
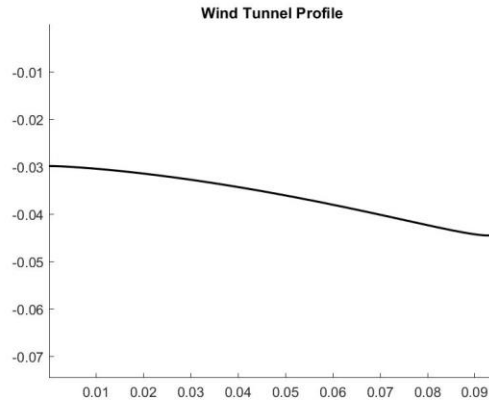
Figure 6-8: Wind tunnel profile for intake.

$$Re = \frac{\rho_1 * u_1}{\mu} * \frac{A_2 - A_1}{l} \qquad (6\text{-}3)$$

6.3: Experimental Plan

With the Reynolds number defined and an appropriate experimental model selected, an experimental plan can be defined. At cruise conditions, with a domain inlet of M0.9, the intake reaches M0.75 at its inlet. In Chapter 5, the effects of reducing the Mach number on the pressure recovery were noted, and the effects of the Reynolds number on the flow diffusion were noted. The experiments to be conducted should be used to validate the performance of the optimized geometry as well as calibrate the off-design CFD results.

6.3.1: Test Matrix

The primary Mach number of interests at the start of the test piece is M0.75. At this Mach number different Reynolds numbers can be tested to assess the numerical study performed on Reynolds number effects in Chapter 5. Then, by adjusting the area of the sonic throat, the Mach number at the inlet of the test article can be adjusted and the effects of the Mach number on the pressure recovery can be investigated. The table below summarizes an experimental campaign that will calibrate the numerical analysis done in the preceding chapters.

Table 6-3: Proposed test matrix for intake.

Test Case	Mach Number	Reynolds Number	Massflow (kg/s)	Total Temperature (K)
1	0.75	9.4E5	3.14	295
2	0.75	2.5E5	1.59	295
3	0.75	1.8E6	6.00	295
4	0.9	9.4E5	3.02	295
5	0.5	9.4E5	3.28	295
6	0.3	9.4E5	3.32	295

Test case 1 is the nominal cruise simulation. Test cases 2 and 3 maintain the same Mach number (sonic throat remains unchanged) while varying the massflow. Case 2 will closely resemble operation at 10000m, where performance of the intake will decay slightly, while case 3 resembles operation at 1000m, where performance should remain largely unaffected. Then in cases 4-6 the Reynolds number returns to the cruise operation, while the Mach number at the inlet of the domain is changed. This is done by varying the area of the sonic throat and modifying the massflow slightly. Cases 2 and 3 will be used to determine the effect of Reynolds number on intake diffusive capabilities as well as on the development of the boundary layer. Cases 4-6 will be used to determine the effects of Mach number on the pressure recovery of the intake.

6.3.2: Measurement Techniques

To calibrate the numerical analysis performed in this thesis several different measurements are needed. The static pressure distribution along the profile wall can be measured to ensure that the numerical tools are successfully determining the boundary layer development and the deceleration of the flow. Below in Figure 6-9 is the static pressure distribution of the optimized profile which will be mounted in the linear wind tunnel, along with the locations for the static pressure taps. Within the PETAL facility, the pressure taps measurements can be resolved to within 5 millibars.
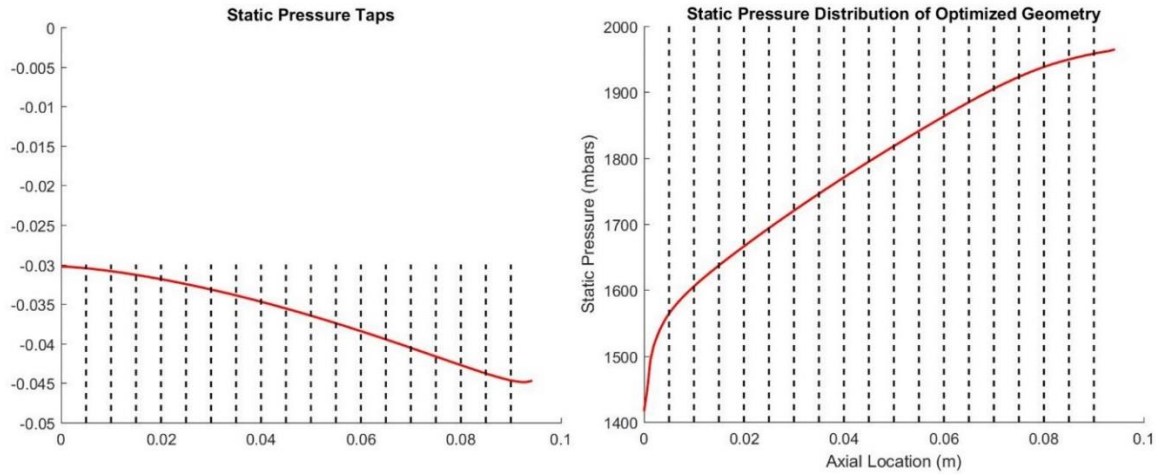
Figure 6-9: Proposed static pressure taps for experiments.

To measure flow diffusion and flow distortion, total pressure rakes will be installed upstream and downstream of the test piece. Upstream and downstream there are flat regions which will allow for the probes to be placed in a manner that won't disturb the flow in the actual test section. The total to static pressure ratios will be used to determine the inlet and outlet Mach numbers in the experiment, thus allowing for determination of the flow diffusion. The rakes will also be used to measure the radial variation in the total pressure at the inlet and the outlet to verify how well the numerical tools capture the boundary layer development. Figure 6-10 below shows the predicted inlet and outlet total pressure variations in the experimental model. The total pressure rakes within the PETAL facility are capable of resolving the flow within 25 millibars.
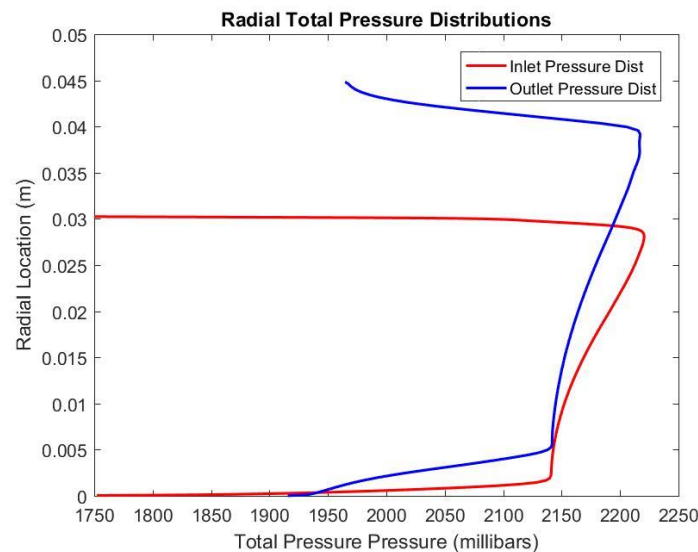

Figure 6-10: Radial total pressure distributions predicted in experimental model.

The windows of the wind tunnel allow for optical access. Using this unique feature, the test matrix above can be subjected to several experimental campaigns that take advantage of the optical access. Oil flow visualizations [48] can be used to detect the surface shear stress. This will be used to verify the local minimum near the inlet and outlet of the experimental piece that is predicted by the numerical tools. Furthermore, PIV [49] can be used in future campaigns to identify separation features in the baseline geometries which have large separation bubbles. The wind tunnel operation can be modified to pull vacuum, which can be used to simulate takeoff conditions by imposing no inlet flow and using vacuum to simulate suction produced by the fan. With the unsteady nature and large separation bubbles present in the takeoff simulations, the numerical results in Chapter 4 can be compared to PIV data.

6.4: 3D CAD Model

The experimental model described above is modeled in CAD and will be machined in aluminum. The model consists of 3 parts: an acceleration ramp, the experimental test article, and a flat plate trailing edge to insert measurement probes in. Figure 6-11 below shows these 3 components.
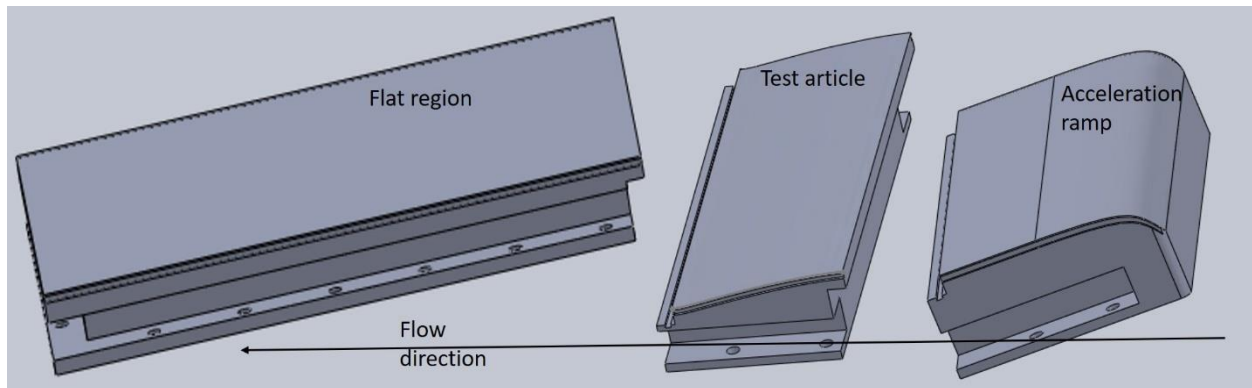

Figure 6-11: CAD model for experiments.

Between the acceleration ramp and the start of the test article is a flat region of 3 cm. This flat region will allow for measurements slightly upstream of the test article which are representative of the test article inlet. Additionally, the test article curvature starts 0.25mm above the end of the flat region to simulate the separation near the intake lips. The assembly of the separate components are shown below in Figure 6-12. The fully assembled experimental model

inside of the wind tunnel is shown below in Figure 6-13 with the optical access to the experimental piece shown.
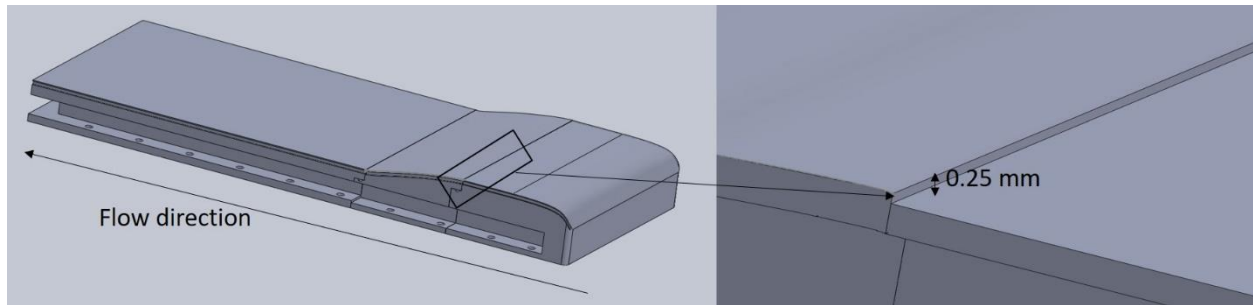

Figure 6-12: Assembly of experimental pieces (left). (Right) shows the bump to trip separation in the test article.
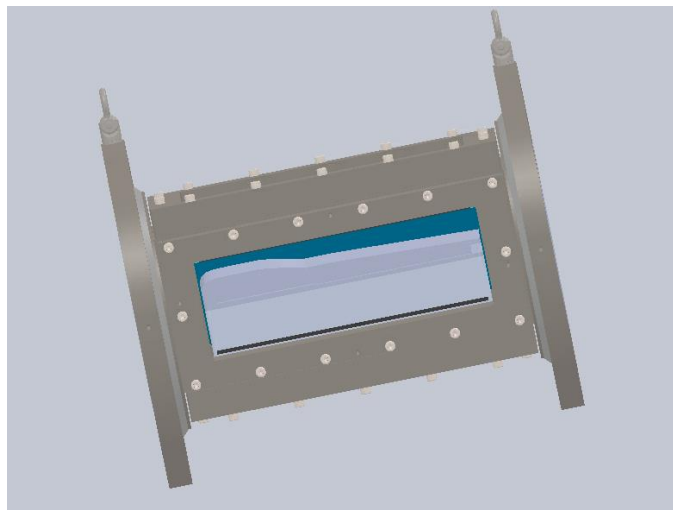

Figure 6-13: Experimental model mounted in linear wind tunnel with windows for optical access.

6.5: Conclusions and Takeaways

In this chapter, an experimental model and procedure was fully defined for future work on intake analysis. The model is developed for use in a linear wind tunnel with optical access, which will allow for experimental campaigns to derive a great deal of information about intake performance and boundary layer development.

The work to determine how to model the intake revealed that intake performance is primarily guided by separation and boundary layer development. This in turn is primarily controlled by the local curvature of the intake. However, the investigations in this chapter also revealed that the effects of the area ratio cannot be neglected as the cone serves to compress the

area and aid in prevention of flow separation. To properly analyze the intake, the characteristic length when going from cruise to wind tunnel operations was defined. The correct definition of Reynolds number primarily effects the performance of the flow diffusion parameter and is mostly negligible in terms of shear stress development and pressure losses.

Finally, this chapter laid out an experimental campaign that will be used to properly validate the numerically optimized engine intake. The campaign will use various test points to independently assess the effects of Mach number and Reynolds number on intake performance. These results will be used to calibrate the numerical tools that developed the off-design analysis done in Chapter 5. The optical techniques available within the PETAL facility will also allow for a deep study of the boundary layer within internal flow fields.

CHAPTER 7 : CONCLUSIONS AND KEY TAKE-AWAYS FOR FUTURE DESIGNERS

The work presented in this thesis focuses on improving understanding of high subsonic speed intakes for future applications to compact micro turbofan applications. These applications are focused around future UAVs which have a wide operational envelope. Engine intakes for these high-speed applications must be compact and highly diffusive. These requirements present challenges to fulfilling the full operational envelope for future engines; with difficulties primarily in meeting both cruise and takeoff performance requirements.

To further design methodologies for such engine intakes, first an engine intake design procedure is set for creating optimized cruise geometries. Based on previous work, intake size and inlet lip design are determined and fed into an optimization routine. The optimization revealed a pareto front of optimal intake geometries. This pareto front revealed key features that will help guide future designers create diffusive, compact intakes for a variety of high-speed applications.

However; these optimized geometries suffer significantly reduced performance during takeoff operation. Depending on the application, a cruise optimized geometry may not be sufficient for takeoff operation. Depending on the amount of enhancement needed at takeoff, several potential methods exist to improve takeoff operation. For small improvements, a series of small slots could be used, or the nose cone can be slid. For larger improvements, fan suction can be increased or large slots between the engine intake and turbofan can be introduced. If these methods are not sufficient, a variable geometry intake must be designed that is capable of significantly increasing the inlet area. Variable area intakes offer enhancements across a wide-range of engine conditions since the geometry can be varied to several different conditions.

The optimized engine intake geometry is evaluated at several off-design engine points including: reduced flight speed, non-axial inlet flow, various altitudes, and unsteady operation (due to unsteady turbofan operation). The effects of engine operation are fully considered on intake performance to demonstrate sensitivity of intake performance to engine operation. Then, the effects of engine intake performance are integrated into an overall engine analysis to demonstrate the importance of considering intake performance when doing mission analysis and determining flight operation.

An experimental model is developed for testing annular engine intakes in a linear wind tunnel. The developed model replicates relevant flow physics from the annular intake geometry, including non-dimensional parameters, shear stress distribution trends, and enhancements in relevant aerodynamic objectives (such as pressure losses and flow diffusion) between baseline and optimized geometries.

Optimized engine intakes for high-speed applications were successfully developed, with a method for design developed and design recommendations presented. The tradeoffs between cruise and takeoff operations were discussed, with several methods of enhancements evaluated and ranked. Off-design engine operation is considered on optimized intake performance, and the performance of the intake is integrated into an engine model to show potential impacts of intake on engine operation. Finally, an experimental model and method to test intakes in a linear wind tunnel is presented.

This work can be utilized by future engine intake designers in a variety of ways. The results shown here can help guide future designers create highly compact diffuser technology, capable of operating across a wide breadth of conditions. Methods to assess intake performance affects on overall engine performance are demonstrated; and an experimental approach to intake analysis is developed.

List of Key Takeaways:

- High-speed intake design recommendations:
    i. Peak angle of curvature of roughly 15° (between 12-15°)
        o Peak angle of curvature occurring near 75% of diffuser axial span, or 50% of cone axial span (between 70-75% axial span of diffuser)
    ii. An area compression zone near the outlet to help reduce separation and minimize pressure losses (obtained through aggressive cone compression near the domain outlet as well as the diffuser itself compressing the flow)
        o The area compression should not happen before 90% of the axial diffuser span
    iii. Inlet lips designed elliptically, with a fineness ratio near 2 and a contraction ratio near 1.2
    iv. Intake length sized according to the following criteria:

- $\dfrac{A_2}{A_1} = 1 + \dfrac{2L(r_2 - r_1)}{L_{ref}\sqrt{L^2 + (r_2 - r_1)^2}}$

- $L_{ref} = \dfrac{r_1 + (r_2 + r_{2,cone})}{2}$

- Large takeoff enhancements (>80%) require variable geometry intake designs. Moderate enhancements (10-50%) require large slots between fan and intake. Small enhancements (<10%) can be achieved through small slots in diffuser walls or through sliding inlet nose cone. Enhancements measured as a function of takeoff massflow ingestions

- Cruise and takeoff conditions are aerodynamically different and designing specifically for one condition reduces the ability to meet requirements at the other. This design trade-off should be considered throughout the design process and methods to evaluate and enhance performance at takeoff need to be considered early in the design process

- Intake performance is highly sensitive to inlet flow angle, and at high speeds the decay in intake performance is significant with respect to angle of attack

- Intake performance is sensitive to downstream fluctuations that effect boundary conditions at the intake outlet. As such, the effects of downstream fluctuations in intake design should be considered, and if these fluctuations are significant, methods to damp the effects should be considered

- Intake performance is sensitive to altitude and Reynolds number. For altitudes above 10,000m at high speeds, the design recommendation presented here become less effective

- Overall engine performance is significantly impacted by off-design intake performance. As such, when conducting mission analysis and mission planning, it is vital to implement intake performance

- To test annular engine intakes in a linear wind tunnel, the curvature of the diffuser wall is the important geometric factor to replicate. When determining the Reynolds number, the characteristic length to convert from intake operation to experimental operation depends on the diffusion rate: $d_{char} = \dfrac{\Delta A}{length}$

REFERENCES

1. Kadosh, K., & Cukurel, B. (2016). Micro-Turbojet to Turbofan Conversion via Continuously Variable Transmission: Thermodynamic Performance Study. *Volume 8: Microturbines, Turbochargers and Small Turbomachines; Steam Turbines*. doi:10.1115/gt2016-56274.
2. Onal, O., & Turan, O. (2016). Calculation and Comparison of a turbofan engine performance parameters with various definitions. *International Journal of Aerospace and Mechanical Engineering,10*(10).
3. Turbofan Engine. (n.d.). Retrieved from https://www.grc.nasa.gov/www/k-12/airplane/aturbf.html
4. Chiang, H. D., Hsu, C., Lai, A., & Lin, R. (2002). An Investigation of Steady and Dynamic Performance of a Small Turbojet Engine. *Volume 1: Turbo Expo 2002*. doi:10.1115/gt2002-30577
5. Traverso, A., & Massardo, A. F. (2005). Optimal design of compact recuperators for microturbine application. *Applied Thermal Engineering,25*(14-15), 2054-2071. doi:10.1016/j.applthermaleng.2005.01.015
6. Vyas, U., Andreoli, V., & Paniagua, G. (2018). Effect of transonic inlet design on the performance of a mico-turbojet engine. *2018 AIAA Aerospace Sciences Meeting*. doi:10.2514/6.2018-1624
7. Douglas W. Murphy, James Cycon, "Applications for mini VTOL UAV for law enforcement," Proc. SPIE 3577, Sensors, C3I, Information, and Training Technologies for Law Enforcement, (7 January 1999).
8. Adbelhafiz, M., Mostafa, A., & Girard, A. (2010). Vehicle Routing Problem Instances: Application to Multi-UAV Mission Planning. *AIAA Guidance, Navigation, and Control Conference*. doi:10.2514/6.2010-8435
9. Kanistras, K., Martins, G., Rutherford, M. J., & Valavanis, K. P. (2014). Survey of Unmanned Aerial Vehicles (UAVs) for Traffic Monitoring. *Handbook of Unmanned Aerial Vehicles,*2643-2666. doi:10.1007/978-90-481-9707-1_122
10. Ryan, A., Zennaro, M., Howell, A., Sengupta, R., & Hedrick, J. (2004). An overview of emerging results in cooperative UAV control. *2004 43rd IEEE Conference on Decision and Control (CDC) (IEEE Cat. No.04CH37601)*. doi:10.1109/cdc.2004.1428700
11. Candiago, S., Remondino, F., Giglio, M. D., Dubbini, M., & Gattelli, M. (2015). Evaluating Multispectral Images and Vegetation Indices for Precision Farming Applications from UAV Images. *Remote Sensing,7*(4), 4026-4047. doi:10.3390/rs70404026
12. Torun, E. (n.d.). *UAV Requirements and Design Considerations*. doi:https://apps.dtic.mil/dtic/tr/fulltext/u2/p010321.pdf
13. Evers, L., Dollevoet, T., Barros, A.I. et al. Ann Oper Res (2014) 222: 293. https://doi.org/10.1007/s10479-012-1261-8
14. Luidens, R. W., Stockman, N. O., & Diedrich, J. H. (1979). An Approach to Optimum Subsonic Inlet Design. *Volume 1A: Gas Turbines*. doi:10.1115/79-gt-51
15. A. Albers, J & A. Miller, B. (1974). Effect of subsonic inlet lip geometry on predicted surface and flow Mach number distributions.

16. Miller, B. A., Dastoli, B. J., & Wesoky, H. L. (1975). *Effect of entry-lip design on aerodynamics and acoustics of high-throat-Mach-number inlets for the quiet, clean, short-haul experimental engine*. Washington, D.C.: National Aeronautics and Space Administration.

17. Tindell, R. H. (1988). Highly compact inlet diffuser technology. *Journal of Propulsion and Power,4*(6), 557-563. doi:10.2514/3.23100

18. Kline SJ, Abbott DE, Fox RW. Optimum Design of Straight-Walled Diffusers. ASME. *J. Basic Eng.* 1959;81(3):321-329. doi:10.1115/1.4008462

19. Mayer, D., Anderson, B., & Johnson, T. (1998). 3D subsonic diffuser design and analysis. *34th AIAA/ASME/SAE/ASEE Joint Propulsion Conference and Exhibit*. doi:10.2514/6.1998-3418

20. Hoyle, N., Bressloff, N. W., & Keane, A. J. (2006). Design Optimization of a Two-Dimensional Subsonic Engine Air Intake. *AIAA Journal,44*(11), 2672-2681. doi:10.2514/1.16123

21. Zhang, W., Knight, D. D., & Smith, D. (2000). Automated Design of a Three-Dimensional Subsonic Diffuser. *Journal of Propulsion and Power,16*(6), 1132-1140. doi:10.2514/2.5688

22. Tormalm, M. (2006). Design and Analysis of Compact UAV Ducts. *24th AIAA Applied Aerodynamics Conference*. doi:10.2514/6.2006-2828

23. Tyler, R. A., & Williamson, R. G. (1967). Paper 11: Diffuser Performance with Distorted Inflow. *Proceedings of the Institution of Mechanical Engineers, Conference Proceedings,182*(4), 115-125. doi:10.1243/pime_conf_1967_182_136_02

24. Wolf, S., & Johnston, J. P. (1969). Effects of Nonuniform Inlet Velocity Profiles on Flow Regimes and Performance in Two-Dimensional Diffusers. *Journal of Basic Engineering,91*(3), 462. doi:10.1115/1.3571155

25. Kennedy, S., Robinson, T., Spence, S., & Richardson, J. (2014). Computational Investigation of Inlet Distortion at High Angles of Attack. Journal of Aircraft,51(2), 361-376. doi:10.2514/1.c031789

26. Scott B. Norin, "Propulsion System Modeling for High Angle of Attack Simulation", Propulsion Controls and Diagnostics Workshop, NASA, 2017

27. Aircraft Propulsion Systems Technology and Design. (1989). 253-289. doi:10.2514/4.861499

28. Cantwell, B (2007). Aircraft and Rocket Propulsion. Course Reader. Stanford Univeristy.

29. Reddy, E., & Reddy, D. (1995). Aerodynamic shape optimization of a subsonic inlet using 3-D Euler computation. *31st Joint Propulsion Conference and Exhibit*. doi:10.2514/6.1995-2757

30. Majić, F., Efraimsson, G., & Oreilly, C. J. (2016). Potential improvement of aerodynamic performance by morphing the nacelle inlet. *Aerospace Science and Technology,54*, 122-131. doi:10.1016/j.ast.2016.04.006

31. Klein, A. "Review: effects of inlet conditions on conical-diffuser performance." Journal of Fluids Engineering 103 (1981): 250-257

32. Anderson, M. (2008). Fluent CFD Versus Sovran and Klomp Diffuser Data Benchmark Study. *46th AIAA Aerospace Sciences Meeting and Exhibit*. doi:10.2514/6.2008-665

33. Chakravarthy, S., Peroomian, O., Goldberg, U., & Palaniswamy, S. (1998). The CFD computational fluid dynamics software suite. *AIAA and SAE, 1998 World Aviation Conference*. doi:10.2514/6.1998-5564

34. Maesschalck, C. D., Lavagnoli, S., Paniagua, G., Verstraete, T., Olive, R., & Picot, P. (2015). Heterogeneous Optimization Strategies for Carved and Squealer-Like Turbine Blade Tips. *Volume 5B: Heat Transfer*. doi:10.1115/gt2015-42983

35. Verstraete TT, Alsalihi ZZ, Van den Braembussche RA. Multidisciplinary Optimization of a Radial Compressor for Microgas Turbine Applications. ASME. J. Turbomach. 2010;132(3):031004-031004-7. doi:10.1115/1.3144162

36. Verstraete T, Amaral S, Van den Braembussche R, Arts T. Design and Optimization of the Internal Cooling Channels of a HP Turbine Blade: Part II—Optimization. ASME. Turbo Expo: Power for Land, Sea, and Air, Volume 4: Heat Transfer, Parts A and B ():977-987. doi:10.1115/GT2008-51080.

37. Juangphanich, P., Maesschalck, C.D., and Paniagua, G., 2017, "From Conceptual 1D Design To Full 3D Optimization of a Highly Loaded Turbine Stage," *Proceedings of the 55th Aerospace Sciences Meeting*, January 9-13, Grapevine, TX. AIAA 2017-0110. DOI: https://arc.aiaa.org/doi/pdf/10.2514/6.2017-0110

38. Andreoli, V., Braun, J., Paniagua, G., De Maesschalck, C., Bloxham, M., Cummings, W., and Langford, L., 2019, "Aerothermal Optimization of Fully Cooled Turbine Blade Tips," *Journal of Turbomachinery*, Vol. 141, No. 6, p. 061007. DOI: https://doi.org/10.1115/1.4041961

39. Storn, R. & Price, K. Journal of Global Optimization (1997) 11: 341. https://doi.org/10.1023/A:1008202821328

40. Deb, K., Pratap, A., Agarwal, S., Meyarivan, T., 2002, "A fast and elitist multiobjective genetic algorithm: NSGA-II", IEEE Transactions on Evolutionary Computation, 6(2):182–197

41. Piotrowski, A. P. (2017). Review of Differential Evolution population size. *Swarm and Evolutionary Computation,32*, 1-24. doi:10.1016/j.swevo.2016.05.003

42. Williams, E. A., & Crossley, W. A. (1998). Empirically-Derived Population Size and Mutation Rate Guidelines for a Genetic Algorithm with Uniform Crossover. *Soft Computing in Engineering Design and Manufacturing,*163-172. doi:10.1007/978-1-4471-0427-8_18

43. Celik, I. B., Ghia, U., and Roache, P. J., 2008, "Procedure for Estimation and Reporting of Uncertainty due to Discretization in CFD Applications," *Journal of Fluids Engineering*, Vol. 130, p. 078001. DOI: https://doi.org/10.1115/1.2960953

44. Ou-Yang, Hui & Zhu, Zhi-li & Chen, Min. (2008). Conceptual Design of Geometry-Variable Hypersonic Intake for TBCC. 10.2514/6.2008-4587.

45. Leylek, Zafer, Wesly S. Anderson, Glen Rowlinson, and Nigel Smith. "An investigation into performance modeling of a small gas turbine engine." In ASME Turbo Expo 2013: Turbine Technical Conference and Exposition, pp. V05AT23A007-V05AT23A007. American Society of Mechanical Engineers, 2013

46. Chapman, J. W., Lavelle, T. M., May, R. D., Litt, J. S., & Guo, T. H., "Toolbox for the Modeling and Analysis of Thermodynamic Systems (T-MATS) User's Guide", 2014.

47. Paniagua, G., Cuadrado, D., Saavedra, J., Andreoli, V., Meyer, T., Meyer, S., & Lawrence, D. (2016). Design of the Purdue Experimental Turbine Aerothermal Laboratory for Optical and Surface Aero-Thermal Measurements. *Volume 6: Ceramics; Controls, Diagnostics and Instrumentation; Education; Manufacturing Materials and Metallurgy*. doi:10.1115/gt2016-58101

48. Pierce, A., Lu, F., Bryant, D., & Shih, Y. (2010). New Developments in Surface Oil Flow Visualization. *27th AIAA Aerodynamic Measurement Technology and Ground Testing Conference*. doi:10.2514/6.2010-4353

49. Roberts, W. B. (1980). Calculation of Laminar Separation Bubbles and Their Effect on Airfoil Performance. *AIAA Journal,18*(1), 25-31. doi:10.2514/3.50726

APPENDIX A: EFFECTS OF FINENESS RATIO ON INTAKE PERFORMANCE

The figure below shows the outlet Mach number distributions as a function of the fineness ratio. The bottom image shows that a fineness ratio of 2 had the lowest flow distortion. In the literature, this fineness ratio is suggested as optimal at off-design conditions for an elliptical inlet lip, so a fineness ratio of 2 is selected.
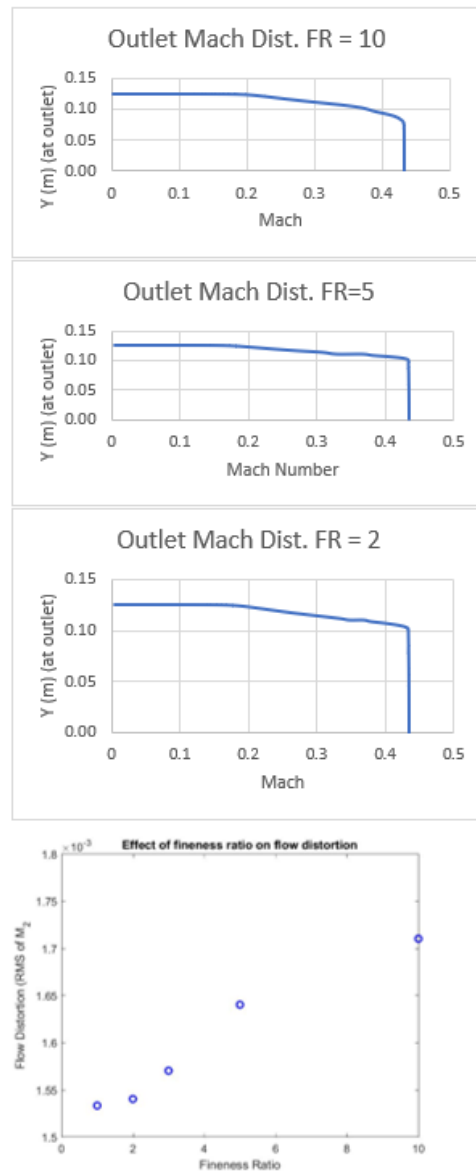

Figure A-1: Outlet flow distortions for various fineness ratios.

Below, the effects of the fineness ratio on total pressure losses is shown. These effects are relatively small compared to flow distortion effects, but once again, a fineness ratio of 2 is shown to be optimal.
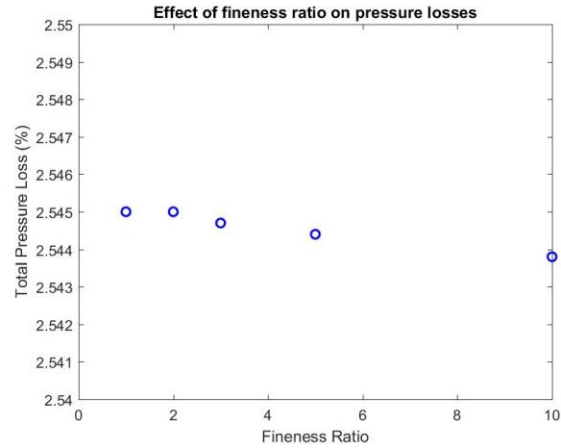
Figure A-2: Effects of fineness ratio on pressure losses.

APPENDIX B: MISCELLANEOUS OPTIMIZATION RESULTS

The figures below show the dependence of various geometric parameters on intake performance. Minimizing the values of most geometric parameters is shown to preferable, however values of x_4, which represents the last control point for the diffuser is shown to control performance along the pareto.
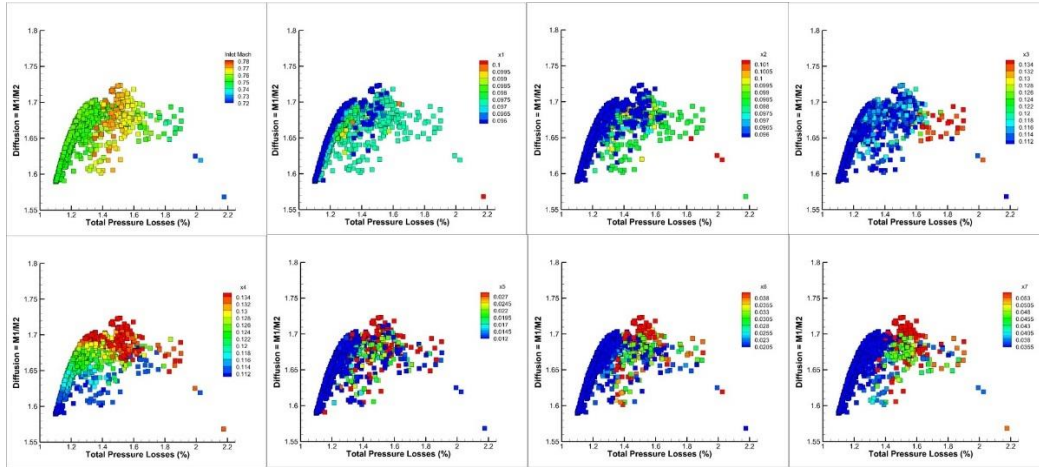

Figure B-1: Relationship of different optimization geometric parameters on intake performance. Contours represent values of geometric parameters.

Figure B-2 below depicts the relationship between inlet and outlet Mach numbers and the achievable flow diffusion. The left figure shows a mostly linear relationship between outlet Mach and flow diffusion. However, the impact of the achievable inlet Mach number is noticeable, clearly demonstrating the need to measure flow diffusion as a function of both. The right figure shows that there is no true relationship between inlet and outlet Mach achieved by the intake.
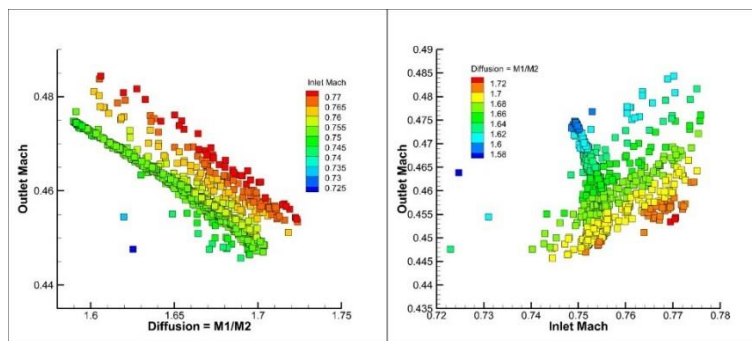

Figure B-2: Relationship between M_1, M_2, and flow diffusion.

APPENDIX C: CONTOURS FROM TAKEOFF SIMULATIONS

Below Figures C1 and C2 depict the methods for sliding intake components. These methods are implemented to assess the potential for sliding intake geometries to enhance takeoff performance. The geometries are shifted upstream in the intake and are extended by physical walls.
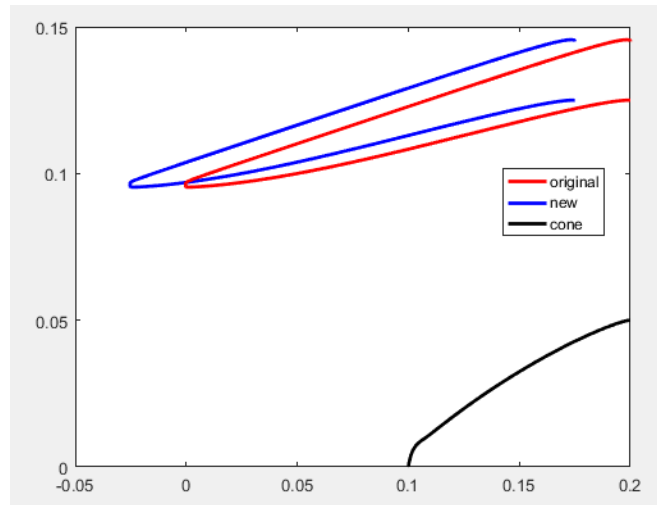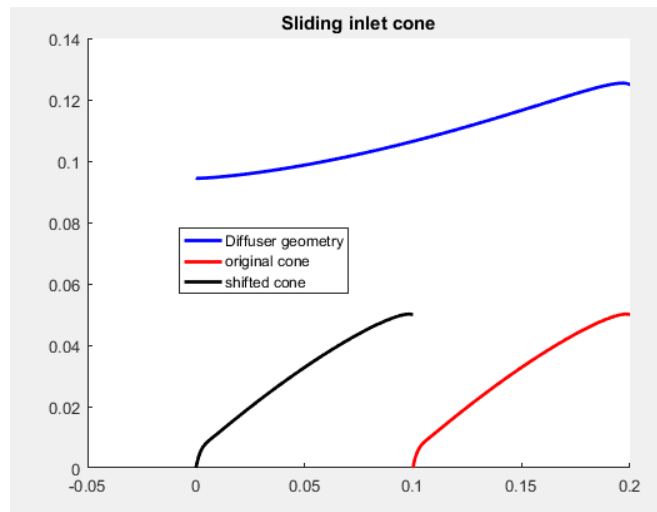

Figure C-1: Sliding nacelle geometry.

Figure C-2: Sliding cone geometry.

The contours below show intake performance at takeoff conditions with various fan back pressures. Decreasing the fan back pressure past 65 kPa results in choked flow, and the massflow is not enhanced past this point. The maximum massflow passed by decreasing fan back pressure is 5.25 kg/s (improved from 3.59 kg/s).
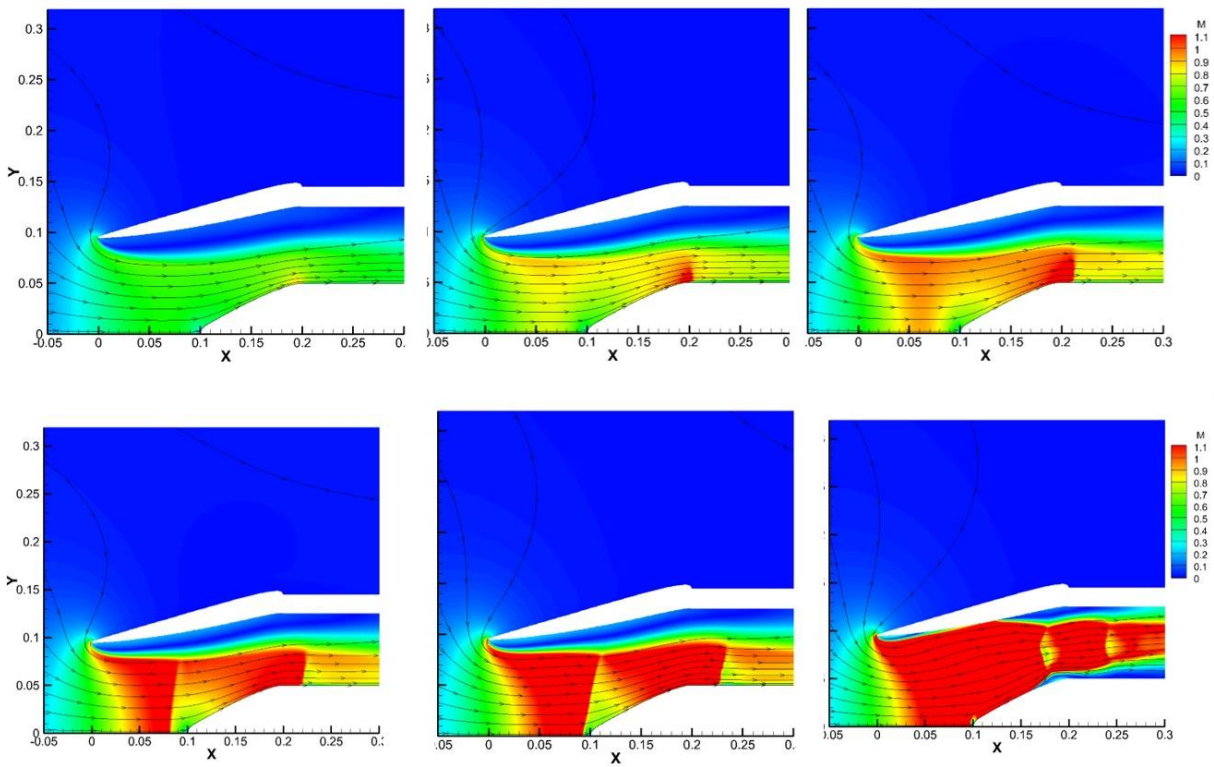
Figure C-3: Takeoff contours ranging from a back pressure of 85 kPa (top left) to 60 kPa (bottom right). At 65 kPa the intake is effectively choked and massflow enhancements are limited.